# Destabilization of Boron-Based Compounds for Hydrogen Storage in the Solid-State: Recent Advances

Carlos Castilla-Martinez, Romain Moury, Salem Ould-Amara, Umit Demirci

energies

MDPI

*Review*

# Destabilization of Boron-Based Compounds for Hydrogen Storage in the Solid-State: Recent Advances

**Carlos A. Castilla-Martinez [1,*], Romain Moury [2], Salem Ould-Amara [3] and Umit B. Demirci [4]**

[1] Laboratoire des Fluides Complexes et leurs Réservoirs, UMR 5150, Université de Pau et des Pays de l'Adour, E2S UPPA, CNRS, 64600 Anglet, France
[2] Institut des Molécules et Matériaux du Mans (IMMM), UMR 6283, Le Mans Université, CNRS Avenue Olivier Messiaen, CEDEX 9, 72085 Le Mans, France; romain.moury@gmail.com
[3] Laboratoire Analyse, Modélisation, Matériaux pour la Biologie et l'Environment, LAMBE—UMR 8587, Université D'Evry Val d'Essonne, CNRS, 91025 Evry, France; salemouldamara54@outlook.fr
[4] Institut Européen des Membranes, IEM—UMR 5635, Université de Montpellier, ENSCM, CNRS, 34095 Montpellier, France; umit.demirci@umontpellier.fr
* Correspondence: ccastilla90@gmail.com

**Abstract:** Boron-based materials have been widely studied for hydrogen storage applications. Examples of these compounds are borohydrides and boranes. However, all of these present some disadvantages that have hindered their potential application as hydrogen storage materials in the solid-state. Thus, different strategies have been developed to improve the dehydrogenation properties of these materials. The purpose of this review is to provide an overview of recent advances (for the period 2015–2021) in the destabilization strategies that have been considered for selected boron-based compounds. With this aim, we selected seven of the most investigated boron-based compounds for hydrogen storage applications: lithium borohydride, sodium borohydride, magnesium borohydride, calcium borohydride, ammonia borane, hydrazine borane and hydrazine bisborane. The destabilization strategies include the use of additives, the chemical modification and the nanosizing of these compounds. These approaches were analyzed for each one of the selected boron-based compounds and these are discussed in the present review.

**Keywords:** borohydride; borane; hydrogen storage; destabilization; thermolysis; hydrogen carrier; boron



**Citation:** Castilla-Martinez, C.A.; Moury, R.; Ould-Amara, S.; Demirci, U.B. Destabilization of Boron-Based Compounds for Hydrogen Storage in the Solid-State: Recent Advances. *Energies* **2021**, *14*, 7003. https://doi.org/10.3390/en14217003

Academic Editor: Muhammad Aziz

Received: 28 September 2021
Accepted: 21 October 2021
Published: 26 October 2021



## 1. Introduction

Energy is essential for humanity. Nowadays, the primary source of energy is fossil fuels (oil, gas, coal) and secondarily, alternative sources (solar, wind, nuclear, etc.). Fossil fuels are limited, non-renewable resources that are being depleted; their extraction is becoming harder and their combustion produces greenhouse gases (carbon dioxide, $CO_2$; methane, $CH_4$; nitrogen oxides, $NO_x$; and fluorinated compounds). Thus, energy consumption has a direct impact on global warming and the environment [1]. To overcome these negative effects, it is necessary to obtain energy from sources that produce zero or near-zero noxious emissions.

Hydrogen ($H_2$) has arisen as the best energy vector to use as a substitute for fossil fuels [2,3]. It possesses a high energy density, it is nontoxic, it produces zero emissions during its combustion in a fuel cell and it overcomes the intermittent nature of other renewable energy sources (such as solar and wind energy). Thanks to its potential, the concept of a hydrogen economy has been developed: a whole new energy model, based on the production, storage, distribution and utilization of hydrogen [4–6]. At present, great effort is being made in order to develop and mature hydrogen technologies. However, different challenges still lie ahead. Hydrogen storage is one of them. Different factors have to be considered to obtain a good storage system, such as the weight, volume, efficiency, safety and cost of the system. At present, hydrogen is stored in high-pressure

tanks, in liquefaction tanks at subzero conditions and stored into a host material. The latter seems to be the most promising approach, due to its superior potential storage capacity. Depending on the interaction between hydrogen and the host material (physical or chemical), different materials have been proposed to store hydrogen (zeolites, carbon-based materials, clathrates, metal organic frameworks, ammonia, hydrides and liquid organic carriers, for example) [7–14]. Boron-based materials have been widely studied as potential candidates to store hydrogen [15,16]. Usually, these compounds present a high hydrogen gravimetric density due to the lightness of the boron atom (10.8 amu) and its capacity to form multiple bonds. Borohydrides and boranes are good examples of these materials. The present review aims to provide a general overview of recent studies (from the period 2015–2021) on the approaches towards destabilizing lightweight boron-based compounds (Figure 1): borohydrides (lithium, sodium, magnesium and calcium) and boranes (ammonia borane, hydrazine borane and hydrazine bisborane). A general overview of these compounds is presented in Section 2, and a general description of the destabilization approaches is briefly provided in Section 3. From Section 4 to Section 9, recent advances on these materials are presented, and finally, the perspectives and conclusions are given in Section 10.

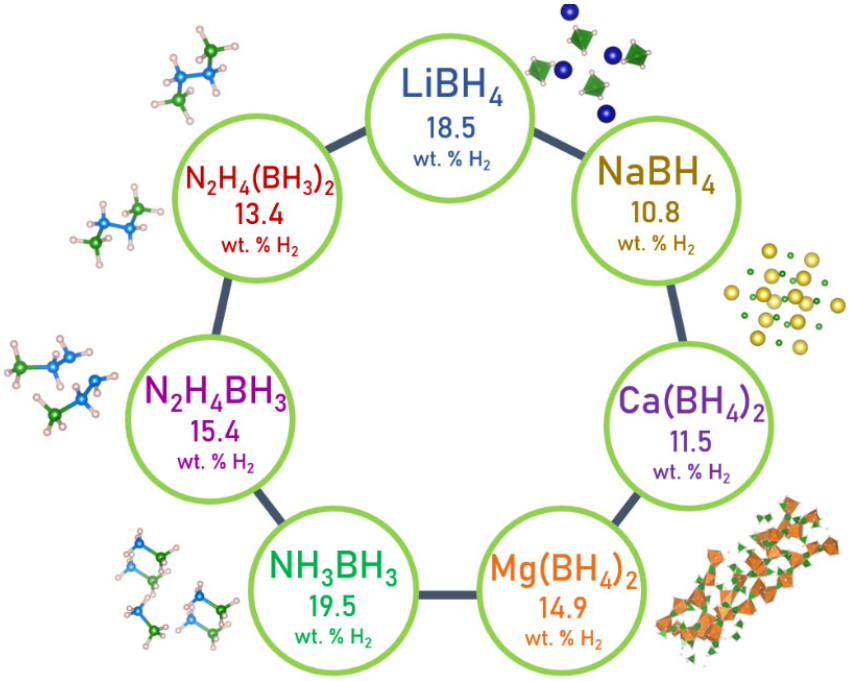


**Figure 1.** Selected B-based compounds and their gravimetric storage capacity.

## 2. Overview

Sodium borohydride ($NaBH_4$) and ammonia borane (AB, $NH_3BH_3$) are typical examples of chemical hydrides that have been much studied as boron-based hydrogen storage materials. Both were originally discovered in the 1940s–1950s, and both were rediscovered in the late 1990s and the mid-2000s, respectively. They thus have a history, and this history can be divided into three periods: the discovery in the 1940s–1950s as mentioned above; the oblivion in the 1960–1980s (a period in which both were scarcely considered in research) [17,18] and the resurgence since the late 1990s (as summarized hereafter).

Sodium borohydride was discovered by Schlesinger and co-workers in the 1940s in the context of military research for the use of hydrogen [19]. Different synthesis pathways were explored and each one allowed the successful preparation of the borohydride. One of the paths, the simpler one (Equation (1)) [20], is currently the key reaction for its industrial production:

$$4NaH + B(OCH_3)_3 \rightarrow NaBH_4 + 3\ NaOCH_3 \quad (1)$$

The as-synthesized sodium borohydride was found to be appropriate for the targeted application because it is a solid, with a remarkable stability when heated in air at 300 °C and under vacuum at 400 °C, it dissolves in cold water, and it is able to release pure $H_2$ via hydrolysis (Equation (2)) in the presence of a catalyst:

$$NaBH_4 + 4H_2O \rightarrow NaB(OH)_4 + 4H_2 \quad (2)$$

These are the properties that have made sodium borohydride so attractive as a chemical hydride and a potential hydrogen carrier (10.8 wt. % $H_2$) in recent years [21]. It is classified as chemical hydride because the storage of hydrogen via this compound is thermodynamically irreversible. Dehydrogenation by hydrolysis is exothermic [22], and rehydrogenation by $H_2$ is thermodynamically impossible under affordable conditions. The only way to close the hydrogen cycle with 'hydrolytic' sodium borohydride is to chemically reduce the borate product, sodium tetrahydroxyborate $NaB(OH)_4$, to hydrogenate it and regenerate sodium borohydride [23] (Figure 2).

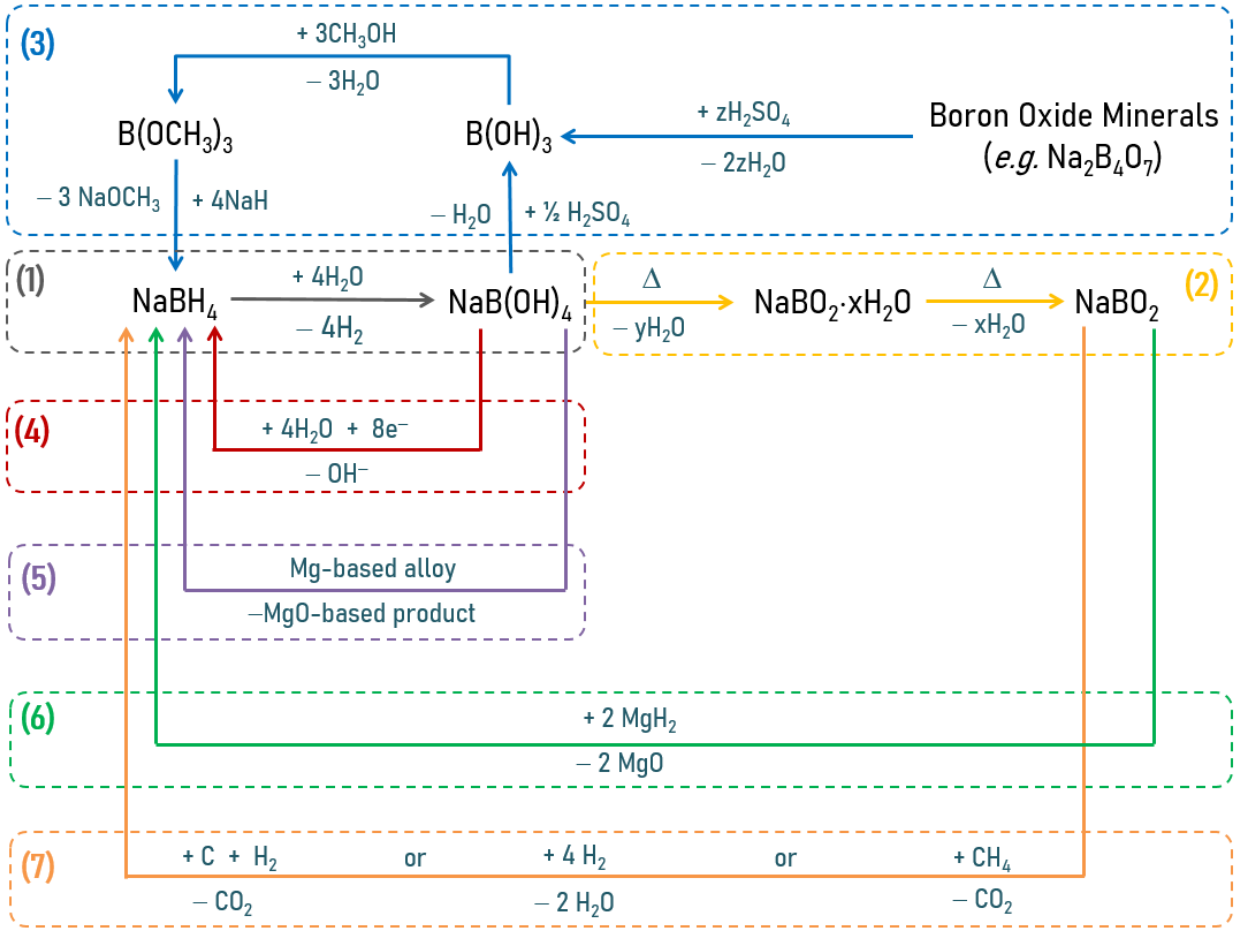


**Figure 2.** Hydrogen cycle with sodium borohydride: (1) hydrolysis of $NaBH_4$; (2) dehydration of the hydrated borate product $NaB(OH)_4$; (3) Brown–Schlesinger process used for the commercial production of $NaBH_4$; (4) electroreduction of $NaB(OH)_4$ for regenerating $NaBH_4$; (5) chemical reduction of $NaB(OH)_4$ by means of a Mg-based alloy; (6) chemical reduction of $NaBO_2$ using magnesium hydride; (7) chemical reduction of $NaBO_2$ using various reducing agents.

A recent example of the regeneration path is as follows. For example, Le et al. successfully produced sodium borohydride (99.5% conversion) via mechanical milling of the hydrolysis product sodium tetrahydroxyborate in dihydrated form, $NaB(OH)_4 \cdot 2H_2O$, with an Mg-Al-based alloy (76.1 wt. % Mg, 13.6 wt. % Al, with the rest being Ca, Cu, Mn, Nd, Zn, Y and Ag) at 25 °C–40 °C and 1 bar Ar [24]. Interestingly, this regeneration path

uses the hydrogen of OH and/or $H_2O$ of $NaB(OH)_4 \cdot 2H_2O$ to reform the B–H bonds of sodium borohydride.

Still in the 1940s, Schlesinger and co-workers developed a number of other metal borohydrides, such as $Al(BH_4)_3$ [25], $Be(BH_4)_2$ [26], $LiBH_4$ [27] $Ga(BH_4)_3$ [28] and $U(BH_4)_4$ [29]. Among these, lithium borohydride ($LiBH_4$) has also been studied as a hydrogen storage material [30], but unlike sodium borohydride, it has been mainly considered as a complex hydride. In contrast with a chemical hydride, a complex hydride can be rehydrogenated, at least partially, by increasing the temperature under a certain $H_2$ pressure. $LiBH_4$ dehydrogenates from 275 °C [31], leading to a mixture of LiH and B via a complex mechanism (Equation (3)) [32].

$$LiBH_4 \rightarrow LiH + B + 3/2\ H_2 \quad (3)$$

Such a dehydrogenation path allows the release of 13.9 wt. % $H_2$ over the 18.5 wt. % $H_2$ that corresponds to the theoretical gravimetric hydrogen density of lithium borohydride. As mentioned, the strength of lithium borohydride lies in the fact that the dehydrogenation products can be hydrogenated under $H_2$ to regenerate the borohydride. For instance, Orimo et al. showed that a mixture of LiH and B was hydrogenated at 600 °C and 350 bar $H_2$, which resulted in the formation of lithium borohydride [33]. Though feasible, reversibility in such conditions is not appropriate for technological applications, and this is why strategies for destabilizing lithium borohydride have been developed within recent decades. This is discussed in Section 4, with a particular emphasis on the developments reported within the last 6 years. It is worth mentioning that lithium borohydride opened the way for alternate borohydrides. Two examples are magnesium borohydride $Mg(BH_4)_2$ and calcium borohydride $Ca(BH_4)_2$. The former is able to release almost 15 wt. % $H_2$ when heated up to 500 °C [34] and the dehydrogenation product can be hydrogenated at >260 °C and 400 bar $H_2$ to regenerate magnesium borohydride [35]. The latter borohydride dehydrogenates (9 wt. % $H_2$) between 360 °C and 500 °C [36], and dehydrogenation products such as $CaH_2$ and $CaB_6$ can be hydrogenated in the presence of additives [37]. As for lithium borohydride, both of these alkaline-earth borohydrides have been more deeply studied in order to develop destabilization strategies, allowing them to store hydrogen reversibly under milder conditions. This is discussed in Section 6.

Schlesinger and co-workers long sought to synthesize AB but they never succeeded [38]. This was accomplished by Shore and Parry in the 1950s and the related article was released in 1955 [39]. AB was found to be a white solid when kept under ambient conditions, and stable in water at neutral pH and in solid state when kept under ambient conditions. A simple path (Equation (4)) for synthesizing pure AB is based on the use of sodium borohydride [40]:

$$2\ NaBH_4 + (NH_4)_2SO_4 \rightarrow 2\ NH_3BH_3 + Na_2SO_4 + 2\ H_2 \quad (4)$$

In the recent period, AB has also been considered as a promising hydrogen storage material owing to its very high gravimetric hydrogen density of 19.5 wt. % $H_2$ [41]. With AB, the aforementioned two dehydrogenation approaches have been widely investigated. On the one hand, a number of catalysts have been developed to accelerate the release of $H_2$ through the hydrolysis of AB (Equation (5)) under ambient conditions [42]:

$$NH_3BH_3 + 3H_2O \rightarrow NH_3 + B(OH)_3 + 3H_2 \quad (5)$$

Nevertheless, one might wonder whether such an approach is relevant when it is compared to the hydrolysis of sodium borohydride, because the hydrolysis of AB does not present any advantage (Figure 3), and worst of all, it has drawbacks that the hydrolysis of sodium borohydride does not have [43]. Examples of these drawbacks are as follows: the release of $NH_3$ together with $H_2$ [44], the mixture of borate species after hydrolysis [45], a lower effective gravimetric hydrogen storage capacity [46], and a higher cost of AB (because it is synthesized from sodium borohydride; Equation (5)) [47].

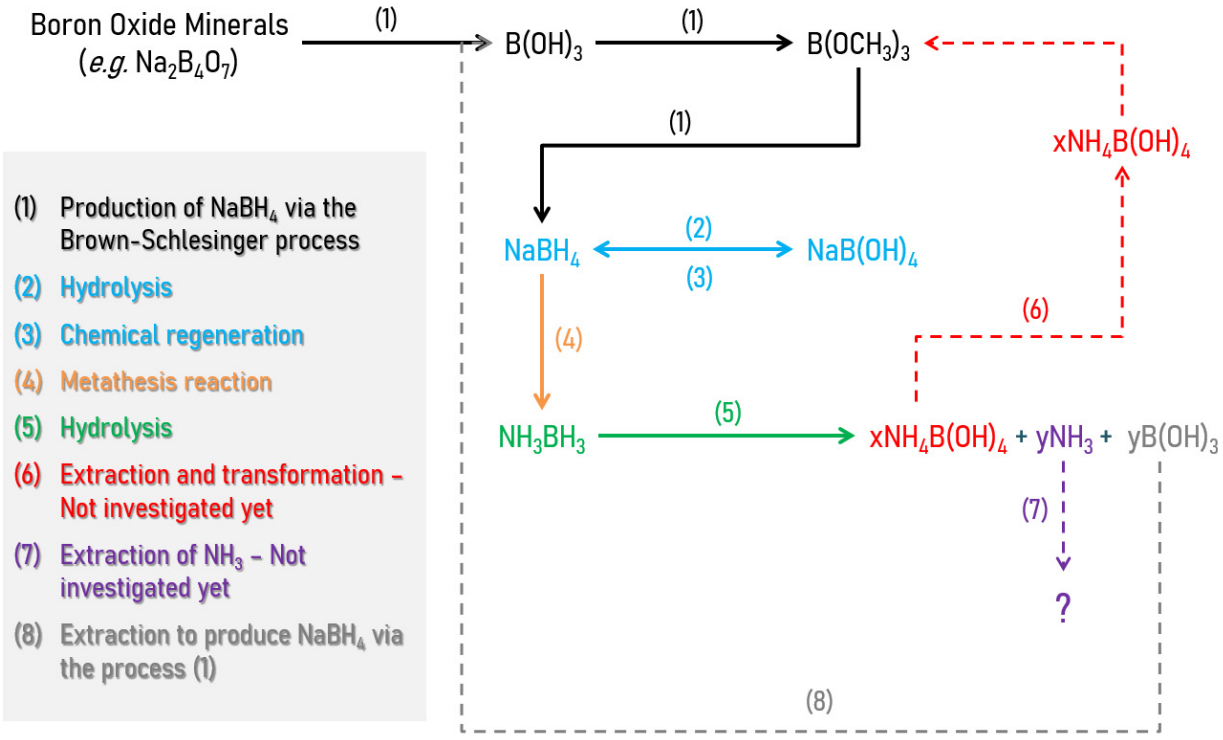


**Figure 3.** Sodium borohydride vs. ammonia borane for $H_2$ generation via hydrolysis at ambient conditions.

On the other hand, thermal dehydrogenation of AB has been widely investigated. This compound has a few specific features that make it attractive for solid-state hydrogen storage and dehydrogenation under heating. First, AB carries three protic hydrogens ($H^{\delta+}$) and three hydridic hydrogens ($H^{\delta-}$) that can combine through inter- and/or intra-molecular interactions to give 3 $H_2$ [48]. Second, the solid state of AB is rationalized by these two types of hydrogens and the subsequent dihydrogen $H^{\delta+}\cdots H^{\delta-}$ bonding network [49]. Third, AB is stable at ambient conditions, when stored under inert atmosphere, and it readily dehydrogenates when it is heated above 80 °C [50]. For instance, it has often been reported that AB is able to release two equivalents of $H_2$ (13 wt. % $H_2$) between 100 °C and 200 °C (Equations (6) and (7)) when heated at 5 °C or 10 °C $min^{-1}$ [51]:

$$NH_3BH_3 \rightarrow [NH_2BH_2] + H_2 \quad (6)$$

$$[NH_2BH_2] \rightarrow [NHBH] + H_2 \quad (7)$$

The dehydrogenated product denoted [NHBH] is in fact a polymeric residue made of polyaminoborane $[NH_2BH_2]_n$, polyiminoborane $[NHBH]_n$ and polyborazylene $[BNH_{x<2}]_n$ [52]. The dehydrogenation of [NHBH] (Equation (8)) takes place above 500 °C [53]:

$$[NHBH] \rightarrow [BNH_{x<2}] + H_2 \quad (8)$$

Full dehydrogenation has to be avoided because of the formation of boron nitride BN that, as a ceramic, is very stable and cannot be hydrogenated back into AB [54]. AB in a pure state is, however, not suitable as a chemical hydride for hydrogen storage. One of the main issues is related to its decomposition. Under heating, AB decomposes more than it dehydrogenates, and it releases significant amounts of volatile products such as borazine ($B_3N_3H_6$), diborane ($B_2H_6$) and ammonia ($NH_3$) [55]. Another issue is the complex composition of the polymeric residue that does not allow the development of an affordable process of AB regeneration. Hence, all of the efforts in this arra have focused on developing strategies for destabilizing AB. The aim is to dehydrogenate the borane below 100 °C, to avoid its decomposition, and to favor the formation of polyborazylene as a single polymeric

residue (because there is an existing efficient recycling strategy using hydrazine ($N_2H_4$) as a reducing agent and ammonia ($NH_3$) as a solvent to regenerate AB [56]). The strategies and the main achievements are discussed in Section 7.

One of the strategies developed for destabilizing AB is based on its chemical modification, which means that derivatives of this borane are synthesized by substituting one protic hydrogen $H^{\delta+}$ of the molecule with a metal cation such as $Na^+$. Though the idea of destabilizing AB in this way is new, the resulting derivatives are not recent. The sodium derivative, namely, sodium amidoborane $NaNH_2BH_3$ (9.5 wt. % $H_2$), was mentioned for the first time in the 1940s by Schlesinger and Burg [57]. It was the only representative of the metal amidoboranes for a long time, until the second one, namely, lithium amidoborane $LiNH_2BH_3$ (13.6 wt. % $H_2$), was reported in 1996 by Myers et al. [58] as a powerful new reductant. In 2007, the potential of using an amidoborane as a hydrogen storage material was mentioned for the first time by Diyabalanage et al. [59], who synthesized the calcium counterpart, $Ca(NH_2BH_3)_2$ (10 wt. % $H_2$). This solid was found to release cleaner $H_2$ than AB does, even though dehydrogenation took place above 100 °C. The potential of amidoboranes as hydrogen storage materials was definitively confirmed by Xiong et al. [60] one year later, when they reported exceptional $H_2$ release properties in lithium amidoborane and sodium borohydride. For example, lithium amidoborane dehydrogenates below 100 °C, following a near-thermally-neutral event ($-3$ kJ $mol^{-1}$). Since then, a number of metal amidoboranes have been reported [61]. They are discussed in detail in Section 7.2.

The 1940s–1950s were relatively fruitful for boranes as well [62]. In 1961, Goubeau and Ricker released an article reporting a borane that has to be seen as one of the derivatives of AB, namely, hydrazine borane (HB, $N_2H_4BH_3$, 15.4 wt. % $H_2$) [63]. Like AB, it is a white crystalline solid and it can be synthesized through salt metathesis using sodium borohydride as the reactant (Equation (9)):

$$2NaBH_4 + (N_2H_4)_2SO_4 \rightarrow 2N_2H_4BH_3 + Na_2SO_4 + 2\,H_2 \quad (9)$$

As with AB, the dehydrogenation of HB can be performed via hydrolysis or thermolysis. Hydrolytic dehydrogenation of HB is more attractive than that of AB because the $N_2H_4$ group of HB can be dehydrogenated in the presence of a suitable catalyst. Accordingly, both of the $BH_3$ and $N_2H_4$ groups of HB are dehydrogenated under near-ambient conditions (Equation (10)):

$$N_2H_4BH_3 + 3H_2O \rightarrow B(OH)_3 + 5\,H_2 + N_2 \quad (10)$$

For example, Yurderi et al. reported Ni@Ir core-shell nanoparticles supported on manganese oxide that was able to catalyze the release of five equivalents (equiv.) of $H_2$ (10 wt. % $H_2$) and one equivalent of $N_2$ from HB (0.2 M) in an aqueous alkaline (5 M NaOH) solution heated at 50 °C [64]. However, this reaction has not been the subject of many studies because of critical issues. The main challenge with HB is to find a catalyst that allows its complete dehydrogenation, does not deactivate, and does not deteriorate towards an incomplete dehydrogenation of $N_2H_4$ into the unwanted $NH_3$ [65]. Otherwise, HB and AB present the same drawbacks when they are compared to sodium borohydride. The second approach to the dehydrogenation of HB is based on its thermolysis [66]. Like AB, it carries protic hydrogens ($4H^{\delta+}$) and hydridic hydrogens ($3H^{\delta-}$) that combine when heated above 60 °C and form $H_2$. Between 60 °C and 100 °C, HB dehydrogenates, but above 100 °C, it decomposes and releases volatile products such as $N_2H_4$ and $NH_3$ [67]. If heated above 300 °C, the residue that forms upon the release of the second equivalent of $H_2$ is shock-sensitive, which makes pure HB not suitable for solid-state hydrogen storage. As a result, there has been research into alternatives to HB, out of which came alkali and alkaline-earth derivatives called hydrazinidoboranes. These new compounds are discussed in Section 8.2. Though it has been little studied to date, hydrazine bisborane (HBB, $BH_3N_2H_4BH_3$, 13.4 wt. % $H_2$) is another derivative of ammonia borane that was synthesized (from sodium borohydride as well) and reported for the first time in the 1960s by Gunderloy [68]. Hydrazine bisborane is in fact a hazardous solid. Gunderloy observed

that it "may explode violently if heated rapidly much beyond 100 °C" and it "may also be detonated by impact". The first feature was recently confirmed by Pylypko et al. [69], but not mentioned by Sun et al. [70].

As mentioned throughout this section, there are some disadvantages that have hindered the implementation of pristine boron-based compounds for hydrogen storage applications. For this reason, the destabilization of such compounds has been widely studied and the main approaches will be discussed in the next section.

## 3. Destabilization Approaches

In general, there are three approaches that have been considered to destabilize boron-based compounds: the incorporation of an additive, the chemical modification and the nanosizing of the compound (Figure 4).

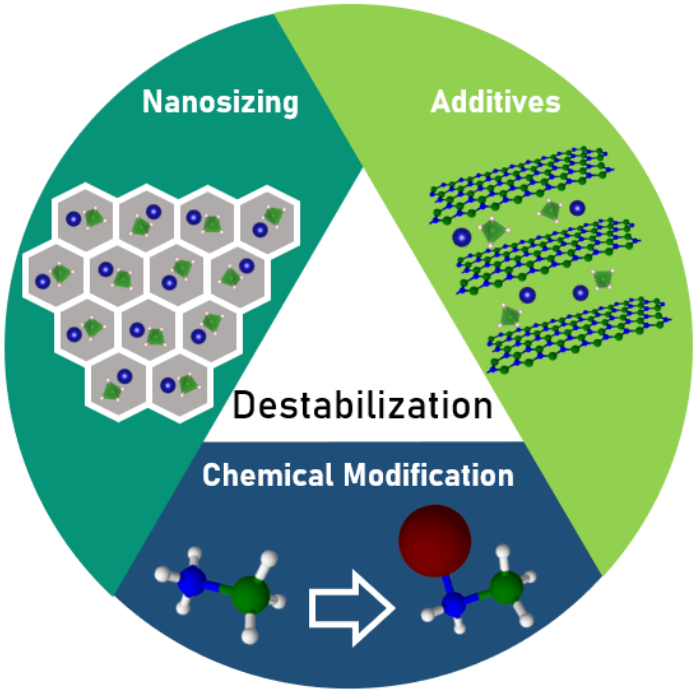


**Figure 4.** The three destabilization approaches for B-based materials.

The incorporation of an additive to the B-based compound consists of obtaining a composite, either by mechanically mixing the components (usually by ball milling, but also by simple hand mixing) or by its preparation via a wet method. The composite contains particles of the B-based compound and of the additive(s). The additive destabilizes the B-based compound through interactions between atoms and/or presents catalytic activity towards the compound, favoring its dehydrogenation at a lower temperature. One example of these interactions is that between protic atoms ($H^{\delta+}$) of a selected additive and the hydridic atoms ($H^{\delta-}$) of a borohydride.

The chemical modification approach consists in either the substitution of one of the H atoms of the compound by another atom or the synthesis of a new complex between the B-based compound and another molecule. For example, as briefly discussed in the previous section, the substitution of an H atom of AB by an alkali or alkaline-earth atom led to the obtention of amidoboranes, which present better dehydrogenation properties than the parent borane.

The nanosizing approach consists in obtaining particles of the compound at the nanoscale. Usually, these particles are confined in a porous host, named the scaffold, which limits and stabilizes these nanoparticles. The introduction of the compound into the scaffold is usually done using one of two approaches: the solvent impregnation method, where the dissolved compound is infiltrated via capillary forces, or melt infiltration, where

the compound is directly infiltrated by melting the compound under an $H_2$ atmosphere. Scaffolds with different chemical nature have been studied to confine borohydrides or boranes. For example, carbon is a cheap and thermally stable compound that can form different porous structures with a wide selection of pore size, specific surface area (SSA) and pore volume. Due to this versatility, C-based scaffolds are among the most common materials used to confine B-based compounds. However, they are not the only ones, as there are several types of scaffolds based on Al, Ni, $SiO_2$ and others. Finally, the possibility of obtaining nanoparticles from B-based compounds without a scaffold is also feasible. To achieve this, surfactants are generally used. These nanoparticles present different behavior in comparison with the bulk material.

The purpose of these three approaches is to improve the dehydrogenation thermodynamics and kinetics of the compound. Recent advances in the destabilization of B-based compounds using these methods are discussed below for each one of the selected compounds from Sections 4–9.

## 4. $LiBH_4$

Being the lightest of the borohydrides, $LiBH_4$ is a crystalline solid (orthorhombic, space group *Pnma*) with a density of 0.66 g $cm^{-1}$ [71]. $LiBH_4$ has been widely studied as a material for hydrogen storage applications due to its high gravimetric (18.5 wt. % $H_2$) and volumetric (121 $kg_{H2}$ $m^{-3}$) hydrogen storage capacity. Unfortunately, the potential use of $LiBH_4$ in the pristine state for hydrogen storage applications presents great disadvantages. First of all, the thermodynamics of $LiBH_4$ presents a problem. Bulk $LiBH_4$ undergoes different changes with the effect of temperature (Figure 5) [72]. A structural phase transition occurs at about 110 °C, changing from orthorhombic symmetry to the hexagonal one, followed by its melting at about 278 °C. Afterwards, the release of $H_2$ begins [73]. A first desorption step was reported, starting at 320 °C, with a mass loss of 1 wt. % $H_2$. The main dehydrogenation step starts at about 450 °C and peaks towards 500 °C. A total weight loss of 9 wt. % was measured up to 600 °C, which represents half of the hydrogen content of the compound. For practical applications, only 13.8 wt. % $H_2$ can be released up to 680 °C. Temperatures above 700 °C are required to completely dehydrogenate LiH. It is obvious that these dehydrogenation temperatures are not suitable for practical applications.

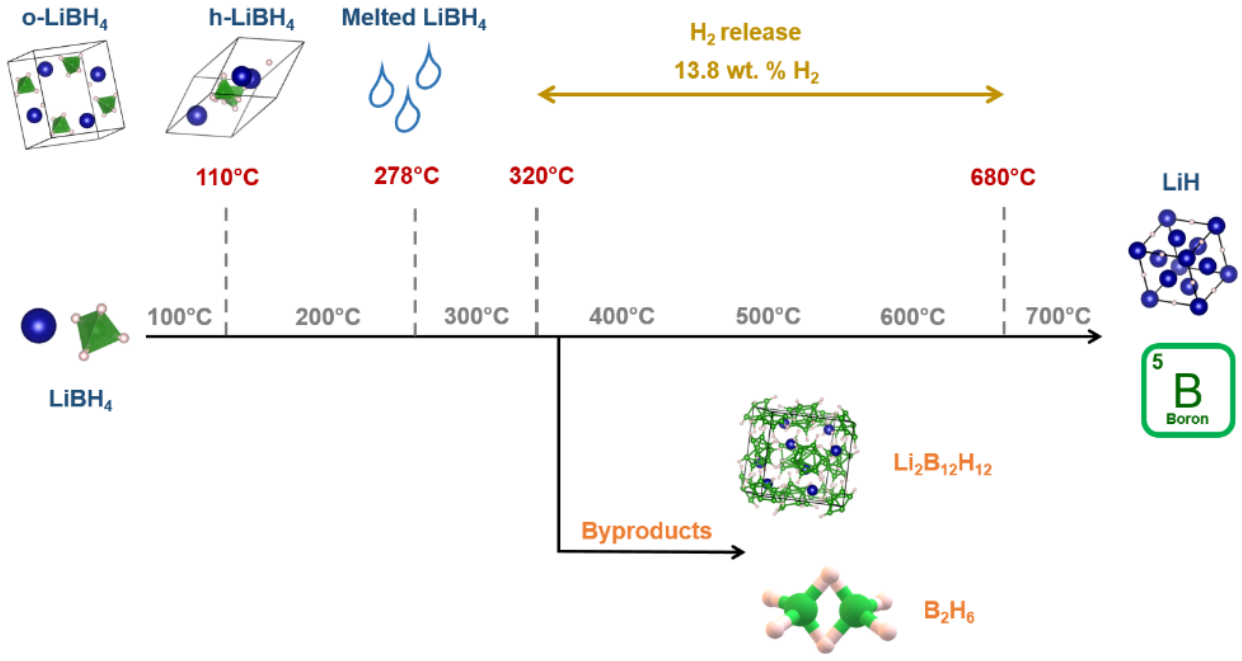


**Figure 5.** Thermal decomposition of $LiBH_4$.

A second drawback is the formation of unwanted products by the dehydrogenation reaction [74,75]. For example, $B_2H_6$, which is a hazardous gas, is released in the thermal dehydrogenation of $LiBH_4$ (Equation (11)). Another undesirable byproduct is $Li_2B_{12}H_{12}$, which plays a role in the decomposition of $LiBH_4$ (Equation (12)). $Li_2B_{12}H_{12}$ is thermally stable up to 650 °C, and it prevents the direct rehydrogenation, affecting the overall performance of $LiBH_4$-based systems.

$$LiBH_4 \rightarrow LiH + \frac{1}{2}B_2H_6 \quad (11)$$

$$12LiBH_4 \rightarrow Li_2B_{12}H_{12} + 10LiH + 13H_2 \quad (12)$$

The sluggish kinetics of the dehydrogenation reaction also prevents its use in practical applications. A last disadvantage is the rehydrogenation of the dehydrogenated products (Equation (3)), which requires harsh conditions: heating at 600 °C under 35 MPa $H_2$ [33]. All of these disadvantages have made the use of pristine $LiBH_4$ difficult for hydrogen storage applications. For this reason, several efforts have been made in order to overcome these disadvantages and improve the thermodynamics, kinetics and reversibility of $LiBH_4$.

### *4.1. Destabilization by Additives*

The addition of different compounds in order to destabilize $LiBH_4$ have been studied. For example, it is known that the $H^{\delta-}$ of $LiBH_4$ can be destabilized through the introduction of a $H^{\delta+}$-containing species. Different research groups have tested several materials (Figure 6), and recent studies will be discussed in the following sections.

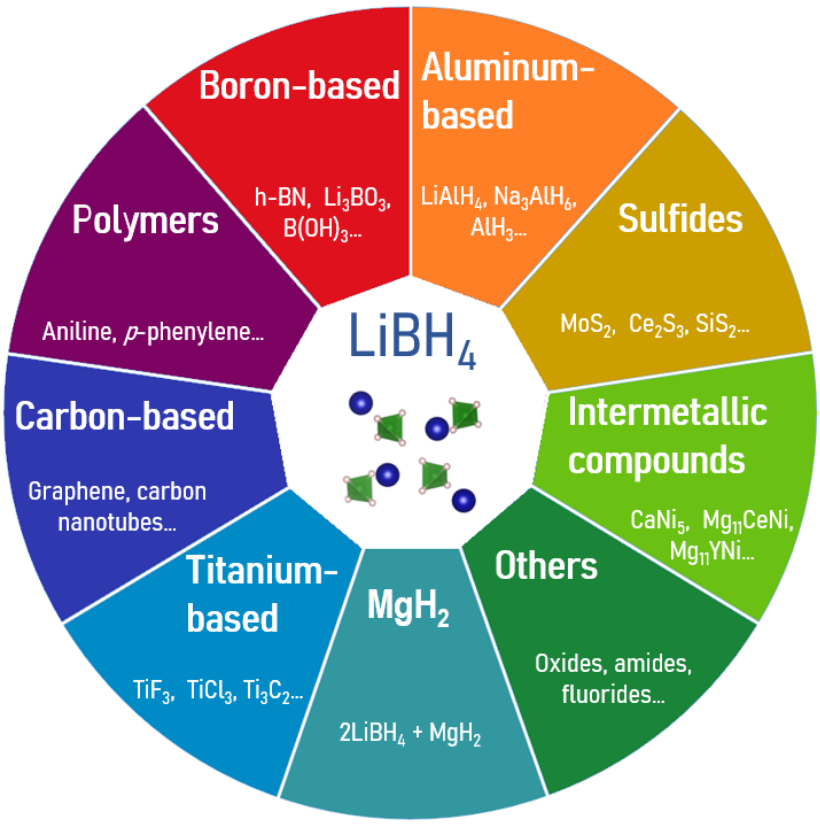


**Figure 6.** Categories and some examples of the additives used to destabilize $LiBH_4$ in the solid state.

#### 4.1.1. Boron-Containing Compounds

Hexagonal boron nitride (h-BN) has been tested as an additive to improve the dehydrogenation of $LiBH_4$. Some features of h-BN favor the destabilization of $LiBH_4$, such as the lone pair of electrons of the N atom, the presence of dangling bonds and defects in the

structure, and B–H$\cdots$B–N interactions [76–78]. Zhu et al. [79] used nanoporous h-BN to prepare a composite with $LiBH_4$ through ball milling. The composite released 13.9 wt. % $H_2$ up to 400 °C. The storage capacity decreased under cycling, but it stabilized at 7.6 wt. % $H_2$ after five cycles. The formation of $Li_2B_{12}H_{12}$ and $Li_xBN$ was observed; the first explained the loss of reversibility, whereas the last participated in and improved the rehydrogenation of $LiBH_4$. Muthu et al. [80] used h-BN activated by an acid treatment, which prevented the agglomeration of the particles during the rehydrogenation of the composite. The release of $H_2$ took place between 110 °C and 150 °C and the composite maintained 85.7% of its original hydrogen storage capacity after four cycles of sorption/desorption. Tu et al. [81] analyzed the effect of h-BN and $NbCl_5$ to destabilize $LiBH_4$. Pure $H_2$ was released without traces of unwanted $NH_3$ or $B_2H_6$. With the addition of $NbCl_5$, the apparent activation energy of the dehydrogenation step decreased to 122 kJ $mol^{-1}$, proving the catalytic effect of the $NbCl_5$. NbH particles formed in situ and they acted as nucleation sites and shortened the distance of the solid–liquid phase boundary in the decomposition of $LiBH_4$.

Other B-containing compounds have been used as destabilization agents for $LiBH_4$. For example, $Li_3BO_3$ can act a catalyst during the dehydrogenation of $LiBH_4$, providing active centers, weakening the Li–B bond, favoring $[BH_4]^-$ decomposition and keeping the Li, B and H atoms close to each other [82]. Li et al. [83] ball-milled $LiBH_4$ with $Nb(OEt)_5$, with the latter acting as a precursor of $Li_3BO_3$ and NbH. At 400 °C, the composite released 7.9 wt. % $H_2$ in 20 min. After 30 cycles of absorption/desorption, the composite retained 91 % of its original capacity. The reversibility loss was ascribed to the formation of stable $Li_2B_{12}H_{12}$. Wu et al. [84] used $B(OH)_3$, as the strong interaction between the $O–H^{\delta+}$ of the boric acid and the $B–H^{\delta-}$ of the borohydride can reduce the dehydrogenation temperature of $LiBH_4$. The composite released 5.6 wt. % $H_2$ below 180 °C, with some traces of $H_2O$. The main product obtained after dehydrogenation was $LiB_5O_9H_2$. With fast kinetics, the composite released 4.5 wt. % $H_2$ in 2 min at 180 °C. However, due to the exothermicity of the dehydrogenation, the reversibility of the reaction is not favorable.

Eutectic mixtures between $LiBH_4$ and other borohydrides ($MBH_4$) have been studied. These mixtures tend to melt at lower temperatures than the parent compounds and possess high theoretical storage capacities of about 10 wt. % $H_2$. However, it is likely that the dehydrogenation temperature depends on the nature of the second component rather than on the melting point of the mixture [85]. Some borohydrides that have been used include $La(BH_4)_3$, $Er(BH_4)_3$, $KBH_4$ and $NaBH_4$ [85–87]. However, it appears that the eutectic mixtures in the bulk state are not able to destabilize $LiBH_4$. The release of hydrogen occurs above 300 °C, and often above 500 °C. For this reason, the notion of their use as hydrogen storage materials has been discarded.

#### 4.1.2. Aluminum-Containing Compounds

Alanates are complex hydrides that have also been considered for hydrogen storage. $LiAlH_4$ has a storage capacity of 7.9 wt. % $H_2$ and it decomposes following Equations (13) and (14) [88].

$$3LiAlH_4 \rightarrow Li_3AlH_6 + 2Al + 3H_2 \ (150–200\ ^\circ C;\ 5.3\ wt.\ \%\ H_2) \quad (13)$$

$$Li_3AlH_6 \rightarrow 3LiH + Al + \frac{3}{2}H_2 \ (200–270\ ^\circ C;\ 2.6\ wt.\ \%\ H_2) \quad (14)$$

The rehydrogenation of $Li_3AlH_6$ is not favorable under mild conditions. Some studies have shown that the addition of alanates to $LiBH_4$ can improve the dehydrogenation behavior of the borohydride. He et al. [89] analyzed a mixture of $LiBH_4/xLiAlH_4$. All the composites presented a four-step dehydrogenation pathway. An unidentified Li-Al-B-H intermediate was reported during dehydrogenation. The formation of LiH, $AlB_2$ and LiAl was also reported; the last two were detrimental to the system, as they formed a passivation layer on the Al, inhibiting the dehydrogenation reaction. The inclusion of other additives in the alanate system has also been investigated. Gu et al. [90] studied a $LiBH_4/LiAlH_4/MgF_2$ system that released 8.9 wt. % $H_2$ up to 480 °C. This system was

able to rehydrogenate at 400 °C under 6 MPa of $H_2$, releasing 4.9 wt. % $H_2$ on the 2nd cycle. Thaweelap and Utke [91] added Ti-doped multiwall carbon nanotubes (MWCNTs) to the $LiBH_4/LiAlH_4$ system. MWCNT promoted the dehydrogenation of $LiAlH_4$ at room temperature, during the preparation of the composites. Despite the enhancement of the kinetics, the system presented a poor cycling capacity due to the formation of the thermodynamic sink $Li_2B_{12}H_{12}$ and the irreversible dehydrogenation of $Li_3AlH_6$. Li et al. [92] proposed a $LiBH_4{\cdot}NH_3/LiAlH_4$ composite, where the $H^{\delta+}$ of $NH_3$ worked as destabilizing agent. In this way, the onset dehydrogenation temperature of $LiBH_4$ was reduced by 70 °C and the composite released 6.53 wt. % $H_2$. Halim-Yap et al. [93] investigated the effect of $MgFe_2O_4$ on an $Na_3AlH_6/LiBH_4$ composite, which released 9.5 wt. % $H_2$ when heated up to 550 °C. The in situ formation of Fe and MgO during dehydrogenation was responsible for the improved dehydrogenation properties of this material.

Other Al-containing compounds have been used to improve the dehydrogenation properties of $LiBH_4$. Liu et al. [94] formed a composite with $AlH_3$. This composite decomposed in two stages, releasing 3.5 and 7.7 wt. % $H_2$ around 310 °C and 470 °C. Another example is an AlN functionalized with –OH, which allowed the destabilization of $LiBH_4$ [95]. The dehydrogenation occurred in two steps at 337 °C and 357 °C. In addition, in situ formation of $Li_3BO_3$ was identified, which favored the decomposition of $LiBH_4$. The composite retained a 6 wt. % $H_2$ capacity after several cycles of rehydrogenation.

Al-based compounds are successful in destabilizing $LiBH_4$, but the formation of stable compounds such as $Li_3AlH_6$ hinders the reversibility of the composites. Moreover, unidentified phases of Li-Al-B-H have been detected and the nature of their participation in the dehydrogenation mechanism is still unknown. Moreover, the formation of passivation layers of $AlB_2$ and LiAl on the surface of Al also limits the dehydrogenation of the composites (Figure 7).

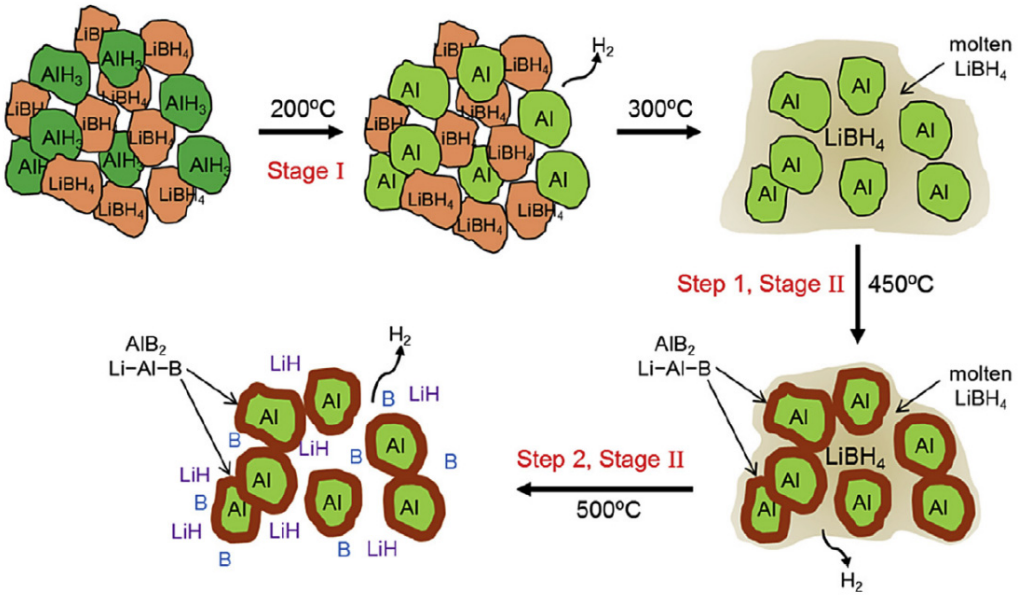


**Figure 7.** Microstructure evolution of a $LiBH_4/AlH_3$ composite up to 500 °C, with a heating rate of 4 °C $min^{-1}$. Reprinted with permission from [94]. Copyright (2016), Elsevier.

#### 4.1.3. Intermetallic Compounds

The use of different types of intermetallic compounds has also been considered to destabilize $LiBH_4$. Meggouh et al. [96] used the $CaNi_5$ alloy to form a composite that released only 1.1 wt. % $H_2$ up to 220 °C. The sample was partially rehydrogenated at 85 °C and 8.5 MPa, due to the formation of nickel borides ($Ni_xB$) that hindered the reversibility of the system. Other examples are the $Mg_{11}CeNi$ (6.6 wt. % $H_2$) and $Mg_{10}YNi$-

H (6.7 wt. % $H_2$) alloys [97,98]. The destabilization of $LiBH_4$ occurred due to the formation of intermediates such as Mg, $Mg_2Ni$, $CeH_2$ and $YB_4$.

#### 4.1.4. Carbon-Based Materials

Carbon-based compounds have been widely studied as destabilizing agents for $LiBH_4$. It appears that composites of $LiBH_4$ and Ni-decorated graphene present remarkable performance. For example, Zhang et al. [99] used a one-pot solvothermal method which formed $LiBH_4$ nanoparticles of 5–10 nm, supported on graphene that was decorated with Ni crystals of 2–4 nm (Figure 8). The dehydrogenation of the composite started from 130 °C, peaked at 285 °C, and released pure $H_2$. The apparent activation energy of this process is 106 kJ $mol^{-1}$. Under isothermal conditions at 300 °C, 9.2 wt. % $H_2$ was released after 175 min. The rehydrogenation was carried out under 10 MPa $H_2$. The composite achieved an outstanding reversible capacity of 100 cycles, with a remarkable 8.5 wt. % $H_2$. One of the key factors required to achieve such good reversibility was to prevent the formation of $Li_2B_{12}H_{12}$ and the agglomeration of $LiBH_4$ particles. In fact, the small size of the Ni crystals favored a closer contact between these particles and $LiBH_4$. The Ni nanoparticles also showed their catalytic effect during cycling: even after 70 cycles, the nanoparticles did not agglomerate; they were still stuck to the $LiBH_4$ particles and their chemical state remained unchanged.

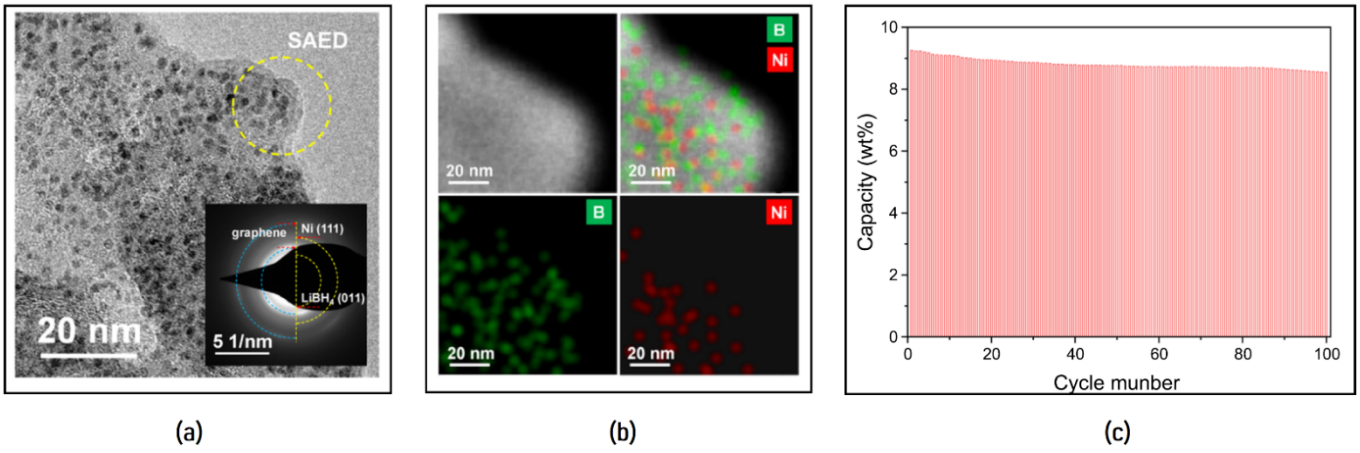


**Figure 8.** (**a**) Transmission electron microscopy (TEM) image; (**b**) energy-dispersive X-ray spectroscopy (EDX) mapping and (**c**) hydrogen cycling stability of nano-$LiBH_4$ supported on graphene decorated with Ni. Reprinted with permission from [99]. Copyright (2021), Elsevier.

A similar system was presented by Xu et al. [100], who prepared a composite with Ni-doped graphene and $LiBH_4$ through ball milling. The composite started to dehydrogenate at 180 °C and it presented two dehydrogenation events that peaked at 275 °C and 465 °C, with a total release of 15.2 wt. % $H_2$. Regarding the kinetics, the composite released 12.8 wt. % $H_2$ in 45 min at 450 °C. The rehydrogenation was performed at 400 °C under 3 MPa $H_2$ for 10 h. Between the 10th and the 30th cycles, the storage capacity of the composite remained stable at a remarkable 9.8 wt. % $H_2$. The loss in the capacity was explained by the formation of stable compounds such as $Li_{12}B_{12}H_{12}$, LiC and $Ni_4B_3$ that inhibited the reversibility of the composite. Other compounds have been used to decorate graphene, though they are not as effective as the Ni-based ones. It seems that the formation of some species during dehydrogenation (such as LiF, $Li_3BO_3$) has a contradictory effect on the systems: they acted as catalysts, improving the kinetics and favoring the dehydrogenation of $LiBH_4$, but at the same time, they hindered the reversibility of the system due to their stability [101–104].

Lai et al. [105] formed $LiBH_4$ nanoparticles (2–18 nm) (Figure 9) and then they deposited these particles onto a Ni(II) phtalocyanine substrate. The Ni(II) phtalocyanine acted

as an electron-active substrate, lowering the charge transfer from $Li^+$ to $BH_4^-$, destabilizing the composite. The composite dehydrogenated through a single step at 350 °C, releasing 14.1 wt. % $H_2$ with some traces of oleic acid used in the synthesis of the material. The reversibility capacity fell to 3.2 wt. % $H_2$ after five cycles of rehydrogenation.

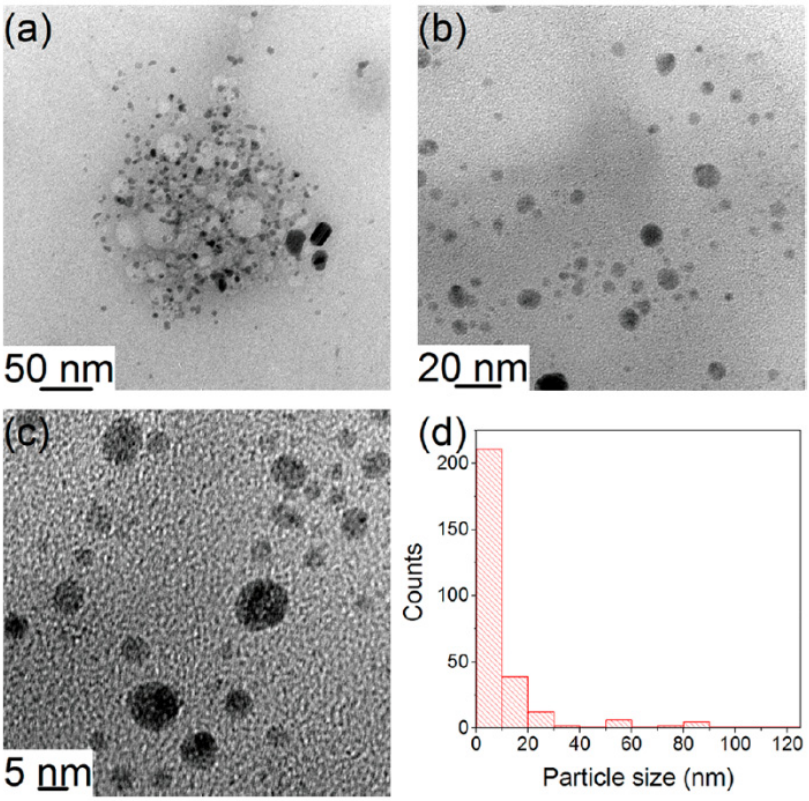


**Figure 9.** (**a**–**c**) TEM images of the $LiBH_4$ nanoparticles and (**d**) corresponding size distribution. Reprinted with permission from [105]. Copyright (2018), American Chemical Society.

Other structures, such as activated carbon, mesoporous carbon and single walled carbon nanotubes (SWCNT), have also been used to obtain composites with $LiBH_4$ [106–109]. In the case of the SWCNT-$LiBH_4$ system, the composite was oxidized under air to prevent the losses of B and Li during dehydrogenation, and in order to obtain a composite that can be managed under air. $LiB(OH)_4$ and $Li_2CO_3$ were found on the surface of the material and the O–$H^{\delta+}\cdots H^{\delta-}$–B interactions favored the kinetics of the composite.

#### 4.1.5. Polymers

Different polymers have been proposed to destabilize $LiBH_4$. Poly (*p*-phenylene) was used to obtain a composite with $LiBH_4$ through ball milling by Bao et al. [110]. The composite released 17.12 wt. % $H_2$ up to 600 °C; however, after three cycles of rehydrogenation at 450 °C the storage capacity fell to 5.5 wt. % $H_2$. This severe degradation was explained by the separation of the B from the carbon substrate during cycling, reducing the catalytic effect of the carbon. Ding et al. [111] studied a system of pyrolyzed aniline and $LiBH_4$. The composite was able to release 4.1 wt. % $H_2$ and after five cycles of sorption/desorption, the storage capacity stabilized at 3.6 wt. % $H_2$.

#### 4.1.6. Sulfides

Metal sulfides can destabilize $LiBH_4$. Some examples are $MoS_2$ and $Ce_2S_3$ [112,113]. The destabilization of the sulfide/$LiBH_4$ composites is due to the formation of several intermediate species during dehydrogenation, such as $Li_2S$, which can decrease the energy to break the B–H bonds [112]. In addition, the formation of borides such as $MoB_2$ and $CeB_6$

can accelerate the kinetics and act as a nucleation medium for the rehydrogenation reaction. Another example is $SiS_2/LiBH_4$ [114]. The composite was able to release 8.2 wt. % $H_2$ up to 385 °C, with an onset temperature of 92 °C. After the 2nd cycle of rehydrogenation, the hydrogen storage capacity fell to 2.4 wt. % $H_2$. It seems that the formation of $Li_x(SiS_2)_y(BH_4)_x$ during the preparation of the composite is responsible for the destabilization of $LiBH_4$, as the $SiS_2$ group can block the Li-coordination sites, reducing the number of Li–H–B interactions.

#### 4.1.7. Ti-Based Additives

Some Ti-based additives can modify the thermodynamics and kinetics of $LiBH_4$, such as titanium halides, including $TiF_3$ [115]. During the synthesis of a $TiF_3/LiBH_4$ composite, the formation of LiF and Ti was identified, indicating the evolution of the sample during the milling process. Furthermore, the $LiBH_4/TiF_3$ composite is not stable over time, as it released 3 wt. % $H_2$ after a few months when stored at room temperature. Lai et al. [116] synthesized $LiBH_4$ nanoparticles doped with $TiCl_3$ using a wet method. These particles released hydrogen via a two-step mechanism that peaked at 260 °C and 340 °C. The destabilization was achieved through the substitution of Ti in $LiBH_4$ and the formation of some species that destabilized the borohydride, such as $TiB_2$. However, the nanoparticles agglomerated during rehydrogenation, leading to a loss of storage capacity. Fan et al. [117] obtained a composite of $LiBH_4$ with a MXene $Ti_3C_2$ through ball milling. The composite started to dehydrogenate at 120 °C and the main dehydrogenation peak occurred at 408 °C. In terms of kinetics, the sample released 5.37 wt. % $H_2$ at 350 °C in 1 h. The apparent activation energy of the dehydrogenation is 70.3 kJ $mol^{-1}$.

#### 4.1.8. $MgH_2$ Reactive Hydride Composite

The mixture of $2LiBH_4/MgH_2$ (11.45 wt. % $H_2$) has been proposed as a reactive hydride composite for hydrogen storage applications. This system starts to release $H_2$ via a two-step mechanism (Equation (15)) [118]. On the one hand, the composite desorbs $H_2$ at elevated temperatures (above 300 °C). On the other hand, the rehydrogenation can be performed under milder conditions in comparison to $LiBH_4$ (between 250 °C and 300 °C and under 5 MPa $H_2$). Due to the high dehydrogenation temperature of the $2LiBH_4/MgH_2$ composite, different approaches have been considered for its destabilization.

$$2LiBH_4 + MgH_2 \leftrightarrow Mg + 2LiBH_4 + H_2 \leftrightarrow MgB_2 + 2LiH + 4\,H_2 \quad (15)$$

In a group of studies, Ding et al. [119–121] prepared a mixture of nano-$LiBH_4$ and nano-$MgH_2$ via a novel method known as ball milling with aerosol spraying (BMAS). With this approach, a mixture of graphite and $MgH_2$ was milled, and at the same time, a $LiBH_4$-THF solution was sprayed. This method allowed the formation of a nanocomposite of $LiBH_4/MgH_2$, which is able to absorb and to desorb 5 wt. % $H_2$ at 265 °C. These results opened up the possibility of obtaining other composites with improved dehydrogenation properties through nano-engineering.

The incorporation of additives to the $2LiBH_4/MgH_2$ composite has also been considered. For example, different carbon materials were suggested: activated carbon nanofibers, $TiO_2$-doped MWCNT and carbonized starch [122–125]. All of these systems were able to decrease the onset dehydrogenation temperature and accelerate the dehydrogenation kinetics of the $2LiBH_4/MgH_2$ composite. Nb-based additives have also been tested. Zhou et al. [126] compared the addition of NbC and $NbF_5$ to the $2LiBH_4/MgH_2$ composite. They found that $NbF_5$ has a bigger destabilization effect, due to the formation in-situ of $Nb(BH_4)_5$, which improves the dehydrogenation kinetics of the $2LiBH_4/MgH_2$ mixture. Cheng et al. [127] studied a $LiBH_4/MgH_2/Al/NbF_5$ system. The idea was to combine the good reversibility of the $LiBH_4/MgH_2$ system with the fast dehydrogenation of the $LiBH_4/Al$ composite. The addition of $NbF_5$ prevented the alloying between Mg and Al, as well as the formation of the stable $Li_2B_{12}H_{12}$. Despite the good reversibility of this

composite (7.5 wt. % $H_2$), the temperature required to release $H_2$ is still high (>400 °C). The addition of Fe was also considered elsewhere [128].

#### 4.1.9. Other Dopants

Some oxides, fluorides, amides and selenides have been tested as destabilizing agents for $LiBH_4$ [129–132]. These composites allowed the improvement of $LiBH_4$ dehydrogenation properties due to the in situ formation of various species, such as $Fe_3O_4$, LiF, $Li_3Bi$, $SrH_2$ and $Li_2Se$. The formation of borides (NiB, $Fe_3B$, $SrB_6$) on these composites also has a positive effect on the destabilization of $LiBH_4$.

### *4.2. Chemical Modification*

The chemical modification of $LiBH_4$ is another strategy to destabilize the borohydride. Liu et al. [133] prepared a new crystalline compound between $LiBH_4$ and urea (monoclinic, space group $C2/c$), through mechanochemistry. The complex started to dehydrogenate at 120 °C and it released 8.13 wt. % of pure hydrogen. Wu et al. [134] obtained $LiBH_4 \cdot H_2O$ nanosheets with a thickness of 20–30 nm. This complex released 10 wt. % $H_2$ in the range of 50 °C–110 °C. However, as the dehydrogenation process is exothermic, the reversibility of the compound is unfavorable. In both cases, the destabilization was achieved due to $H^{\delta+} \cdots H^{\delta-}$ interactions.

Richter et al. [135] used another approach. They substituted some of the H atoms in $LiBH_4$ with F atoms, as the strong electronegative character of the latter can favor the destabilization of the B–H bonds. Two composites were prepared: one by simple hand mixing $LiBH_4$ and $LiBF_4$, and a sample in which some H atoms were substituted with F atoms via the reaction between $LiBH_4$ and triethylamine trihydrofluoride. On the one hand, the composite obtained by mixing started to decompose at 100 °C, releasing a substantial quantity of $B_2H_6$. On the other hand, the other sample was highly unstable and it decomposed through a violent reaction. The implementation of such compounds for hydrogen storage applications seems to be difficult.

### *4.3. Nanoconfinement*

There are different factors that can modify the behavior of nanoconfined $LiBH_4$. The infiltration method is one of them [136]: for the same scaffold (hollow carbon nanospheres, HCS), the solvent impregnation method was more efficient to destabilize $LiBH_4$ compared to the melting approach. The $LiBH_4$ confined by solvent impregnation presented a lower dehydrogenation temperature and it was rehydrogenated at milder conditions (300 °C, 6 MPa $H_2$). Another important parameter is the chemical nature of the scaffold (e.g., carbon-based, silica-based and alumina-based) [137]. For silica- and carbon-based materials with similar textural properties, the effect of the confinement and the hydrogen mobility on the confined $LiBH_4$ was more pronounced for the $SiO_2$ scaffold. In any case, different types of materials have been used for the nanoconfinement of $LiBH_4$. The following sections describe recent studies about the confinement of $LiBH_4$, classified by the nature of the matrix.

#### 4.3.1. Carbon-Based Scaffolds

The use of unique types of carbon structures has shown good results for confined $LiBH_4$. In a recent study, Wu et al. [138] obtained double-layered carbon nanobowls through the melt infiltration of $LiBH_4$ in HCS. Under isothermal conditions at 300 °C, the system released 9.0 wt. % $H_2$ after 20 h. The rehydrogenation was carried out at 300 °C under 10 MPa $H_2$, and the sample was able to absorb a remarkable 8.5 wt. % $H_2$. The destabilization of $LiBH_4$ was achieved due to the shortened diffusion distance and the specific surface area of the nanobowls. Wang et al. [139] worked with porous HCS, which were loaded with 70 wt. % $LiBH_4$ by means of melt infiltration. The system released 8.1 wt. % $H_2$ within 25 min, at a constant temperature of 350 °C. The storage capacity fell to 4.0 wt. % $H_2$ after five cycles of rehydrogenation. Shao et al. [140] used a zeolite-template carbon to infiltrate $LiBH_4$ (41.5 wt. %), and they densified the sample at 750 MPa. The

system started to desorb $H_2$ at 194 °C and the main dehydrogenation event was recorded at 332 °C. At a constant temperature of 300 °C, the composite released 10.5 wt. % $H_2$ in 1 h. The rehydrogenation of the composite was performed under mild conditions, at 260 °C and 12 MPa $H_2$. In addition, they found that over-infiltrated scaffolds were able to maintain a good reversibility, due to an extra infiltration of $LiBH_4$ during rehydrogenation. Guo et al. [141] used carbon nanocages as scaffolds to confine $LiBH_4$. The system started to dehydrogenate at 200 °C, with a main dehydrogenation step at 320 °C. At 550 °C, the composite released 7.18 wt. % $H_2$. However, after five cycles of rehydrogenation under 5 MPa $H_2$ and 400 °C, it delivered only 3.07 wt. % $H_2$. In addition to the confinement effect, $LiBH_4$ was destabilized by $Li_3BO_3$, which was formed due to the presence of −OH groups on the surface of the nanocages. Finally, Xian et al. [142] synthesized a core-shell system to confine $LiBH_4$. Carbon nanotubes (CNTs) were used as the core and an amorphous carbon decorated with $TiO_2$ was used as the shell. During the synthesis, $LiTiO_2$ and $Li_2O$ formed, which acted as catalysts. The CNTs favored thermal conductivity and heat transfer during hydrogenation and dehydrogenation. The system presented good reversibility: after 20 cycles, a capacity of 5.1 wt. % $H_2$ was retained.

Graphene is another material that has been used to confine $LiBH_4$. Gasnier et al. have studied the confinement of $LiBH_4$ inside a resorcinol-formaldehyde matrix with entangled graphene [143–145]. They found some trends depending on the pore size of the scaffold—smaller pores reduced the melting temperature of $LiBH_4$, whereas bigger pores improved the reversibility of the system. In a further study, they decorated the scaffold with Ni or Co nanoparticles. The addition of the metal nanoparticles lowered the melting and decomposition temperatures and enhanced the dehydrogenation properties at T < 350 °C. The Ni particles improved the reversibility, whereas the Co particles hindered it.

Other carbon-based materials have been used to confine $LiBH_4$, such as aerogels and activated carbons [146–148]. The decoration of activated carbons with different compounds has presented interesting results [149,150]. For example, an activated carbon doped with $CeF_3$ was used as a scaffold and it started to release $H_2$ between 160 °C and180 °C, and released 12.8 wt. % $H_2$ up to 500 °C [150]. After four cycles of rehydrogenation, the storage capacity remained at 9.3 wt. % $H_2$.

#### 4.3.2. Aluminum-Based Scaffolds

Sofianos et al. [151] reported the synthesis of two Al scaffolds, with pore sizes of 355 nm and 56 nm, respectively, and then they infiltrated $LiBH_4$ using the melting approach. The scaffold with 355 nm showed improved kinetics, but the onset dehydrogenation temperature was similar to that of bulk $LiBH_4$ due to the large size of the pores. The scaffold with pores of 56 nm released 5.86 wt. % $H_2$ when heated up to 550 °C. None of these composites showed reversibility. In a further study, the same group obtained another Al scaffold from $NaAlH_4$, which presented reversibility [152]. The composite released 2.8 wt. % $H_2$, but this storage capacity decayed after three cycles of rehydrogenation.

#### 4.3.3. Polymers

Poly (methyl methacrylate) (PMMA) was tested as a scaffold for $LiBH_4$ [153]. This material released 11 wt. % $H_2$ within 5 h at 360 °C. The destabilization was achieved due to the interaction between the electron-donor O atom of the C=O group of PMMA, and the electropositive B atom of $LiBH_4$. Plerdsranoy et al. [154] increased the thermal stability of a scaffold based on (methyl methacrylate)-co-butyl methacrylate through the addition of MWCNT; however, sluggish kinetics were presented, probably due to poor hydrogen diffusion. Fan et al. [155] synthesized an air-stable composite made of melamine foam and $LiBH_4$ nanoparticles. The composite presented hydrophobic behavior and it released 11 wt. % $H_2$ below 500 °C. No information about the reversibility of the material was reported.

#### 4.3.4. Other Scaffolds

Xu et al. [156,157] confined $LiBH_4$ into $NiMnO_3$ microspheres and porous $ZnO/ZnCo_2O_4$ nanoparticles via a solution impregnation method. These materials released 7.3 wt. % $H_2$ and 8.7 wt. % $H_2$ up to 500 °C, with apparent activation energies of 129.8 kJ $mol^{-1}$ and 120.2 kJ $mol^{-1}$ for the Ni-based and the Zn-based scaffold, respectively. Most likely, the Zn-based nanoparticles acted as active sites for nucleation, hindered the agglomeration of the particles and had a stronger destabilization effect than the $NiMnO_3$ spheres. Zang et al. [158] used $Ti_3C_2$ MXene as a scaffold for $LiBH_4$, which was confined through a solution impregnation method. The composite released 9.6 wt. % under constant heating at 380 °C in 1 h. Metallic Ti and $Ti^{3+}$ species were formed during dehydrogenation, which destabilized the ionic bond between $Li^+$ and $[BH_4]^-$. Other examples of scaffolds are an Ni-nanoporous alloy and silica MCM-41 [159,160].

#### 4.3.5. Nanosizing

Wang and Aguey-Zinsou [161] stabilized nanoparticles of $LiBH_4$ with different surfactants, analyzing the effect of the chain length, head group and steric hindrance of the surfactants. When using tiol-based surfactants, the size of the $LiBH_4$ particles decreased as the alkyl chains increased (Figure 10). The opposite was observed for ammonium-based surfactants. The reason for this is the stronger steric hindrance of the latter. Regarding the effect of the head group, the smallest nanoparticles were obtained using –COOH and $–NH_2$ surfactants. This was explained through Pearson's hard and soft acid and base principle—as $Li^+$ is a hard acid and –COOH and $–NH_2$ are hard bases, they coordinate in a stronger way to $LiBH_4$ and hinder the aggregation of small $LiBH_4$ nanoparticles. In addition, the introduction of $NH_2$-based surfactants lowered the desorption temperature of $LiBH_4$, due to $H^{\delta+}\cdots H^{\delta-}$ interactions.

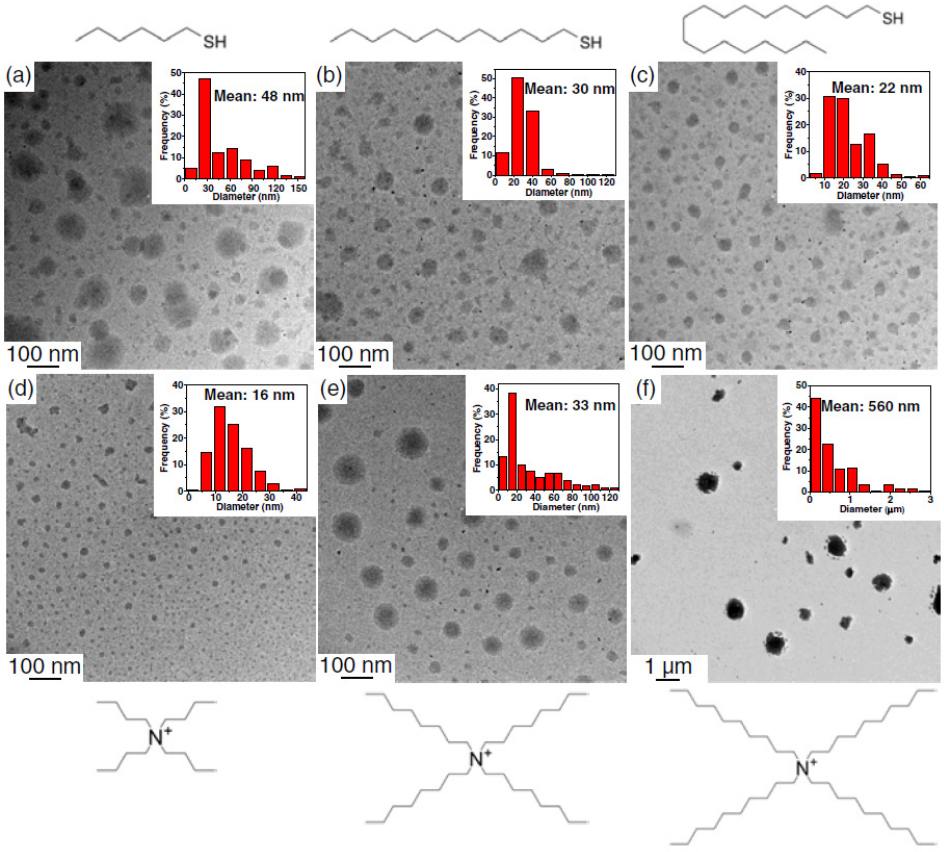


**Figure 10.** TEM images of $LiBH_4$ nanoparticles prepared with (**a**–**c**) tiol-based surfactants; (**d**–**f**) ammonium-based surfactants with different chain lengths. Reprinted with permission from [161]. Copyright (2019), John Wiley and Sons.

### *4.4. General Remarks*

$LiBH_4$ has enormous potential to become a viable option for hydrogen storage systems due to its high gravimetric capacity. However, there are some issues regarding this borohydride. The most challenging is its partial reversibility. As discussed throughout Section 4, many systems have been proposed in order to destabilize $LiBH_4$ and although many of them were successful, their reversibility was not optimal. However, it is likely that the incorporation of $LiBH_4$ in unique-shaped carbon materials decorated with Ni can achieve promising reversibility performance. This opens new possibilities for the scaling up of this kind of materials.

## 5. $NaBH_4$

$NaBH_4$ is a crystalline compound (cubic, space group *Fm*-3*m*), which, with its high gravimetric hydrogen density (10.8 wt. % $H_2$), is an attractive material for hydrogen storage [162]. However, similarly to $LiBH_4$, it suffers from some drawbacks [163,164]: it decomposes at high temperatures (above 500 °C) and it shows sluggish dehydrogenation kinetics and a limited reversibility. The overall thermal decomposition of $NaBH_4$ takes place through Equations (16) and (17), but it is known that there are unwanted side reactions that can produce $Na_2B_{12}H_{12}$ or $B_2H_6$, for example [164,165].

$$NaBH_4 \rightarrow NaH + B + \frac{3}{2} H_2 \quad (16)$$

$$NaBH_4 \rightarrow Na + B + 2H_2 \quad (17)$$

With the purpose of overcoming these limitations, various studies have been performed. In this sense, the incorporation of additives, as well as the chemical modification and the nanosizing of $NaBH_4$ have been considered and are discussed below [166–168].

### *5.1. Additives*

The dehydrogenation properties of $NaBH_4$ can be improved through the use of additives. Different studies have showed that metal transition fluorides can act as catalysts towards the dehydrogenation of $NaBH_4$. For example, $TiF_3$ decreased the first step of dehydrogenation from 490 °C to 300 °C; the composite was able to release 2.3 wt. % $H_2$ up to 340 °C [169,170]. Llamas et al. [171] investigated the addition of metal fluorides (first- and the second-period transition metals) to $NaBH_4$ (Figure 11).

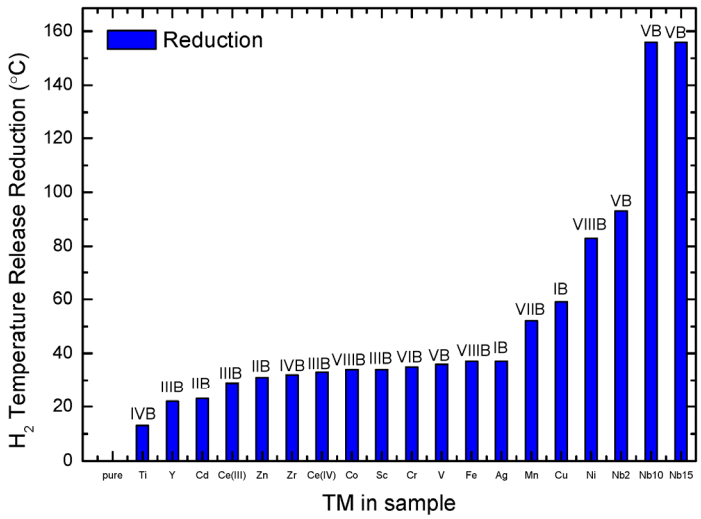


**Figure 11.** Temperature difference between the main decomposition peak of the samples with additives and the one of pure $NaBH_4$, observed by TPD. Reproduced with permission from [171].

The composites were prepared through ball milling; as a result, the decomposition and melting temperature of $NaBH_4$ were decreased. The highest destabilization effect on $NaBH_4$ was found for $NbF_3$ and $MnF_3$. Another parameter analyzed was the amount of additive: a high amount of the additive will lead to the decomposition of $NaBH_4$ during ball milling, thus decreasing the hydrogen storage capacity of the composite.

Zhao et al. [172] investigated a $NaBH_4/ScF_3$ system. $H_2$ was released in three steps, with a total amount of 5.54 wt. % $H_2$ up to 530 °C. The products obtained after the second dehydrogenation step were able to rehydrogenate; however, after the third step, the rehydrogenation was irreversible. Huang et al. [173] proposed the addition of $YF_3$ to the $NaBH_4/ScF_3$ system in order to improve the reversibility of the composite. With this approach, the composite was able to reabsorb around 50% of the desorbed hydrogen, at 380 °C and under 3.2 MPa $H_2$. Another additive that has been tested is $ZrCl_4$ [174], which decreased the dehydrogenation temperature of $NaBH_4$. The composite started to release $H_2$ below 300 °C and the total dehydrogenation was achieved at 600 °C. The catalytic mechanism of $ZrCl_4$ remains unclear, but it seems that the formation of $ZrCl_2$ and Zr plays a role in the destabilization of $NaBH_4$.

### *5.2. Chemical Modification*

As previously mentioned, the $H^{\delta+}$ atoms present in some species can destabilize the $H^{\delta-}$ of borohydrides [175]. In this way, the use of $NH_3$ as a source of $H^{\delta+}$ has been investigated, and the synthesis of various metal borohydride ammoniates has been reported. The decomposition temperature for borohydride ammoniates is lower in comparison with the parent borohydride [176–179]. Hydrazine ($N_2H_4$, 12.5 wt. % $H_2$) has also been used as a source of $H^{\delta+}$ to synthesize borohydride hydrazinates (such as $LiBH_4{\cdot}xN_2H_4$ or $NaBH_4{\cdot}xN_2H_4$) [180,181]. He et al. [180] were the first to synthetize a sodium borohydride hydrazinate via ball milling. More recently, Mao et al. [175] synthesized both $NaBH_4{\cdot}N_2H_4$ and $NaBH_4{\cdot}2N_2H_4$ using an easy solvent-based approach, based on the reaction between $NaBH_4$ and $N_2H_4$ in tetrahydrofuran (THF). Both materials are crystalline (monoclinic, space group $P2_1/c$ and $A1a1$, respectively). The thermal decomposition of these compounds occurred below 200 °C, releasing some byproducts ($N_2H_4$, $NH_3$, $N_2$) along with $H_2$. The emission of these byproducts is explained by Equations (18) and (19). To reduce the release of unwanted byproducts, the strengthening of the coordination bond between the cation and the N atoms has been suggested elsewhere [182,183].

$$N_2H_4 \rightarrow N_2 + 2H_2 \quad (18)$$

$$3N_2H_4 \rightarrow N_2 + 4NH_3 \quad (19)$$

The synthesis of bimetallic borohydrides has been investigated to improve the hydrogen storage proprieties of $NaBH_4$ [184–186]. For example, $NaZn(BH_4)_3{\cdot}en$ and $NaZn(BH_4)_3{\cdot}2en$ (en=ethylene diamine, $(CH_4)_2(NH_4)_2$) were synthetized by means of ball milling and through a solvent-based approach [187]. $NaZn(BH_4)_3{\cdot}en$ starts to dehydrogenate around 134 °C, and $NaZn(BH_4)_3{\cdot}2en$ at 154 °C, without traces of unwanted byproducts. A wide range of Na/rare-earth borohydrides has also been synthetized by ball-milling (Y, La, Ce, Pr, Er, Gd) [185,186]. Bimetallic rare earth borohydrides have shown a high stability and the formation of unwanted gaseous by products, such as $B_2H_6$, hindering the potential of these compounds as materials for hydrogen storage.

### *5.3. Nanosizing*

Nanosizing is an effective approach to improve the thermodynamics and kinetics of $NaBH_4$. Various methods have been used to obtain $NaBH_4$ nanoparticles [162,188,189]. One of them is the solvent evaporation method, which is based on the use of surfactants. Depending on the nature of the surfactant, it is possible to control the size, the shape and the structure of the nanoparticles. Thus, the choice of an appropriate surfactant is a crucial element to ensure optimal control over the synthesis of the nanoparticles [189–191]. It has

been reported that surfactants can also minimize the surface energy of the nanoparticles, limiting their agglomeration; moreover, the chain length and the nature of the functional groups of the surfactant strongly impact the final morphology of the nanoparticles [191]. The particle size is controlled by the interactions and steric repulsion of the surfactants. A recent study showed that the size of $NaBH_4$ nanoparticles was proportional to the length of the carbon chain of the surfactant, and that surfactants with hard head groups lead to the formation of smaller $NaBH_4$ particles [189,190]. Salman et al. [191] reported that the choice of the surfactant allows one to control the shape of the $NaBH_4$ nanoparticles (Figure 12).

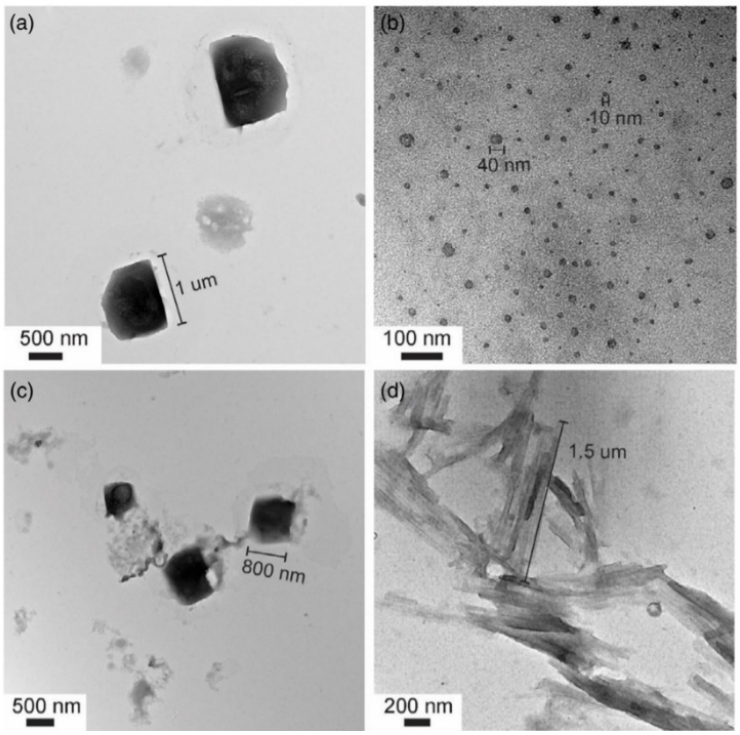


**Figure 12.** Representative TEM images of the $NaBH_4$ nanostructures of (**a**) $NaBH_4$—isopropylamine, (**b**) $NaBH_4$—tetrabutylammonium bromide, (**c**) $NaBH_4$—octadecylamine and (**d**) $NaBH_4$—tridecanoic acid. Reproduced with permission from [191].

Depending on the surfactant, they observed sphere-, cube- or bar-shaped particles. The $NaBH_4$ nanoparticles released $H_2$ at temperatures lower than 50 °C, but the gas stream was polluted with the residues of the surfactants used during the synthesis. This group also observed that increasing the rate of evaporation of the surfactant induced a reduction of the nanoparticles' size.

To avoid the pollution originating from the surfactants, the development of direct methods for the synthesis of $NaBH_4$ nanoparticles is desirable, and different strategies have been developed to achieve this goal. However, these approaches have been performed under extreme conditions; such as high temperatures and pressures, using solvents such as ethyl ether, diglyme and THF, and also using highly reactive and volatile materials such as NaH or $B_2H_6$ [192]. Lai et al. [163] proposed the synthesis of $NaBH_4$ nanoparticles from trimethyl-borate $B(OHC_3)_3$ and NaH in THF, at moderate temperatures (65 °C–70 °C). The formation of $NaBH_4$ occurred in two steps. First, $NaB(OCH_3)_4$ formed, and second, during its thermal decomposition the $NaBH_4$ nanoparticles formed. Wang et al. [192] carried out the synthesis of $NaBH_4$ nanoparticles from $NaOCH_3$ and $B_2H_6$, which was generated in situ from the decomposition of $NaZn_2(BH_4)_5$ via a solid–gas reaction. $NaBH_4$ nanoparticles with high purity (98%) were obtained from this reaction. The $NaBH_4$ nanoparticles decreased the onset dehydrogenation temperature by 100 °C in comparison with bulk $NaBH_4$.

### *5.4. General Remarks*

The $H_2$ release from $NaBH_4$ in the solid-state occurs at high temperatures (>500 °C), and the dehydrogenation reaction presents sluggish kinetics. Three strategies have been tested in order to improve the thermal decomposition of this compound: the use of additives, such as metal fluorides; chemical modification through the synthesis of $NaBH_4$ hydrazinates or Na-based bimetallic borohydrides; and the nanosizing of the compound. It seems that the latter strategy is the most efficient approach to improving the dehydrogenation properties of $NaBH_4$. Unfortunately, in the analyzed studies, the $NaBH_4$ nanoparticles released $H_2$ polluted by some residues that originated from the surfactants used in the synthesis of these particles. Therefore, the direct synthesis of $NaBH_4$ nanoparticles is desirable to obtain a purer $H_2$ stream. In addition, due to the poor reversibility of the $NaBH_4$ dehydrogenation reaction [164], this borohydride has been less studied than $LiBH_4$, for example.

## 6. $Mg(BH_4)_2$ and $Ca(BH_4)_2$

$Mg(BH_4)_2$ and $Ca(BH_4)_2$ are very promising hydrogen storage materials, owing to their high gravimetric hydrogen capacity (14.9 wt. % $H_2$ and 11.5 wt. % $H_2$, respectively) and they have attracted great interest in recent years. Compared to alkali borohydrides, $Mg(BH_4)_2$ and $Ca(BH_4)_2$ release $H_2$ at lower temperatures due to their lower stability. The stability of borohydrides is directly related to the charge transfer between the metal cation and the $[BH_4]^-$ group. The weaker the charge transfer, the lower the desorption temperature due to weaker B-H bonds, which can be correlated to the Pauling electronegativity ($\chi_p$) of the cation ($\chi_p(Mg^{2+}) > \chi_p(Ca^{2+}) > \chi_p(Li^+) > \chi_p(Na^+)$) [193]. Nonetheless, alkaline-earth borohydrides still present high dehydrogenation temperatures, sluggish kinetics and poor reversibility. The overall decomposition reactions for $Mg(BH_4)_2$ and $Ca(BH_4)_2$ can be written as follows (Equations (20) and (21)):

$$Mg(BH_4)_2 \rightarrow MgB_2 + 4H_2 \quad (20)$$

$$Ca(BH_4)_2 \rightarrow 2/3\ CaH_2 + 1/3\ CaB_6 + 10/3\ H_2 \quad (21)$$

However, multiple intermediates steps have been identified. The reader can refer to the comprehensive reviews for more information about the thermal decomposition and rehydrogenation of these borohydrides [194]. Hence, the destabilization of $Mg(BH_4)_2$ and $Ca(BH_4)_2$ improves their hydrogen storage properties and eventually, it will lead to room temperature hydrogen storage systems. Therefore, one can modify the thermodynamics and/or the kinetics of the hydrogen storage system. For the former, minimizing the enthalpy difference between the initial and final states can be achieved through chemical modification or by alloying the compound. The nanosizing of complex hydrides can also affect the thermodynamics [195]. Regarding the kinetics, a reduction in the activation energy of the involved processes is usually achieved using catalysts or via nanostructuration [196].

### *6.1. Additives*

To improve the thermodynamic properties of hydrogen storage systems, reactive hydrides composites are used. Composites such as $Mg(BH_4)_2/NaAlH_4$ [197], $Mg(BH_4)_2$ and $Ca(BH_4)_2/MNH_2$ with M = Na or Li [198,199], $Mg(BH_4)_2/AlH_3$ [200], $Mg(BH_4)_2/NaBH_4$ [201], $Mg(BH_4)_2/AlH_3/LiH$ [202] or $Mg(B_3H_8)_2/MgH_2$ [203] have been reported. The $Mg(B_3H_8)_2/MgH_2$ system, for which $Mg(B_3H_8)_2$ is a decomposition intermediate [204], constitutes the first example of an almost-full conversion of $Mg(B_3H_8)_2$ into $Mg(BH_4)_2$ at 100 °C without hydrogen back pressure [203]. With respect to the other composites, they have demonstrated a decrease in the onset temperature ($T_{onset}$) of dehydrogenation, in the range of 124 °C–240 °C [197–202], compared to pure $Mg(BH_4)_2$ or $Ca(BH_4)_2$, which start to dehydrogenate above 300 °C. Moreover, for some of these composites, a partial reversibility up to 3.8 wt. % $H_2$ has been reported [197,200,202]. These improvements were ascribed to the formation of intermediate species during thermal decomposition. For example, the

reduction in $T_{onset}$ during the thermal decomposition of the $Mg(BH_4)_2/AlH_3$ composite and its partial reversibility was explained by the formation of $Mg_2Al_3$ [200].

The improvement of the hydrogen storage properties can also be achieved through the reduction of the activation energy for the different dehydrogenation steps. Additives such as carbon-based materials have been demonstrated to be effective. Carbon nanotubes (CNTs) have also been envisaged [205,206]. Nanosized layers of $Mg(BH_4)_2$ on CNTs were reported, revealing a synergic effect between nanosizing and catalysis. A decrease in the $T_{onset}$ of 117 °C and a drastic improvement in the kinetics was observed, with a drop in the apparent activation energy from 45.9 kJ $mol^{-1}$ for pure $Mg(BH_4)_2$ to 14.4 kJ $mol^{-1}$ under isothermal conditions [207]. In this system, partial rehydrogenation was also observed. Reduced graphene oxide (rGO) has also improved the thermal decomposition of $Mg(BH_4)_2$ and $Ca(BH_4)_2$ by lowering the $T_{onset}$ by 130 °C for $Mg(BH_4)_2$ and by 50 °C for $Ca(BH_4)_2$ [208]. Ni-doped MWCNT decreased the $T_{onset}$ to 80 °C, with a significant reduction of the apparent activation energy to 119 kJ $mol^{-1}$ compared to 451.5 kJ $mol^{-1}$ for pure $Mg(BH_4)_2$. The apparent activation energy was determined in dynamical conditions using the Kissinger method [209]. Oxides such as $MoO_3$ and $TiO_2$ allowed faster desorption kinetics with a reversible hydrogen capacity of 2.4 wt. % $H_2$ at 270 °C in the first cycle [210]. Cobalt-based catalysts have also been studied: $Co_3O_4$, $CoF_3$, $Co_2B$ and $CoCl_2$ [211,212]. In these studies, the authors showed that cobalt additives enhance the decomposition kinetics, but hinder the absorption ones, except for $Co_3O_4$. Finally, $ZrCl_4$ [174], $Nb_2O_5$, $Ni_3B$ [213], Ti nanoparticles [214], $K_2TiF_6$ and $K_2NbF_7$ [215] have been reported as efficient catalyst for the dehydrogenation and rehydrogenation of $Mg(BH_4)_2$ and/or $Ca(BH_4)_2$.

### *6.2. Chemical Modification*

Another strategy to destabilize $Mg(BH_4)_2$ or $Ca(BH_4)_2$ is their chemical modification. The first example consists of introducing $H^{\delta+}$ atoms into the molecule to facilitate the interaction with $H^{\delta-}$ atoms, and to increase the hydrogen density. The ammoniation of $Mg(BH_4)_2$ or $Ca(BH_4)_2$ has been proposed [177,178]; however, the emission of $NH_3$ and the lack of reversibility of these compounds have prevented any practical application. Accordingly, the introduction of a third component to these compounds has been suggested. Systems such as the $Mg(BH_4)_2{\cdot}2NH_3/MAlH_4$ composite (with M = Li or Na [216,217]), nanoconfined or nanozised $Mg(BH_4)_2{\cdot}6NH_3$ [218,219] and F-substituted $Mg(BH_4)_2{\cdot}2NH_3$ [220] were developed. These systems showed a reduction in the $T_{onset}$ of up to 30 °C without the emission of $NH_3$ [221]. In the case of $Ca(BH_4)_2{\cdot}2NH_3$, the release of pure $H_2$ was achieved using transition metal chloride catalysts (such as $CoCl_2$, $NiCl_2$ and $FeCl_3$) [222]. Ethylenediamine ($C_2H_4(NH_2)_2$, denoted en) has been used to synthesize the complex $Mg(BH_4)_2{\cdot}$en, which exhibited good dehydrogenation properties [223]. In that study, the author demonstrated that the driving force in hydrogen desorption is caused by the redox reaction between $H^{\delta+}$ (H-N) and $H^{\delta-}$ (H-B). Finally, complexes between $N_2H_4$ and $Ca(BH_4)_2$, and between guanidinate ($CN_3H_5$) and $Mg(BH_4)_2$ and $Ca(BH_4)_2$ were studied [224,225]. These compounds have shown enhanced dehydrogenation properties compared to the sole borohydrides. $Ca(BH_4)_2{\cdot}4/3N_2H_4$ released around 10.8 wt. % of hydrogen at 240 °C; the temperature can be further decreased to 140 °C using an $FeCl_3$ catalyst. The borohydride guanidinate $MBH_4{\cdot}nCN_3H_5$ (M = Mg and Ca) can release up to 10 wt. % $H_2$ below 200 °C with minimized contamination with $B_2H_6$ or $NH_3$. Unfortunately, for all of these adducts, no reversibility was observed due to the formation of stable B-N bonds.

The destabilization of $Mg(BH_4)_2$ by Lewis-based adducts has also been envisaged as a strategy to drive the decomposition mechanism to a specific by-product, and thus to facilitate the reversibility of the system. The decomposition mechanisms of several solvated complexes of $Mg(BH_4)_2$ were examined, using different Lewis bases as solvents, such as dimethyl sulfide, triethylamine, diethyl ether, diglyme, dimethoxy ethane and THF. According to this work, $Mg(BH_4)_2{\cdot}$THF was selectively decomposed into a $B_{10}H_{10}^{2-}$ by-product, over $B_3H_8^-$ or $B_{12}H_{12}^{2-}$. The $B_{12}H_{12}^{2-}$ anion is highly stable and is a kinetic

dead-end. Hence, driving the decomposition mechanism to avoid the formation of this compound could pave the way to potential cycling between $Mg(BH_4)_2$ and $MgB_{10}H_{10}$ [226].

### *6.3. Nanoconfinement*

As previously mentioned, another way to improve the kinetics of hydrogen desorption consists of confining the borohydrides within a porous matrix. For instance, $Mg(BH_4)_2$ and $Ca(BH_4)_2$ confined in nanoporous $Cu_2S$ hollow spheres were studied, and they have shown significant improvements with a $T_{onset}$ values as low as 50 °C for both borohydrides, with a slight hydrogen uptake of 0.5 wt. % $H_2$ and 0.9 wt. % $H_2$ upon cycling [227]. Several carbon-based matrices have also been used, such as hollow carbon nanospheres, where $Mg(BH_4)_2$ and $Ca(BH_4)_2$ were confined using the solvent or melt impregnation methods (Figure 13) [136]. Both methods exhibited an improvement in terms of hydrogen storage properties, but the solvent impregnation resulted in better properties, revealing the sensitiveness to the synthetic routes. The hydrogen release peaked at 330 °C and 375 °C for the $Mg(BH_4)_2$ confined using melt impregnation, whereas the solvant impregantion method allowed a release peaking at 108 °C. The same trend was observed for $Ca(BH_4)_2$. Later on, the same group claimed that the nanoconfinement also modifies as well the thermodynamic of the borohydrides, though no thermodynamic values were given [228].

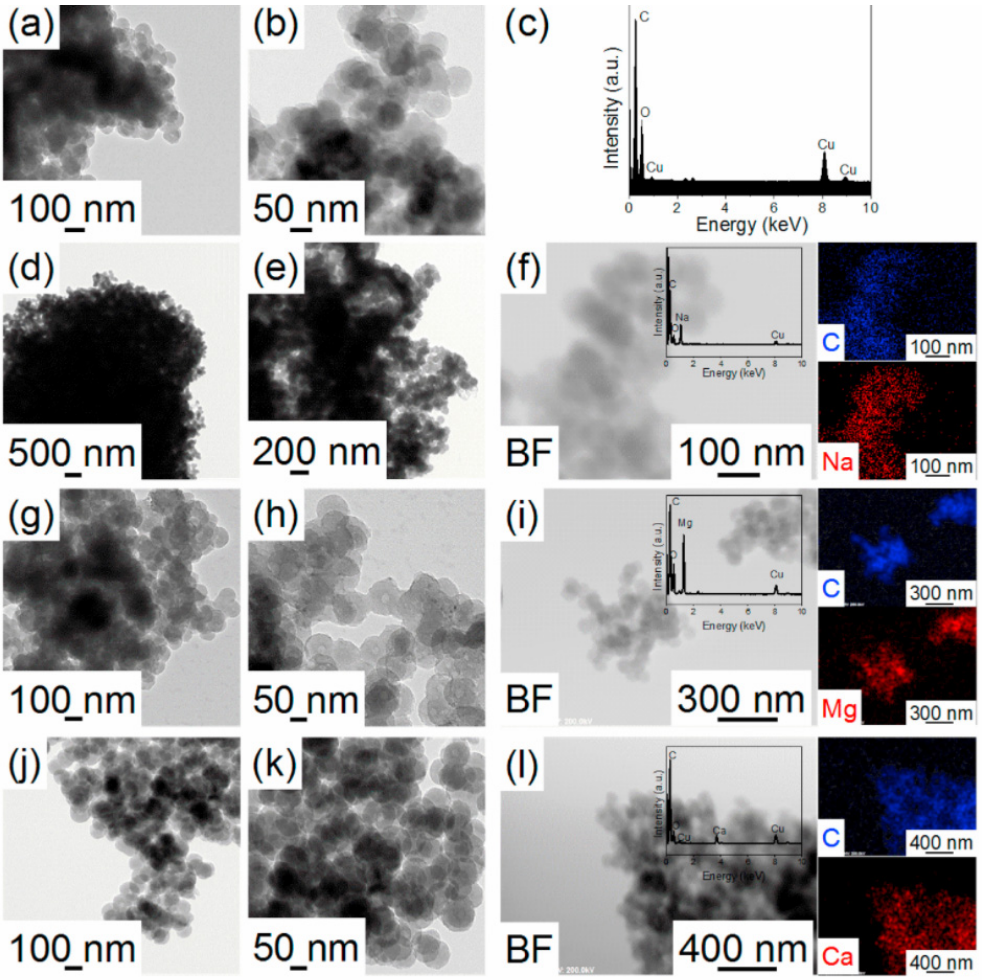


**Figure 13.** Typical TEM images, elemental mapping and EDS analysis of (**a**–**c**) $LiBH_4$-HCNs, (**d**–**f**) $NaBH_4$-HCNs, (**g**–**i**) $Mg(BH_4)_2$-HCNs and (**j**–**l**) $Ca(BH_4)_2$-HCNs via the melt infiltration method. Reprinted with permission from [136]. Copyright (2019), Elsevier.

Metal organic frameworks (MOF) have been used for the confinement of $Mg(BH_4)_2$. For example, the UiO-67bpy MOF ($Zr_6O_4(OH)_4(bpydc)_6$ with $bpydc^{2-}$=2,2′-bipyridine-5,5′-dicarboxylate) was impregnated using an $Mg(BH_4)_2$ solution [229]. The authors suggested that molecular confinement was achieved, instead of the agglomeration of nanoparticles. A substantial improvement was reported, with complete dehydrogenation at 200 °C, evidenced by $^{11}B$ MAS NMR results. The reason for this low dehydrogenation temperature was explained by the lower activation energy of the dissociation of the B-H bond, which was supported by density functional theory calculations. Further improvements were achieved through synergic effects by combining different strategies, including catalyzed composites [197,230–232], by incorporating catalysts directly onto the scaffold [233–235], by nanoconfining composites [236,237] or by synthesizing nanoparticles (NPs) on fluorographites (FGi) [201,238]. As an example of the latter strategy, homogeneous dispersed NPs of $Mg(BH_4)_2$ and $LiAlH_4$ were achieved on an FGi substrate to form a "chocolate cookie" structure. The $T_{onset}$ decreased to 68.2 °C, releasing 7.12 wt. % $H_2$ in a few seconds. These improvements were attributed to the shape of the NPs, for which aggregation was prevented by the FGi substrate and by the exothermic reaction between $LiAlH_4$ and FGi that triggered the $Mg(BH_4)_2$ decomposition.

### *6.4. General Remarks*

In summary, the destabilization of the highly promising $Mg(BH_4)_2$ and $Ca(BH_4)_2$ can be achieved by, on the one hand, modifying their thermodynamics by obtaining a composite with another material, or through nanostructuration. On the other hand, modifying the kinetics by minimizing the activation energy using additives or via nanoconfinement also allows destabilization to occur. The combination of these strategies has demonstrated a further improvement in the hydrogen storage properties of both borohydrides. The positive effect of this destabilization has encouraged studies to find a reversible hydrogen storage system near room temperature. Nonetheless, to date, the lack of full reversibility upon cycling remains the bottleneck for real-life applications, and much effort remains to be exerted in this direction.

## 7. Ammonia Borane

Ammonia borane ($NH_3BH_3$) has been widely studied as a material for hydrogen storage applications. It seems that not only the three approaches mentioned on Section 3 are able to affect the decomposition behavior of AB. For example, the reagents used to synthesize AB can have an impact on its dehydrogenation properties [239]. At a certain degree, modifying the synthesis conditions of AB allows us to tune the decomposition conditions. For example, a more stable AB is obtained when it is synthesized from $LiBH_4$, in comparison with other borohydrides. It is likely that the stronger basicity of the $BH_4^-$ in $LiBH_4$ leads to a stronger N–B bond. The solvent used to prepare AB also has an effect on its thermal stability: samples prepared in THF presented a lower-onset decomposition temperature compared with samples prepared in 1,4-dioxane. The reason for this is that THF can complex with $BH_3$ groups, interacting with AB, and thus destabilizing the N–B bond.

### *7.1. Additives*

Different additives have been considered to modify the dehydrogenation properties of AB. Nakagawa et al. [240] performed a systematic work on the destabilization of AB by metal chlorides ($MCl_x$) and transition metals. The content of the metal additive was of 10 % mol. On the one hand, the transition metals of period 4 have no destabilization effect on AB. On the other hand, $MCl_x$ were able to modify the properties of AB, and this behavior was related to the Pauling electronegativity of the metal. $MCl_x$ with a higher $\chi_P$ were able to desorb $H_2$ at lower temperatures without traces of byproducts. For example, composites with $FeCl_2$, $CoCl_2$, $CuCl_2$ and $NiCl_2$ allowed the dehydrogenation of AB below 100 °C (Figure 14). Compounds with a high $\chi_P$ can act as Lewis acids, inducing changes in

the electronic state of the N atom and destabilizing AB. However, as $MCl_x$ additives with a high $\chi_P$ are usually heavy, the ideal amount of the additive might lie in the range of 5–10% mol.

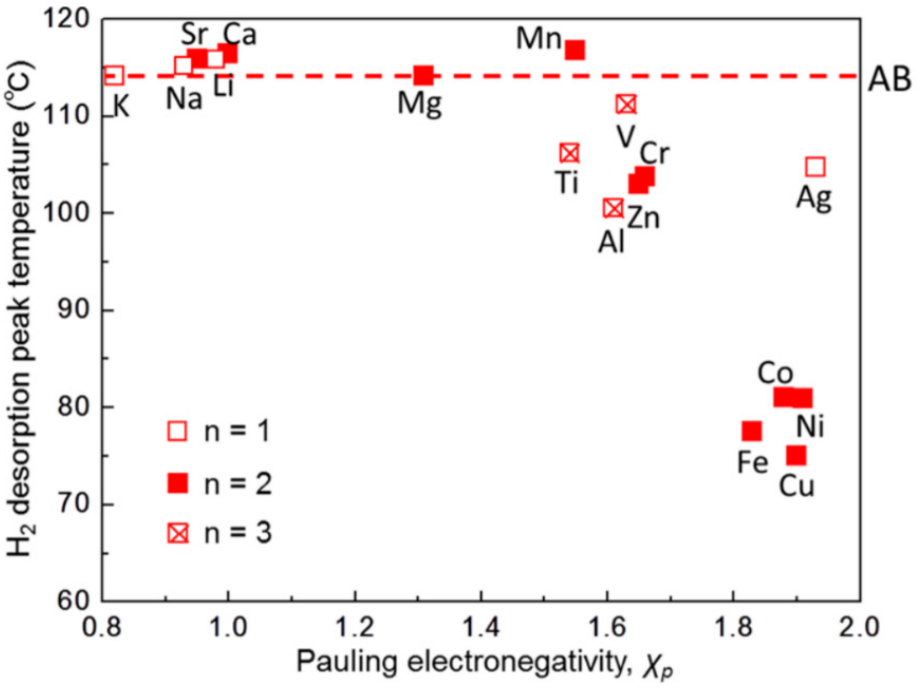


**Figure 14.** $H_2$ desorption peak temperatures of $AB/MCl_x$ mixtures. Reprinted with permission from [240]. Copyright (2016), American Chemical Society.

Different oxygen-containing compounds (such as $TiO_2$, MgO $SiO_2$), can destabilize AB, allowing the release of $H_2$ at about 80 °C [241]. For example, Shin et al. [242] prepared a compressed mixture of $AB/SiO_2$ (the content ranged from 60–80 wt. % AB). The dehydrogenation reaction happened in one minute, releasing 11.2 wt. % $H_2$ with an onset temperature of 85 °C. Despite the improved kinetics, the composite released several byproducts. Ergüven et al. [243] reported an improvement in the kinetics of AB by mixing it with $H_3BO_3$ and $B_2O_3$.

Other additives, such as misch metal (an alloy of rare earth elements), have been reported [244]. Although the destabilization was achieved, the release of unwanted gases hampered further development. Biliskov et al. [245] reported the destabilization effect of KBr on AB. Huang et al. [246] prepared the composite $Zr(BH_4)_4 \cdot 8NH_3/AB$, which released $H_2$ with a purity of 96.1 mol %. Most likely, AB suppresses the release of $NH_3$ and enhances the $H_2$ formation from the borohydride ammoniate, due to the interaction between AB and the $NH_3$ groups. Kim et al. [247,248] proposed two different additives: d-mannitol ($C_6H_8(OH)_6$) and maleic acid ($C_4H_4O_4$). For the first one, it was found that 9.1 wt. % $H_2$ can be obtained by AB at 90 °C, with fast kinetics. In the case of maleic acid, 2.4 wt. % $H_2$ was released at the same temperature. For both compounds, a hydrolysis reaction was detected between AB and the water released from the additives. Due to this, $NH_3$ was produced and the polymeric residues after dehydrogenation presented B–O bonds. In a comparable study, Shin et al. [249] used mucic acid ($C_6H_{10}O_8$) as an additive. The dehydrogenation occurred between 80 °C and 90 °C in 1 min, releasing 10.7 wt. % $H_2$.

Ni-containing compounds have been studied as additives to destabilize AB. Roy et al. [250] prepared transition metal nickel alloys (FeNi, ZrNi and CuNi) and then mixed them with AB. The addition of the alloys reduced the emission of $B_3H_6N_3$. The destabilization effect of the alloys was sorted as follows: CuNi < FeNi < ZrNi. Luo et al. used the $Mg_2Ni$ alloy and milled it with AB [251]. They determined that for an intense milling process, the onset dehydrogenation temperature decreased due to the better mixing of the two components

and a stronger physical interaction between the particles. In addition, $Mg_2NiH_4$ is able to react with AB, forming an Mg–Ni–N–B–H complex.

Some Al-based compounds have also been tested. Wan et al. [252] prepared a composite of $AlH_3$/3AB, which released the 1st and 2nd equiv. $H_2$ at 112 °C and 154 °C (a total of 13 wt. % $H_2$). No volatile products were detected. It seems that AB and $AlH_3$ achieved a mutual destabilization through the Coulombic interaction between the $H^{\delta-}$ of $AlH_3$ and the $H^{\delta+}$ of the $NH_3$ moiety of AB. Dovgaliuk et al. In [253], the authors prepared an $Al(BH_4)_3$·AB complex through an addition reaction. This led to the formation of a new crystalline complex. Although the dehydrogenation of this complex was endothermic, the rehydrogenation of the complex was not achieved.

A different approach to releasing hydrogen from AB was proposed by Huang et al. [254]. $Ti_2O_3$ was used as a full-spectrum light absorber to activate AB photothermally. Under an optimized irradiation at room temperature, 11.8 wt. % $H_2$ was released from the composite in 30 min. The $Ti_2O_3$ nanoparticles were used for four dehydrogenation cycles, without a decay in their reactivity. Seemingly, the photothermal effect was the only one responsible for the improved dehydrogenation of AB. When $CuCl_2$ was added to the system, AB released the same amount (11.8 wt. % $H_2$) at only 70 °C, with a high purity.

### *7.2. Chemical Modification*

The chemical modification of AB is an approach that consists in substituting one of the $H^{\delta+}$ of the $NH_3$ moiety of the molecule with a metal cation. Through this method, ionic salts are obtained and they are called amidoboranes (MABs). The introduction of the metal cation into the molecule destabilizes the dihydrogen bonds and thus improves the dehydrogenation properties by lowering the dehydrogenation temperature and suppressing some (or all) of the volatile unwanted gases. Different amidoboranes have been synthesized and characterized under the scope of hydrogen storage applications (Figure 15) [61,255]. Alkaline and alkaline-earth amidoboranes are usually obtained via the reaction of AB with a metal hydride or a pure metal, releasing $H_2$ (Equations (22) and (23)).

$$xNH_3BH_3 + MH_x \rightarrow M(NH_2BH_3)_x + xH_2 \quad (22)$$

$$NH_3BH_3 + M \rightarrow MNH_2BH_3 + \frac{1}{2}H_2 \quad (23)$$

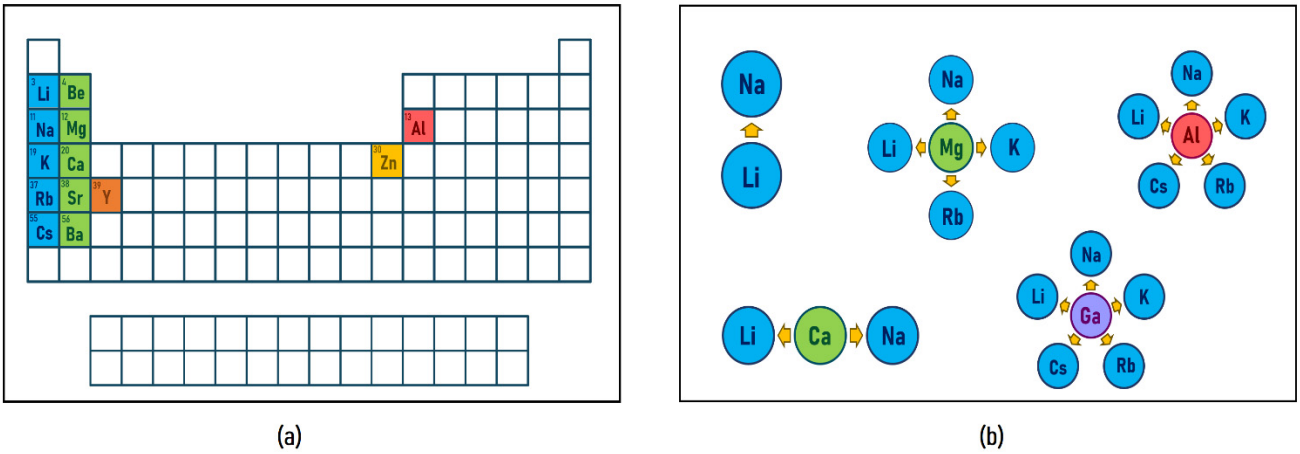


**Figure 15.** (**a**) Reported monometallic amidoboranes, either experimentally or theoretically; (**b**) combinations of metals for bimetallic amidoboranes that have been reported, either experimentally or theoretically.

The synthesis of amidoboranes is usually performed via mechanochemical reactions or through wet synthesis. Various approaches have been tested in order to optimize the synthesis routes or to look for different precursors to obtain these compounds [256,257]. Recent advances in the field of amidoborane compounds are presented below.

7.2.1. Monometallic Amidoboranes

Lithium amidoborane (LiAB, $LiNH_2BH_3$, 13.7 wt. % $H_2$) is a crystalline compound with two allotropes. The α phase forms first through ball milling, whereas the β phase forms through energetic ball milling, as the reaction progresses [258]. β-LiAB can be seen as a metastable phase. Both allotropes have an orthorhombic unit cell with a *Pbca* space group, but the lattice parameters of β-LiAB are almost twice the ones of the α-LiAB. Liu et al. [259] analyzed the dehydrogenation of each allotrope. α-LiAB presents the lowest onset temperature (61 °C) and β-LiAB the highest (76 °C). Besides, the activation energy of α-LiAB is lower in comparison with β-LiAB (157 kJ $mol^{-1}$ vs. 270 kJ $mol^{-1}$). Thus, α-LiAB is a better candidate for hydrogen storage applications. The destabilization of LiAB has also been studied through different approaches. Ghaani and Catti [260] tried to decrease the dehydrogenation temperature of LiAB by increasing the pressure of the system and by using additives ($LiBH_4$ and $MgH_2$). Increasing the pressure between 0–8 MPa $H_2$ has no effect on the decomposition of LiAB, nor does adding $MgH_2$. However, the presence of $LiBH_4$ decreased the dehydrogenation temperature of LiAB from 74 °C to 64 °C. In addition, a composite with a molar ratio 5:1 (LiAB:$LiBH_4$) released 10.9 wt. % $H_2$ in comparison with the 9.8 wt. % $H_2$ released by pristine LiAB upon heating to 180 °C.

Rubidium (RbAB, $RbNH_2BH_3$, 4.3 wt. % $H_2$) and cesium (CsAB, $CsNH_2BH_3$, 3.1 wt. % $H_2$) amidoboranes were synthesized for the first time in [261,262]. When these amidoboranes are heated, they undergo a phase transition. α-RbAB (monoclinic, s.g. $P2_1/c$) and α-CsAB (orthorhombic, s.g. *Pnam*) are the low-temperature allotropes. The high-temperature phases, namely, β-RbAB (cubic, sg. *Fm*-3*m*) and β-CsAB (cubic, sg. *Fm*-3*m*) form when they are heated between 50 °C and 70 °C, prior to the decomposition. Both compounds released $H_2$ and $NH_3$. At this point, it is necessary to present a realistic evaluation of the heaviest amidoboranes as solid-state hydrogen storage materials. First, they fall short in their storage capacity in comparison with other amidoboranes. The weight of heavy elements, such as Rb and Cs, outshine the gravimetric H density of these compounds. Even if they are completely dehydrogenated, this would lead to the formation of boron nitride, which is highly stable, and its rehydrogenation is unfavorable. Second, the management of pure alkali elements is challenging due to their high reactivity. Third, they are unstable. It appears that heavier amidoboranes are not the best candidates for the chemical storage of hydrogen. Nevertheless, from the fundamental point of view it is important to obtain and to analyze these compounds, as they allow a better understanding of their properties, such as the role of the cation on the molecule. In addition, other applications for these compounds have been suggested, such as being used as precursors of decorated boron nitride [255].

Regarding alkaline earth-based amidoboranes, some reports have been published. Computational studies have predicted the crystalline structure and dehydrogenation properties of beryllium-based amidoboranes [263]. However, as a highly toxic element, the use of Be was discarded. The synthesis of $Ba(AB)_2$ was reported by Shcherbina et al. [264] via the reaction of metallic Ba with AB in THF, at −10 °C. $Ba(AB)_2$ released 5 wt. % $H_2$ in the range of 40 °C–240 °C. No volatile byproducts were detected.

7.2.2. Bimetallic Amidoboranes

Bimetallic amidoboranes, which are amidoboranes containing two metal cations, have been studied as potential materials for hydrogen storage. An advantage over monometallic amidoboranes is that the thermodynamics of bimetallic amidoboranes can benefit from the synergic effect of mixed cations. For example, the dehydrogenation process of many bimetallic amidoboranes is endothermic [61], opening up the possibility of rehydrogenating the decomposed amidoborane. The combination of different metal cations also offers the possibility of tailoring the properties of these compounds. With these features on mind, new bimetallic amidoboranes have been synthesized in recent years.

$Na[Al(NH_2BH_3)_4]$ ($NaAl(AB)_4$, 11.8 wt. % $H_2$) was obtained through the mechanochemical reaction between AB and $NaAlH_4$ [265]. $NaAlH_4$ was the first complex hydride re-

ported that was able to deprotonate AB. $NaAl(AB)_4$ crystallized in a triclinic unit cell with a space group *P*1. $NaAl(AB)_4$ decomposes via a two-step process between 120 °C and 160 °C, releasing pure $H_2$ and forming $NaBH_4$ and an amorphous product $AlN_4B_3H_{(0–3.6)}$. The latter was able to reabsorb 27% of the released hydrogen. However, a different group reported the emission of volatile byproducts ($NH_3$, $B_2H_6$ and $B_3H_6N_3$) during the decomposition of $NaAl(AB)_4$ [266].

Milanović et al. [267] presented two new calcium-based amidoboranes, $Li_2Ca(NH_2BH_3)_4$ ($Li_2Ca(AB)_4$, 11.5 wt. % $H_2$) and $Na_2Ca(NH_2BH_3)_4$ ($Na_2Ca(AB)_4$, 9.7 wt. % $H_2$) obtained by the mechanochemical reaction between the respective metal hydrides and AB. The decomposition of both compounds takes place through exothermic events. $Li_2Ca(AB)_4$ dehydrogenates between 85 °C and 95 °C, releasing $H_2$ and traces of $NH_3$. $Na_2Ca(AB)_4$ undergoes a fast decomposition from 66 °C, releasing $H_2$ and a substantial amount of $NH_3$. The authors also identified two general thermal decomposition paths for Na-containing amidoboranes: (i) a dominant path where pure $H_2$ is released, and (ii) a secondary path where $H_2$ and $NH_3$ are released. One theoretical and experimental study was performed by Chernysheva et al. [268], in which they explored the possibility of obtaining different complex amidoboranes $M^1[M^2(NH_2BH_3)_4]$ ($M^1$ = Al, Ga; $M^2$ = Li, Na, K, Rb, Cs) (Equation (24)). The spectral characterization of these compounds was presented, and the feasibility of the synthesis of such amidoboranes was confirmed.

$$M^1Cl_3 + 4M^2NH_2BH_3 \rightarrow M^2\left[M^1(NH_2BH_3)_4\right] + 3M^2Cl \quad (24)$$

#### 7.2.3. Other Systems

Yang et al. [269] reported the synthesis of a metal amidoborane ammoniate $[Al(NH_2BH_3)_6]^{3-}$ $[Al(NH_3)_6]^{3+}$. This compound decomposed in the range 65 °C–180 °C, releasing 7.5 wt. % of $H_2$ and $NH_3$. Under isothermal conditions at 105 °C, the sample released 10.3 wt. % $H_2$, where only 0.05 wt. % $NH_3$ was detected. It is likely that a sufficient partial pressure of $NH_3$ in a closed system would inhibit the formation of further $NH_3$. This provides evidence for the different thermal behavior of boron- and nitrogen-based compounds in open and closed systems. He et al. [270] reported the first metal amidoborane hydrazinate, $LiNH_2BH_3NH_2NH_2$. ($LiAB{\cdot}N_2H_4$, 13.1 wt. % $H_2$). The $4LiAB{\cdot}N_2H_4$ complex can release 7.1 wt. % $H_2$ at 75 °C. Finally, Li et al. [271] synthesized calcium amidoborane hydrazinate ($Ca(AB)_2{\cdot}2N_2H_4$), which started to decompose at around 98 °C, releasing $H_2$ and $NH_3$. The suppression of the $NH_3$ released was achieved using a hydrazinate with the composition $Ca(AB)_2{\cdot}1/2N_2H_4$. The synthesis of complexes with $[BH_4]^-$ anions has been also considered, such as $Al(BH_4)_3{\cdot}NH_3BH_3$ and $Sr(BH_4)_2(NH_3BH_3)_2$ [253,272].

### *7.3. Nanoconfinement*

Different types of scaffolds have been proposed for the nanoconfinement of AB. Each one presents different features and is discussed in the following section. Table 1 summarizes recent investigations on nanoconfined AB.

#### 7.3.1. Silicon-Based Scaffolds

The confinement of AB in mesoporous SBA-15 has different effects on the dehydrogenation properties of the borane. For example, the hydroxyl groups found on the surface of the SBA-15 destabilizes AB via $O–H^{\delta+}\cdots H^{\delta-}–B$ interactions, modifying the dehydrogenation mechanism and suppressing the emission of borazine and the foaming of the compound [273,276,277]. Silanol groups (Si–O–Si) also prevent the formation of B–N volatile products and lower the onset dehydrogenation temperature of AB [274]. The interactions between the surface groups of silicon-based scaffolds and AB have been evidenced through Raman spectroscopy [292]. Other positive effects have been reported, such as the absence of an induction period for the release of $H_2$ and improved kinetics [275].

**Table 1.** List of materials investigated as scaffolds for AB confinement. The material and its textural properties (specific surface area, SSA; average pore size, APS; total pore volume, TPV) are given, when available. Other details about the infiltration method; the onset dehydrogenation temperature, $T_{onset}$; the peak at which $H_2$ is released, $T_{peak}$; the activation energy, $E_a$; and the byproducts detected from the sample are given, when available.

| Material | SSA ($m^2$ $g^{-1}$) | APS (nm) | TPV ($cm^3$ $g^{-1}$) | Infiltration Method | $T_{onset}$ (°C) | $T_{peak}$ (°C) | $E_a$ (kJ $mol^{-1}$) | Byproducts | Ref. |
|---|---|---|---|---|---|---|---|---|---|
| SBA-15 | 609 | 7.8 | 0.96 | THF | 40 | 97 | - | Not detected | [273] |
| SBA-15 | 550 | 6.4 | 0.69 | THF | 40 | 97 | - | $B_2H_6$ | |
| SBA-15 | 497 | 4.3 | - | THF | 75 | 90 | - | $AB_{(g)}$ | [274] |
| MCM-41 | 668 | 3.4 | - | THF | 95 | 108 | - | $AB_{(g)}$ | |
| MCF | 217 | 18.0 | - | THF | 75 | 80 | - | $AB_{(g)}$ | |
| Silica aerogel | 887 | 8.7 | 1.94 | THF | 37 | 62 | - | Not reported | [275] |
| Bentonite | 42.4 | - | - | $CH_3OH$ | R.T. | 120 | - | Not detected | [276] |
| Pd-halloysite | 48.1 | 2.8 | 0.2 | THF | 60 | 80 | 46 | Not detected | [277] |
| MOF-derived carbon | 2222 | 0.4 | 2.49 | THF | 63 | 72 | 61 | $NH_3$ | [278] |
| Microporous carbon | 1652 | 1.0 | 0.87 | $CH_3OH$ | 50 | 86 | 75 | Not detected | [279] |
| AC | - | - | - | Ball milling | 85 | 104 | 34 | $NH_3$, $B_2H_6$, $B_3H_6N_3$ | [280] |
| AC | - | - | - | THF | 96 | 112 | - | $NH_3$ | |
| CMK-5 | 1650 | 4 | 1.69 | THF | 50 | 98 | - | $NH_3$ | [281] |
| MOF-5 | 1032 | - | 0.57 | $CH_3OH$ | 60 | 84 | 68.4 | $NH_3$ | [282] |
| Ni-MOF | - | - | - | Ball milling | 70 | 90 | - | Not detected | [283] |
| Tm(BCT) | - | - | - | $CH_3OH$ | 60 | 77 | 98.1 | Not detected | [284] |
| UiO-66-$NH_2$ | 976 | - | 0.43 | $Et_2O$ | <50 | 78 | - | Not detected | [285] |
| MIL-53-$NH_2$ (Al) | 540 | - | - | THF | 60 | 91 | 38.2 | Not detected | [286] |
| IRMOF-1 | 1060 | 1.3 | 0.43 | $CH_3OH$ | <45 | 75 | - | $NH_3$ | [287] |
| IRMOF-10 | 320 | - | 0.18 | $CH_3OH$ | 50 | 73 | - | $NH_3$ | |
| UiO-66 | 1010 | 1.1 | 0.67 | $CH_3OH$ | <45 | 64 | - | $NH_3$ | |
| UiO-67 | 1920 | - | 0.75 | $CH_3OH$ | <50 | 76 | - | $NH_3$ | |
| MIL-53(Al) | 1110 | 1.8 | 0.58 | $CH_3OH$ | 65 | 85 | - | $NH_3$ | |
| Cu(BDC) | 550 | 1.3 | - | Hand grinding | <60 | 96 | 101.9 | Not detected | [288] |
| PPy nanotubes | 74.9 | 40 | 0.29 | THF | 48 | 90 | 78.5 | Not detected | [289] |
| $MnO_2$ hollow spheres | 256.9 | 2.4 | 0.47 | THF | 70 | 107 | 68.5 | Not detected | [290] |
| h-BN | 584 | - | 0.75 | THF | >40 | 98 | - | Not detected | [291] |

#### 7.3.2. Carbon-Based Scaffolds

So et al. [278] used different carbons with different pore size distribution to confine AB. They found that carbon with pores of about 0.4 nm presented the best performance in their study. As a conclusion, they stated that micropores are optimal to destabilize AB. The same conclusion was drawn by Yang et al., using microporous carbon with an average pore size of 1.0 nm [279]. Due to the geometrical constraints of the scaffold, the activation energy was reduced and the dehydrogenation occurred at 86 °C. Consequently, the N–B bond was not split and the formation of gaseous byproducts was suppressed. Bravo Diaz et al. [280] used activated carbon as a scaffold, introducing AB via both ball milling and a solution impregnation method. The composite obtained using the impregnation method presented better dehydrogenation behavior, as the composite started to dehydrogenate at 96 °C, releasing $H_2$ with small traces of $NH_3$. The composite obtained through ball milling released several byproducts. Cao et al. [281] used a carbon nanotube array CMK-5 as a scaffold to confine AB and $AlH_3$. They observed the formation of organic borates (–OBX) due to the reaction between AB and the surface hydroxyl groups. This also promotes the cleavage of the N–B bond, forming $NH_3$ and $H_2$ during decomposition.

Sun et al. [293] reported the decoration of graphene with 3–10-nm nanoparticles of $NiCl_2$ and $CoCl_2$, and used it as a matrix for AB. An onset temperature between 60 °C and 90 °C was achieved, releasing pure $H_2$ with an apparent activation energy between 61 and 76 kJ $mol^{-1}$. A reduced graphene oxide was also reported as a scaffold that prevented the formation of volatile byproducts from AB [294].

#### 7.3.3. Metal Organic Frameworks

Through the nanoconfinement of AB into a MOF, its dehydrogenation properties are modified; for example, Liu et al. [282] improved the kinetics and the dehydrogenation properties of AB using MOF-5. However, the release of $NH_3$ was detected during decomposition, due to the lack of an unsaturated metal inside the MOF-5. The latter seems to be a key factor in avoiding the formation of volatile byproducts.

In another example, AB confined in an Ni-based MOF released only $H_2$ [283]. It seems that the unsaturated Ni acted as an acidic site, favoring the catalysis of the dehydrogenation and preventing the formation of $NH_3$ and other volatile compounds. Yang et al. [284] used an unsaturated MOF based on $Tm^{3+}$ to infiltrate AB through an impregnation method and by means of ball milling. The samples obtained using both approaches achieved the destabilization of AB. Nevertheless, the sample obtained by wet impregnation did not release any volatile byproduct, whereas the sample obtained by ball milling released $NH_3$. The role of the unsaturated $Tm^{3+}$ in the sample obtained using the impregnation method acted as a Lewis acid, interacting with the electron donor $NH_3$ moiety of AB. Wang et al. [285] used UiO-66-$NH_2$ and then infiltrated a borane adduct to form a complex. The material dehydrogenates without an unwanted gas release, and this was explained by the strong chemical bond between the amino groups of the MOF and the borane. Similar results were obtained by Liao et al. [286].

There are different features of the MOF that can destabilize AB. Chung et al. [287] confined AB in five different MOFs, and they established a linear relationship between the particle size of AB (obtained by the pore size of the MOF) and the dehydrogenation temperature (Figure 16). The smaller the pores are, the lower is the dehydrogenation temperature. In that study, the UiO-66 MOF presented the lowest decomposition temperature (64 °C), with a pore size of 1.17 nm.

In a recent study, Peil et al. [295] analyzed the effect of the confinement of AB in the MIL-53 MOF. In the first instance, the typical MIL-53(Al) was used; thereafter, the terephthalic linkers were modified with OH and $NH_2$ groups, and finally, other metallic nodes were tested (Cr, Fe, V). The AB@MIL-53(Al) started to release $H_2$ at a higher temperature than bulk AB; however, the suppression of volatile byproducts was achieved. The MIL-53 with the functionalized linkers decreased the onset dehydrogenation temperature between 60 °C and 110 °C. It is likely that the interaction between AB and the functional groups can

reduce the energetic barrier to release $H_2$. Regarding the other metallic nodes, only the Fe node decreased the release temperature of AB. Wu and Wang [288] used a Cu-based MOF to infiltrate AB by means of hand grinding. After the dehydrogenation, they washed the MOF to remove the thermolytic residues and reinserted AB into the framework. However, the catalytic effect of the MOF diminished with every cycle, due to the reduction of the copper sites during the hydrogen release. However, the destabilization of AB was achieved (Figure 17).

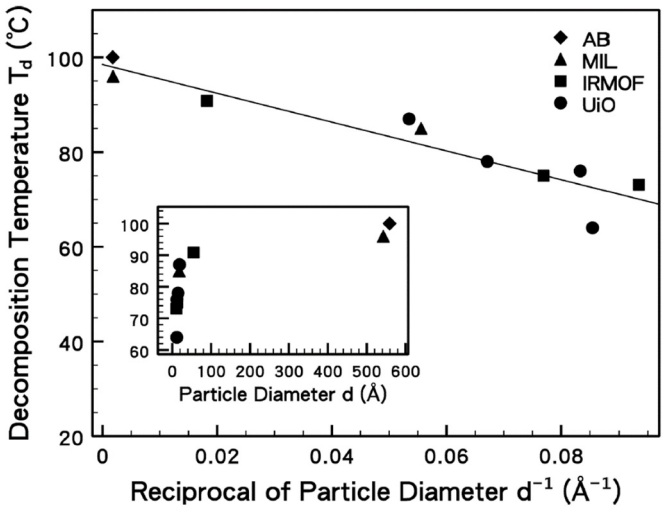


**Figure 16.** Peaked temperatures ($T_d$) of the decomposition of neat AB (¨), and AB confined in MOF of MIL, IRMOF and UiO MOF vs. the reciprocal particle size (d) of the corresponding hydrides. $T_d$ vs. d is shown in the inset. Reprinted with permission from [287]. Copyright (2017), American Chemical Society.

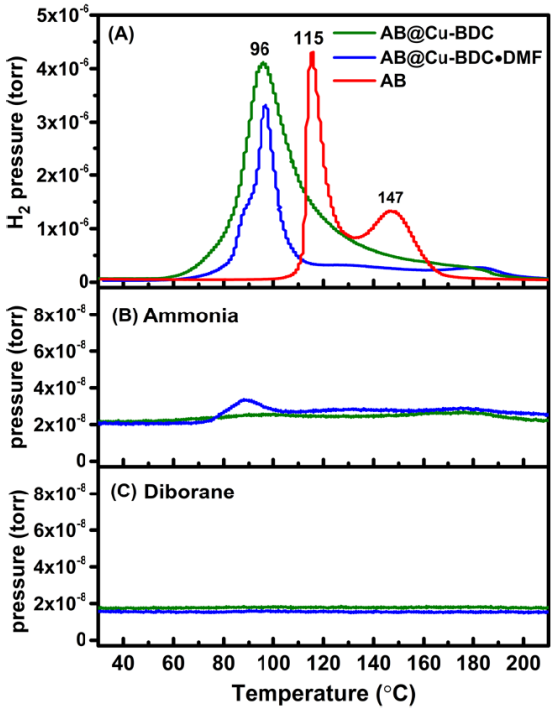


**Figure 17.** Temperature-programmed desorption with mass spectroscopy (TPD-MS) of (**A**) hydrogen, (**B**) ammonia and (**C**) diborane generated from AB (red), AB@Cu-BDC (green) and AB@Cu-BDC·DMF (blue) in the unit of Torr. Reprinted with permission from [288]. Copyright (2019), American Chemical Society.

#### 7.3.4. Polymers

Different kinds of polymers have been tested as scaffolds to infiltrate AB. Zhang et al. [289] used N-doped polypyrrole (PPy) nanotubes. The confined AB started to release hydrogen at 48 °C, releasing a total of 15.3 wt. % $H_2$ below 150 °C, without traces of volatile byproducts. The dopant N atoms acted as a catalyst, improving the dehydrogenation of AB. Another example is polyethylene oxide (PEO). A composite AB@PEO was prepared by Nathanson et al. via the electrospinning technique [296]. AB was destabilized by the interaction between the ethereal oxygen atom (C=O) of the PEO and the $H^{\delta+}$ of AB, and it started to dehydrogenate at 85 °C. However, during decomposition, an increased amount of $B_3H_6N_3$ was released, suggesting that the addition of PEO favors the cyclic dehydrogenation route of AB. This was explained by the fact that the use of ethereal compounds (such as PEO, THF and glyme) favors the dehydrogenation of AB accompanied by a substantial amount of $B_3H_6N_3$. Other findings were reported in further studies [297,298], in which PEO also prevented the foaming of AB, and the formation of a crystalline intermediate during the dehydrogenation of the composite. Seemaladinne et al. [299] used polyvinylpyrrolidone (PVP) embedded with AB particles. The apparent activation energy of the composites decreased in comparison with pristine AB. This was related to the molecular weight and polymer content of the composites. As these two parameters increased, the activation energy decreased. Another polymer that improved the dehydrogenation properties of AB is PMMA [300].

#### 7.3.5. Other Scaffolds

A few reports on scaffolds of different chemical natures have been recently published. Two examples are $MnO_2$ hollow spheres and porous h-BN [290,291]. Due to the confinement effect, in both cases AB dehydrogenates, releasing pure $H_2$ at lower temperatures than bulk AB. Roy et al. [301] used aluminum phosphate to confine AB. Using $^{11}$B MAS NMR spectroscopy, they obtained evidence of a different decomposition mechanism pathway of confined AB, through homopolar interactions. These interactions led to the formation of B-B bonds. The decomposition of AB through homopolar interactions has also been reported and discussed by other groups [48,302,303].

#### 7.3.6. Nanosizing

Song et al. [304] prepared AB nanoparticles (50 nm) through the direct reaction of $B_2H_6$ and $NH_3$ (with an excess of $B_2H_6$). The particles presented the two characteristic dehydrogenation peaks of AB at 101 °C and 149 °C, in comparison with the 121 °C and 156 °C of the bulk phase. They also noted the production of less volatile products, as well as the absence of foaming during dehydrogenation. Lai et al. [305] obtained 50 nm particles of AB using an antiprecipitation method. Though these nanoparticles did not decrease the dehydrogenation temperature compared to pristine AB, the foaming was avoided. In a further experiment, the AB nanoparticles were dispersed in an Ni matrix. In this way, the particles started to release pure $H_2$ in the 50 °C–100 °C range. However, up to 200 °C, traces of $NH_3$ and $B_3H_6N_3$ were detected. Once dehydrogenated, the Ni-AB nanoparticle system showed a partial reversibility, being able to uptake 1 wt. % $H_2$ when rehydrogenated under 6 MPa $H_2$ at 200 °C. Finally, Valero-Pedraza et al. [306] synthesized AB nanospheres (110 nm diameter) through an emulsification approach using a surfactant (Figure 18). These spheres started to decompose at about 80 °C, releasing 1 wt. % $H_2$ up to 103 °C. A second decomposition step took place between 145 °C and 200 °C, losing 10.4 wt. %. Even if the emission of byproducts was reduced and the melting of the compound was delayed, it seems that the diameter of the particles is still too high to achieve an optimal performance.

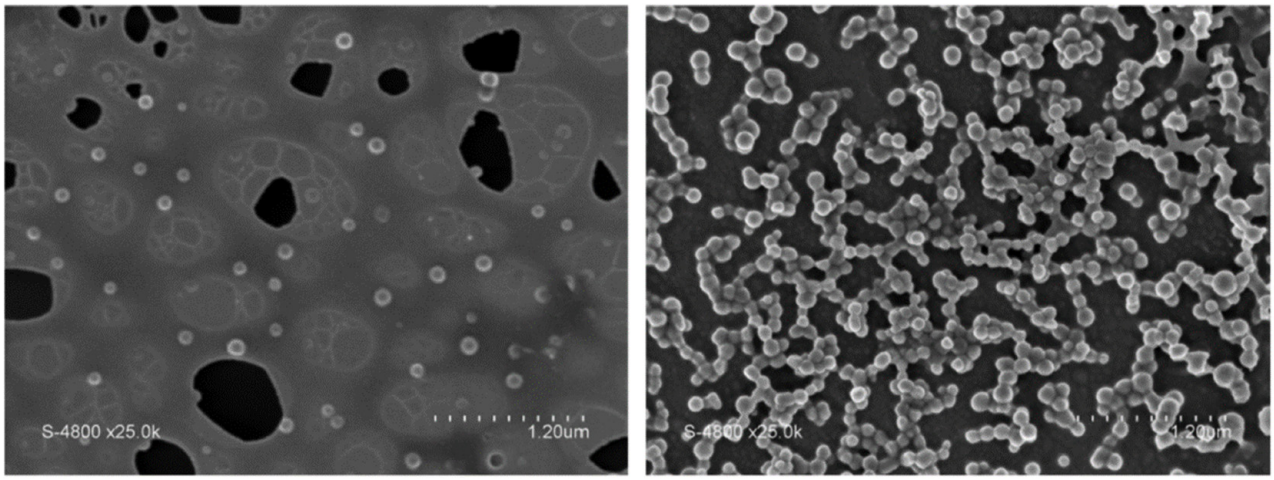


**Figure 18.** Scanning electron microscopy (SEM) micrographs of nanosized AB, dropped onto a carbon film on a cooper grid. Reprinted with permission from [306]. Copyright (2019), American Chemical Society.

### *7.4. General Remarks*

Despite the high gravimetric storage capacity of AB, the use of this compound in the pristine state is difficult, due to the release of unwanted volatile byproducts and due to a lack in the reversibility of the material. Destabilization strategies, such as chemical modification and nanosizing, have allowed the improvement of the dehydrogenation properties of AB, suppressing all or some of the byproducts, and reducing the onset temperature for the release of $H_2$. However, the major challenge regarding AB (and amidoboranes) is reversibility. More efforts have to be undertaken in order to rehydrogenate or recycle AB and its derivatives. The lack of studies regarding the scaling up of AB-based technologies is also notable. The development of prototypes at a larger scale based on AB is desirable.

## 8. Hydrazine Borane

Another boron- and nitrogen-based compound that has been considered for hydrogen storage applications is HB. HB can be seen as a derivative of AB, in which the $NH_3$ moiety of the molecule has been replaced by $N_2H_4$. HB starts to decompose at a lower temperature in comparison to AB, but it presents a similar drawback: the release of unwanted volatile byproducts [67]. Even worse, when HB is heated above 300 °C, a highly unstable (and explosive) residue is produced. Due to the high hydrogen gravimetric content of HB, some destabilization strategies have been considered to improve its dehydrogenation behavior.

### *8.1. Additives*

Pylypko et al. [307] investigated the destabilization of HB by the addition of alkali and alkaline earth hydrides (LiH, NaH, $CaH_2$, $MgH_2$ and $AlH_3$). The samples were prepared by means of ball milling. LiH and NaH reacted with HB to form $LiN_2H_3BH_3$ and $NaN_2H_3BH_3$. In the case of the $MgH_2$/HB and $CaH_2$/HB mixtures, no reaction was reported, and composites were formed. The milling of HB and $AlH_3$ led to the formation of a mixture of $AlH_3$, HB and Al, which probably formed due to the reduction of $AlH_3$ by HB. In terms of dehydrogenation, the HB/$CaH_2$ composite showed the best performance: it released 7.1 wt. % of gas in 30 min at 80 °C, which would represent 70% of its hydrogen storage capacity.

### *8.2. Chemical Modification*

Significant efforts have been exerted to modify HB and improve its dehydrogenation properties. The chemical modification of HB consists in substituting one of the H atoms of the middle N atom of the molecule by a metal cation. Usually, a metal hydride is used to modify HB. The substitution reaction can be carried out through ball milling or through a

solvent-based approach. The ionic salts obtained after the modification of HB are called hydrazinidoboranes (MHB, where M denotes the respective metal cation). Hydrazinidoborane compounds have shown better dehydrogenation properties in comparison with the parent HB. Although the storage capacity and the stability of some alkali hydrazinidoboranes are not practical for hydrogen storage (i.e., the heaviest ones), we believe that the discussion and the analysis of their properties contribute to improving the understanding of the chemistry of B-and N-based compounds.

#### 8.2.1. Alkali Hydrazinidoboranes

In the first half of the 2010s decade, the three first alkaline hydrazinidoboranes were synthesized and characterized [308–311], namely, lithium hydrazinidoborane (LiHB, $LiN_2H_3BH_3$, 11.7 wt. % $H_2$), sodium hydrazinidoborane (NaHB, $NaN_2H_3BH_3$, 8.9 wt. % $H_2$) and potassium hydrazinidoborane (KHB, $KN_2H_3BH_3$, 7.2 wt. % $H_2$). In the second half of the decade, the synthesis of rubidium hydrazinidoborane (RbHB, $RbN_2H_3BH_3$, 4.6 wt. % $H_2$) and cesium hydrazinidoborane (CsHB, $CsN_2H_3BH_3$, 3.4 wt. % $H_2$) were reported by our group [312,313]. Unlike previous hydrazinidoboranes, the synthesis of RbHB and CsHB was carried out by a wet approach using the pure metal (Rb or Cs) and HB dissolved in THF, due to the high reactivity between reactants. It is also due to this high reactivity that RbHB and CsHB could not be obtained as pure phases, as evidenced by $^{11}$B MAS NMR analysis. All the alkali MHBs are crystalline, and RbHB and CsHB presented a monoclinic unit cell (space group $P2_1$). Considering the complete alkali family of hydrazinidoboranes, some trends were identified [255]. For example, as the size of the metal cation increases, the M ··· M distances decrease. The M-N bond becomes longer as the metal cation increases in size: it increases from 2.11 Å for LiHB to 3.22 Å for CsHB. In terms of destabilization, RbHB and CsHB exhibit enhanced dehydrogenation properties compared to HB; however, the $H_2$ released by both hydrazinidoboranes was polluted with some volatile byproducts. In addition, the heaviest alkali hydrazinidoboranes carry a lower quantity of hydrogen (Figure 19). Some strategies to improve the dehydrogenation performance of alkali hydrazinidoboranes include the use of dopants such as NaH, or obtaining MHB ammoniates [314,315].

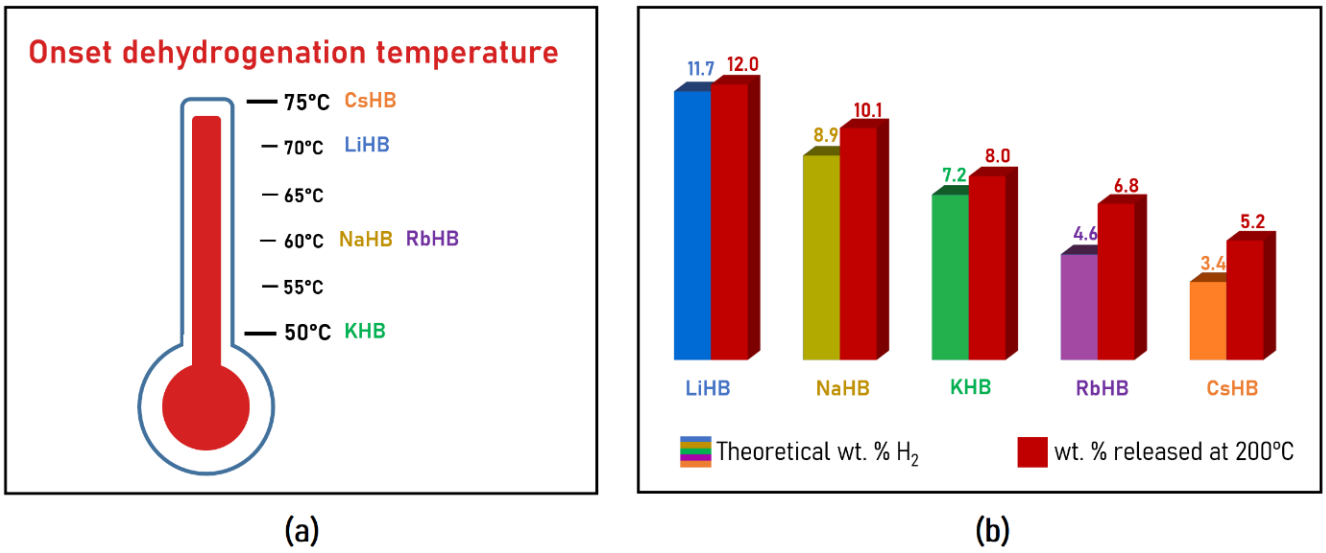


**Figure 19.** (**a**) Onset temperature of dehydrogenation; (**b**) theoretical hydrogen gravimetric capacity vs. weight loss at 200 °C of the alkali hydrazinidoboranes.

#### 8.2.2. Alkaline Earth Hydrazinidoboranes

In our group, different attempts to obtain alkaline earth hydrazinidoboranes ($M(HB)_2$) have been performed, but most of them were unsuccessful. It seems that the synthesis of

these compounds is elusive. For example, the direct ball milling of a mixture of HB with $MgH_2$ or $CaH_2$ leads to the formation of a composite composed of unreacted HB, $CaH_2$ or $MgH_2$ and some amorphous species [307]. The mixing of solubilized HB in THF or 1,4-dioxane and the solid metal hydride produces similar results. However, after various attempts, the synthesis of magnesium hydrazinidoborane ($Mg(HB)_2$, $Mg(N_2H_3BH_3)_2$, 10.6 wt. % $H_2$) and calcium hydrazinidoborane ($Ca(HB)_2$, $Ca(N_2H_3BH_3)_2$, 9.3 wt. % $H_2$) was finally reported [316,317]. In the case of $Ca(HB)_2$, a mixture of HB and $CaH_2$ has to be ball-milled. Then, a particular heat treatment has to be performed—heating the HB/$CaH_2$ mixture at 62 °C for 50 min; after this, the mixture needs to be cooled down rapidly to room temperature. $Ca(HB)_2$ forms around 60 °C, the temperature at which HB melts, and the reaction takes place between the solid $CaH_2$ and the melted HB. Unfortunately, the obtained product was composed of 71% $Ca(HB)_2$ and 29% $CaH_2$. $Ca(HB)_2$ is a crystalline compound with a monoclinic unit cell (*Ic* s.g.) (Figure 20). The insertion of $Ca^+$ into the molecule slightly changes the bond distance of HB, which explains the similar electron repartition around the B atom, in comparison to HB [316]. $Ca(HB)_2$ showed a main decomposition between 90 °C and 170 °C, releasing 5.3 wt. % gas. During decomposition, unwanted volatile gases were detected, such as $N_2$, $NH_3$ and $N_2H_4$. $CaHB_2$ showed better dehydrogenation proprieties than HB; however, it remains less efficient than the MHB or the composite HB/$CaH_2$.

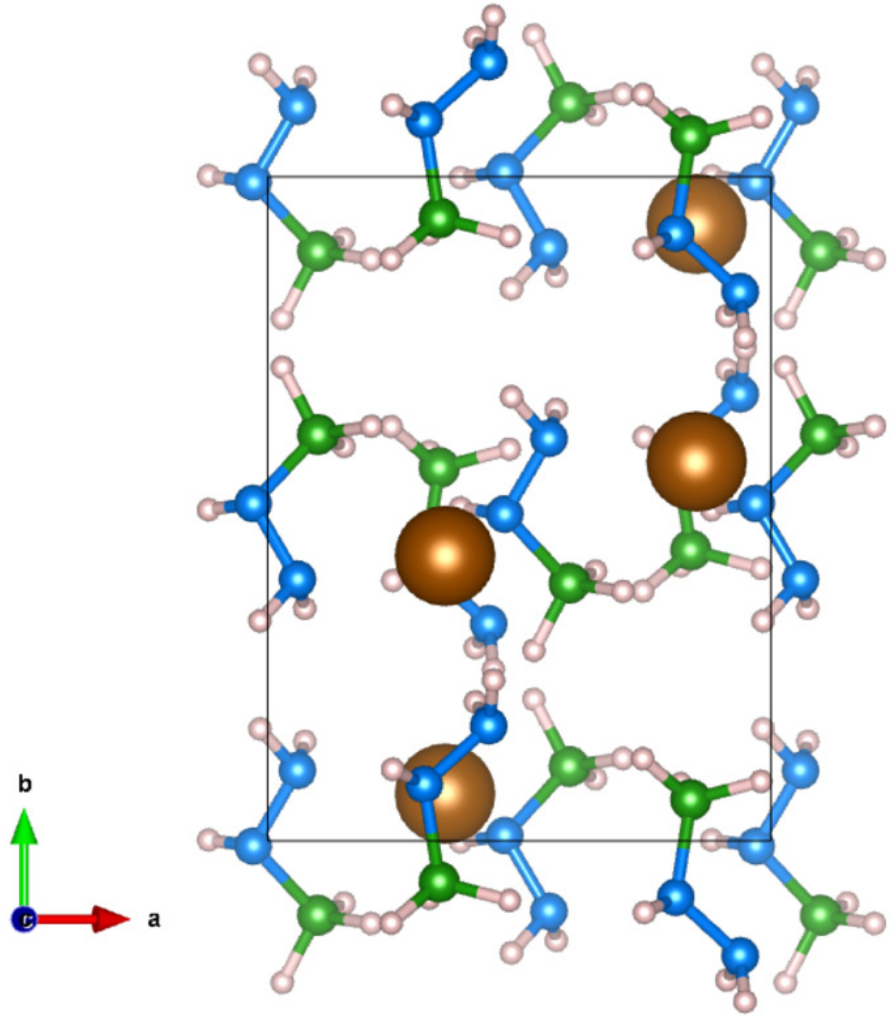


**Figure 20.** Crystal structure of $Ca(HB)_2$ along the [001] direction. The H, B, N and Ca atoms are represented by pink, green, blue and brown spheres, respectively.

$Mg(HB)_2$ was prepared using a solvent-based approach [317]. Di-n-butylmagnesium was used as the Mg precursor, and it was added dropwise into a HB solution in THF. In contrast with all previous hydrazinidoboranes, $Mg(HB)_2$ showed a higher stability than the parent HB. $Mg(HB)_2$ presented a first mass loss of 6 wt. % up to 120 °C, releasing $N_2$ and some $H_2$. Temperatures above 180 °C are required to release the rest of the $H_2$, alongside $N_2$, $NH_3$ and $N_2H_4$. Through this study, different dehydrogenation behaviors of hydrazinidoboranes were observed, depending on whether the thermal treatment was performed in an open or closed system. In the particular case of $Mg(HB)_2$, when heated in a closed system, the dehydrogenation took place mainly via homopolar interactions between the $H^{\delta+}$ of the molecule. Unfortunately, $Mg(HB)_2$ presented an amorphous structure, and no further information about the interatomic distances could be obtained.

### *8.3. General Remarks*

The dehydrogenation behavior of HB is determined by destabilizing the compound using alkali and alkaline earth hydrides. Through the chemical modification of AB, hydrazinidoboranes are synthesized, which have presented improved dehydrogenation properties in comparison with the parent borane. All the alkali derivatives of HB have been obtained, but in comparison with these, the alkaline earth hydrazinidobones are more difficult to obtain due to a lower reactivity between HB and the alkaline earth precursors. To date, only the magnesium and calcium derivatives have been reported. However, as in the case of AB, the lack of reversibility of hydrazinidoboranes is still a challenge in the field.

## 9. Hydrazine Bisborane

Another derivative of AB, hydrazine bisborane (HBB, $N_2H_4(BH_3)_2$, 16.8 wt. % $H_2$), has been considered as a candidate for hydrogen (storage applications due to its high hydrogen gravimetric density. HBB is a crystalline compound that presents two phases, both orthorhombic with a *Pbca* s.g. and different unit cell parameters, with a reversible transition between the α-HBB and the α'-HBB phases in the 10 °C–17 °C range [69]. However, it has been reported that when HBB is heated with a rate of 10 °C $min^{-1}$ it explodes at about 170 °C [69]. For this reason, HBB is not a good candidate for storage applications in the solid state. Only six works (according to the Web of Science) have been published since 2015 regarding HBB. None of these investigated the destabilization of the molecule. There was one work published in 2014 which reported the synthesis of the lithium derivative of HBB [318]. Lithium hydrazidobisborane (LiHBB, $LiN_2H_3(BH_3)_2$) was obtained through the reaction between HBB and n-butyllithium in $EtO_2$. This compound started to decompose at about 100 °C and released 8.2 wt. % $H_2$ up to 350 °C, avoiding the emission of volatile byproducts. The dehydrogenation of LiHBB is less exothermic than the parent HBB. It is possible that other derivatives of HBB can be envisaged as potential materials for hydrogen storage applications. In this way, the safety risks related to the use of HBB could be avoided.

## 10. Conclusions and Opportunities

The destabilization strategies in the solid state for seven selected boron-based compounds have been analyzed through this review. It is clear that light-weight borohydrides have the potential to work as materials for hydrogen storage applications. However, there are still many challenges ahead. The first of these is the reversibility of the systems. Many of the composites analyzed in this work showed low reversibility and, even worse, decaying of the storage capacity with every cycle of dehydrogenation/rehydrogenation. In the case of $LiBH_4$, a promising approach seems to be the use of graphene decorated with Ni-nanoparticles. The works presented in Section 4.1.4 showed a remarkable reversibility, maintaining the storage capacity even after 100 cycles. The key to achieving a good performance is to avoid the formation of closo-hydridoborates, which hinder the reversibility

of the system. The nanoconfinement or nanosizing of borohydrides is also a promising approach. In this way, the suppression of byproducts and the avoidance of the formation of closo-hydridoborates is generally achieved.

If we consider a system based on a nanoconfined compound, various factors have to be considered to attain a feasible system. One of them is the overall weight of the system. If the loading of the compound inside the scaffold is low, the practical hydrogen capacity is reduced. In the same way, heavier scaffolds can decrease the overall capacity of the system. Another important issue related to nanoconfinement is the chemical nature of the scaffold. For example, when O atoms are present on the surface of the scaffold, this leads to their interaction with the B atoms, forming B-O bonds. These bonds are almost as stable as the C-O bond from carbon dioxide, which implies that the rehydrogenation of B-O is challenging. Any B atom involved in a B-O bond would be lost to regenerate $BH_4^-$ (or $BH_3$ groups in the case of the boranes). This is another obstacle in regard to acquiring an acceptable net storage capacity. It is therefore crucial to focus on O-free scaffolds. Another important point to consider is that for some composites, the species formed in situ have a double role in the dehydrogenation of the B-based material: on the one hand, they act as catalysts for the dehydrogenation reaction; on the other hand, they hamper the reversibility of the system. In this way, the fast delivery of $H_2$ is achieved, but with a low reversibility; a practical equilibrium between these two effects should be considered.

One perspective in relation to these materials is the use of catalytically doped scaffolds, which are scaffolds decorated with metal nanoparticles that are able to act as hydrogen catalysts. These metal nanoparticles would be expected to catalyze the hydrogenation of the spent fuels in the presence of $H_2$, at temperatures slightly higher than room temperature. In some way, the objective would be to learn from what has been accomplished to date with the hydrogenation of unsaturated compounds in the oil industry.

AB, HB and HBB have been studied as potential materials for hydrogen storage. The use of pristine AB and HB in the solid state is difficult due to the emission of several byproducts. Even through destabilization strategies have improved the dehydrogenation properties of these boranes, a large challenge remains—the regeneration of such compounds is difficult. The thermal decomposition of AB, HB and HBB leads to the formation of B- and N-based polymers of complex composition. At higher temperatures, the final product of these boranes is boron nitride (BN). As the dehydrogenation of these boranes is exothermic, the rehydrogenation of these polymers (or BN) is non-favorable. Different approaches have been explored in order to achieve the regeneration of AB from these compounds. The general idea is (i) to digest the solid thermolysis residues, (ii) to ammoniate the intermediates and (iii) to perform a chemical reduction [52,319,320]. Nevertheless, it has been difficult to obtain high yields of regeneration. The regeneration of BN to AB has also been reported [321], though the regeneration yield is <5%. Thus, the regeneration of AB, HB and HBB remains as the main challenge for these compounds. The chemical modification of HBB has been scarcely investigated. The synthesis of alkali derivatives of HBB seems to reduce the risk of explosion associated with this compound. Thus, the obtention of alkali derivatives of HBB might open up an opportunity to explore new compounds with potential for hydrogen storage applications.

To date, all of the strategies developed to destabilize AB have aimed at decreasing its dehydrogenation temperature, but without any target and limit. There have been examples in which AB has released $H_2$ between 40 °C and 60 °C, or even at lower temperatures due to acid–base reactions catalyzing the overall process. These results raise one critical question, when the final applications are considered: Is it relevant and realistic to have a hydrogen carrier that releases $H_2$ at 40 °C–60 °C, when this temperature can be easily reached in summertime? This leads to another question: Would it not be more relevant to target a dehydrogenation temperature in line with the operation temperature of fuel cells? We believe that these questions should be considered for future developments.

Finally, in recent years, the field of $H_2$ was given a big push through the creation of roadmaps supported by decision-makers. Laboratories and industry have started to gain substantial political and financial support, and this has provided a great opportunity that researchers have been waiting for. Furthermore, this is the perfect opportunity to devote much more effort to the scaling up of these systems, and on reaching technological readiness levels beyond level 5. In other words, the start of the 2020s should be seen as the time for producing demonstrators and prototypes, so that technologies with commercial potential can emerge in the second half of the 2020s.

Due to their high gravimetric hydrogen density, B-based compounds could be considered for portable and mobile applications over the next five years, such as small-unmanned aircraft systems; and ultimately as fuel for vehicles, if the production and reversibility issues can be addressed. We also believe that reversibility represents the main bottleneck for these compounds. Accordingly, $LiBH_4$ has the best chances to be scaled up due to its favorable reversibility and its high storage capacity. We consider that it might be worthwhile to scale up a synthesis process of confined $LiBH_4$ into decorated porous media and then to evaluate its performance at a larger scale. It will be desirable to reach a TRL of 4–5. $NaBH_4$ has shown a good potential to be used for hydrogen storage, if not in the solid state, by means of its hydrolysis. As discussed above, the main challenge for AB is its regeneration. The use of AB (as well as its alkaline derivatives, such as LiAB and NaAB) at a larger scale is desirable, but it might perhaps be useful to scale up a regeneration process for these compounds with an acceptable yield at the same time. To find an appropriate catalyst to form a single polymeric residue from AB (preferably polyborazylene) is desirable as well. However, reversible storage of $H_2$ by AB cannot be completely ruled out, since 1 wt. % $H_2$ of reversibility was observed for AB oligomers in the presence of Ni nanoparticles [305]; the key may lie in the catalytic hydrogenation of unsaturated B-N bonds.

Research groups and industry should work together to achieve such goals and to channel their efforts for a greener future.

**Author Contributions:** Conceptualization, C.A.C.-M.; resources, C.A.C.-M., R.M., S.O.-A. and U.B.D.; investigation C.A.C.-M., R.M., S.O.-A. and U.B.D.; writing—original draft preparation, C.A.C.-M., R.M., S.O.-A. and U.B.D.; writing—review and editing, C.A.C.-M., R.M., S.O.-A. and U.B.D.; supervision, C.A.C.-M. All authors have read and agreed to the published version of the manuscript.

**Funding:** This research received no external funding.

**Conflicts of Interest:** The authors declare no conflict of interest.

## References

1. Al-Ghussain, L. Global warming: Review on driving forces and mitigation. *Environ. Prog. Sustain. Energy* **2019**, *38*, 13–21. [CrossRef]
2. Oliveira, A.M.; Beswick, R.R.; Yan, Y. A green hydrogen economy for a renewable energy society. *Curr. Opin. Chem. Eng.* **2021**, *33*, 100701. [CrossRef]
3. Brandon, N.P.; Kurban, Z. Clean energy and the hydrogen economy. *Phil. Trans. R. Soc. A* **2017**, *375*, 1–17. [CrossRef]
4. Abdalla, A.M.; Hossain, S.; Nisfindy, O.B.; Azad, A.T.; Dawood, M.; Azad, A.K. Hydrogen production, storage, transportation and key challenges with applications: A review. *Energy Convers. Manag.* **2018**, *165*, 602–627. [CrossRef]
5. Moradi, R.; Groth, K.M. Hydrogen storage and delivery: Review of the state of the art technologies and risk and reliability analysis. *Int. J. Hydrogen Energy* **2019**, *44*, 12254–12269. [CrossRef]
6. Sinigaglia, T.; Lewiski, F.; Santos Martins, M.E.; Mairesse Siluk, J.C. Production, storage, fuel stations of hydrogen and its utilization in automotive applications-a review. *Int. J. Hydrogen Energy* **2017**, *42*, 24597–24611. [CrossRef]
7. Gupta, A.; Baron, G.V.; Perreault, P.; Lenaerts, S.; Ciocarlan, R.-G.; Cool, P.; Mileo, P.G.M.; Rogge, S.; Van Speybroeck, V.; Watson, G.; et al. Hydrogen clathrates: Next generation hydrogen storage materials. *Energy Storage Mater.* **2021**, *41*, 69–107. [CrossRef]
8. Kojima, Y. Hydrogen storage materials for hydrogen and energy carriers. *Int. J. Hydrogen Energy* **2019**, *44*, 18179–18192. [CrossRef]
9. Yu, X.; Tang, Z.; Sun, D.; Ouyang, L.; Zhu, M. Recent advances and remaining challenges of nanostructured materials for hydrogen storage applications. *Prog. Mater. Sci.* **2017**, *88*, 1–48. [CrossRef]

10. Gangu, K.K.; Maddila, S.; Mukkamala, S.B.; Jonnalagadda, S.B. Characteristics of MOF, MWCNT and graphene containing materials for hydrogen storage: A review. *J. Energy Chem.* **2019**, *30*, 132–144. [CrossRef]
11. Ren, J.; Musyoka, N.M.; Langmi, H.W.; Mathe, M.; Liao, S. Current research trends and perspectives on materials-based hydrogen storage solutions: A critical review. *Int. J. Hydrogen Energy* **2017**, *42*, 289–311. [CrossRef]
12. Rao, P.C.; Yoon, M. Potential liquid-organic hydrogen carrier (LOHC) systems: A review on recent progress. *Energies* **2020**, *13*, 6040. [CrossRef]
13. Niermann, M.; Timmerberg, S.; Drünert, S.; Kaltschmitt, M. Liquid organic hydrogen carriers and alternatives for international transport of renewable hydrogen. *Renew. Sustain. Energy Rev.* **2021**, *135*, 110171. [CrossRef]
14. Aziz, M.; Wijayanta, A.T.; Nandiyanto, A.B.D. Ammonia as effective hydrogen storage: A review on production, storage and utilization. *Energies* **2020**, *13*, 3062. [CrossRef]
15. Moussa, G.; Moury, R.; Demirci, U.B.; Şener, T.; Miele, P. Boron-based hydrides for chemical hydrogen storage. *Int. J. Energy Res.* **2013**, *37*, 825–842. [CrossRef]
16. Umegaki, T.; Yan, J.M.; Zhang, X.B.; Shioyama, H.; Kuriyama, N.; Xu, Q. Boron- and nitrogen-based chemical hydrogen storage materials. *Int. J. Hydrogen Energy* **2009**, *34*, 2303–2311. [CrossRef]
17. Abdelhamid, H.N. A review on hydrogen generation from the hydrolysis of sodium borohydride. *Int. J. Hydrogen Energy* **2021**, *46*, 726–765. [CrossRef]
18. Li, H.; Yang, Q.; Chen, X.; Shore, S.G. Ammonia borane, past as prolog. *J. Organomet. Chem.* **2014**, *751*, 60–66. [CrossRef]
19. Schlesinger, H.I.; Brown, H.C.; Hoekstra, H.R.; Rapp, L.R. Reactions of diborane with alkali metal hydrides and their addition compounds. new syntheses of borohydrides. Sodium and potassium borohydrides 1. *J. Am. Chem. Soc.* **1953**, *75*, 199–204. [CrossRef]
20. Schlesinger, H.I.; Brown, H.C.; Finholt, A.E.; Gilbreath, J.R.; Hoekstra, H.R.; Hyde, E.K. Sodium borohydride, its hydrolysis and its use as a reducing agent and in the generation of hydrogen. *J. Am. Chem. Soc.* **1953**, *75*, 215–219. [CrossRef]
21. Fakioglu, E.; Yürüm, Y.; Veziroglu, T.N. A review of hydrogen storage systems based on boron and its compounds. *Int. J. Hydrogen Energy* **2004**, *29*, 1371–1376. [CrossRef]
22. Zhang, J.; Fisher, T.; Gore, J.; Hazra, D.; Ramachandran, P. Heat of reaction measurements of sodium borohydride alcoholysis and hydrolysis. *Int. J. Hydrogen Energy* **2006**, *31*, 2292–2298. [CrossRef]
23. Nunes, H.X.; Silva, D.L.; Rangel, C.M.; Pinto, A.M.F.R. Rehydrogenation of sodium borates to close the $NaBH_4$-$H_2$ cycle: A review. *Energies* **2021**, *14*, 3567. [CrossRef]
24. Le, T.T.; Pistidda, C.; Puszkiel, J.; Milanese, C.; Garroni, S.; Emmler, T.; Capurso, G.; Gizer, G.; Klassen, T.; Dornheim, M. Efficient synthesis of alkali borohydrides from mechanochemical reduction of borates using magnesium–aluminum-based waste. *Metals* **2019**, *9*, 1061. [CrossRef]
25. Schlesinger, H.I.; Sanderson, R.T.; Burg, A.B. Metallo borohydrides. I. Aluminum borohydride. *J. Am. Chem. Soc.* **1940**, *62*, 3421–3425. [CrossRef]
26. Burg, A.B.; Schlesinger, H.I. Metallo borohydrides. II. Beryllium borohydride. *J. Am. Chem. Soc.* **1940**, *62*, 3425–3429. [CrossRef]
27. Schlesinger, H.I.; Brown, H.C. Metallo borohydrides. III. Lithium borohydride. *J. Am. Chem. Soc.* **1940**, *62*, 3429–3435. [CrossRef]
28. Schlesinger, H.I.; Brown, H.C.; Schaeffer, G.W. The borohydrides of gallium. *J. Am. Chem. Soc.* **1943**, *65*, 1786–1787. [CrossRef]
29. Schlesinger, H.I.; Brown, H.C. Uranium(IV) borohydride. *J. Am. Chem. Soc.* **1953**, *75*, 219–221. [CrossRef]
30. Zhang, W.; Zhang, X.; Huang, Z.; Li, H.-W.; Gao, M.; Pan, H.; Liu, Y. Recent development of lithium borohydride-based materials for hydrogen storage. *Adv. Energy Sustain. Res.* **2021**, *2*, 2100073. [CrossRef]
31. Orimo, S.I.; Nakamori, Y.; Eliseo, J.R.; Züttel, A.; Jensen, C.M. Complex hydrides for hydrogen storage. *Chem. Rev.* **2007**, *107*, 4111–4132. [CrossRef] [PubMed]
32. Orimo, S.-I.; Nakamori, Y.; Ohba, N.; Miwa, K.; Aoki, M.; Towata, S.; Züttel, A. Experimental studies on intermediate compound of $LiBH_4$. *Appl. Phys. Lett.* **2006**, *89*, 021920. [CrossRef]
33. Orimo, S.; Nakamori, Y.; Kitahara, G.; Miwa, K.; Ohba, N.; Towata, S.; Züttel, A. Dehydriding and rehydriding reactions of $LiBH_4$. *J. Alloys Compd.* **2005**, *404–406*, 427–430. [CrossRef]
34. Matsunaga, T.; Buchter, F.; Mauron, P.; Bielman, M.; Nakamori, Y.; Orimo, S.; Ohba, N.; Miwa, K.; Towata, S.; Züttel, A. Hydrogen storage properties of $Mg[BH_4]_2$. *J. Alloys Compd.* **2008**, *459*, 583–588. [CrossRef]
35. Li, H.-W.; Miwa, K.; Ohba, N.; Fujita, T.; Sato, T.; Yan, Y.; Towata, S.; Chen, M.W.; Orimo, S. Formation of an intermediate compound with a $B_{12}H_{12}$ cluster: Experimental and theoretical studies on magnesium borohydride $Mg(BH_4)_2$. *Nanotechnology* **2009**, *20*, 204013. [CrossRef] [PubMed]
36. Miwa, K.; Aoki, M.; Noritake, T.; Ohba, N.; Nakamori, Y.; Towata, S.; Züttel, A.; Orimo, S. Thermodynamical stability of calcium borohydride $Ca(BH_4)_2$. *Phys. Rev. B* **2006**, *74*, 155122. [CrossRef]
37. Kim, J.-H.; Shim, J.-H.; Cho, Y.W. On the reversibility of hydrogen storage in Ti- and Nb-catalyzed $Ca(BH_4)_2$. *J. Power Sources* **2008**, *181*, 140–143. [CrossRef]
38. Demirci, U.B. Impact of H.I. Schlesinger's discoveries upon the course of modern chemistry on B−(N−)H hydrogen carriers. *Int. J. Hydrogen Energy* **2017**, *42*, 21048–21062. [CrossRef]
39. Shore, S.G.; Parry, R.W. The crystalline compound ammonia borane,[1] $H_3NBH_3$. *J. Am. Chem. Soc.* **1955**, *77*, 6084–6085. [CrossRef]
40. Ramachandran, P.V.; Gagare, P.D. Preparation of ammonia borane in high yield and purity, methanolysis, and regeneration. *Inorg. Chem.* **2007**, *46*, 7810–7817. [CrossRef]

41. Demirci, U.B. Ammonia borane: An extensively studied, though not yet implemented, hydrogen carrier. *Energies* **2020**, *13*, 3071. [CrossRef]
42. Alpaydin, C.Y.; Gülbay, S.K.; Colpan, C.O. A review on the catalysts used for hydrogen production from ammoniaborane. *Int. J. Energy Res.* **2020**, *45*, 3414–3434. [CrossRef]
43. Demirci, U.B. About the technological readiness of the $H_2$ generation by hydrolysis of B(−N)−H compounds. *Energy Technol.* **2018**, *6*, 470–486. [CrossRef]
44. Brockman, A.; Zheng, Y.; Gore, J. A study of catalytic hydrolysis of concentrated ammonia borane solutions. *Int. J. Hydrogen Energy* **2010**, *35*, 7350–7356. [CrossRef]
45. Chandra, M.; Xu, Q. Dissociation and hydrolysis of ammonia-borane with solid acids and carbon dioxide: An efficient hydrogen generation system. *J. Power Sources* **2006**, *159*, 855–860. [CrossRef]
46. Li, H.; Yan, Y.; Feng, S.; Chen, Y.; Fan, H. Ammonia borane and its applications in the advanced energy technology. *J. Energy Resour. Technol.* **2021**, *143*. [CrossRef]
47. Kantürk Figen, A.; Pişkin, M.B.; Coşkuner, B.; Imamoğlu, V. Synthesis, structural characterization, and hydrolysis of Ammonia Borane ($NH_3BH_3$) as a hydrogen storage carrier. *Int. J. Hydrogen Energy* **2013**, *38*, 16215–16228. [CrossRef]
48. Roy, B.; Pal, U.; Bishnoi, A.; O'Dell, L.A.; Sharma, P. Exploring the homopolar dehydrocoupling of ammonia borane by solid-state multinuclear NMR spectroscopy. *Chem. Commun.* **2021**, 1887–1890. [CrossRef] [PubMed]
49. Chen, X.; Zhao, J.C.; Shore, S.G. The roles of dihydrogen bonds in amine borane chemistry. *Acc. Chem. Res.* **2013**, *46*, 2666–2675. [CrossRef]
50. Baitalow, F.; Baumann, J.; Wolf, G.; Jaenicke-Rößler, K.; Leitner, G. Thermal decomposition of B–N–H compounds investigated by using combined thermoanalytical methods. *Thermochim. Acta* **2002**, *391*, 159–168. [CrossRef]
51. Hu, M.G.; Geanangel, R.A.; Wendlandt, W.W. The thermal decomposition of ammonia borane. *Thermochim. Acta* **1978**, *23*, 249–255. [CrossRef]
52. Summerscales, O.T.; Gordon, J.C. Regeneration of ammonia borane from spent fuel materials. *Dalt. Trans.* **2013**, *42*, 10075–10084. [CrossRef] [PubMed]
53. Frueh, S.; Kellett, R.; Mallery, C.; Molter, T.; Willis, W.S.; King'Ondu, C.; Suib, S.L. Pyrolytic decomposition of ammonia borane to boron nitride. *Inorg. Chem.* **2011**, *50*, 783–792. [CrossRef] [PubMed]
54. Kostoglou, N.; Polychronopoulou, K.; Rebholz, C. Thermal and chemical stability of hexagonal boron nitride (h-BN) nanoplatelets. *Vacuum* **2015**, *112*, 42–45. [CrossRef]
55. Sit, V.; Geanangel, R.A.; Wendlandt, W.W. The thermal dissociation of $NH_3BH_3$. *Thermochim. Acta* **1987**, *113*, 379–382. [CrossRef]
56. Sutton, A.D.; Burrell, A.K.; Dixon, D.A.; Garner, E.B.; Gordon, J.C.; Nakagawa, T.; Ott, K.C.; Robinson, J.P.; Vasiliu, M. Regeneration of ammonia borane spent fuel by direct reaction with hydrazine and liquid ammonia. *Science* **2011**, *331*, 1426–1429. [CrossRef] [PubMed]
57. Schlesinger, H.I.; Burg, A.B. Hydrides of boron. VIII. The structure of the diammoniate of diborane and its relation to the structure of diborane. *J. Am. Chem. Soc.* **1938**, *60*, 290–299. [CrossRef]
58. Myers, A.G.; Yang, B.H.; Kopecky, D.J. Lithium amidotrihydroborate, a powerful new reductant. Transformation of tertiary amides to primary alcohols. *Tetrahedron Lett.* **1996**, *37*, 3623–3626. [CrossRef]
59. Diyabalanage, H.V.K.; Shrestha, R.P.; Semelsberger, T.A.; Scott, B.L.; Bowden, M.E.; Davis, B.L.; Burrell, A.K. Calcium amidotrihydroborate: A hydrogen storage material. *Angew. Chemie–Int. Ed.* **2007**, *46*, 8995–8997. [CrossRef] [PubMed]
60. Xiong, Z.; Yong, C.K.; Wu, G.; Chen, P.; Shaw, W.; Karkamkar, A.; Autrey, T.; Jones, M.O.; Johnson, S.R.; Edwards, P.P.; et al. High-capacity hydrogen storage in lithium and sodium amidoboranes. *Nat. Mater.* **2008**, *7*, 138–141. [CrossRef] [PubMed]
61. Owarzany, R.; Leszczyński, P.J.; Fijalkowski, K.J.; Grochala, W. Mono- and bimetalic amidoboranes. *Crystals* **2016**, *6*, 88. [CrossRef]
62. Staubitz, A.; Robertson, A.P.M.; Sloan, M.E.; Manners, I. Amine– and phosphine–borane adducts: New interest in old molecules. *Chem. Rev.* **2010**, *110*, 4023–4078. [CrossRef]
63. Goubeau, J.; Ricker, E. Borinhydrazin und seine pyrolyseprodukte. *Z. Anorg. Allg. Chem.* **1961**, *310*, 123–142. [CrossRef]
64. Yurderi, M.; Top, T.; Bulut, A.; Kanberoglu, G.S.; Kaya, M.; Zahmakiran, M. Complete dehydrogenation of hydrazine borane on manganese oxide nanorod-supported Ni@Ir core–shell nanoparticles. *Inorg. Chem.* **2020**, *59*, 9728–9738. [CrossRef]
65. Lu, Z.-H.; Yao, Q.; Zhang, Z.; Yang, Y.; Chen, X. Nanocatalysts for hydrogen generation from ammonia borane and hydrazine borane. *J. Nanomater.* **2014**, *2014*, 1–11. [CrossRef]
66. Hügle, T.; Kühnel, M.F.; Lentz, D. Hydrazine borane: A promising hydrogen storage material. *J. Am. Chem. Soc.* **2009**, *131*, 7444–7446. [CrossRef] [PubMed]
67. Moury, R.; Moussa, G.; Demirci, U.B.; Hannauer, J.; Bernard, S.; Petit, E.; Van Der Lee, A.; Miele, P. Hydrazine borane: Synthesis, characterization, and application prospects in chemical hydrogen storage. *Phys. Chem. Chem. Phys.* **2012**, *14*, 1768–1777. [CrossRef] [PubMed]
68. Gunderloy, F.C.; Spielvogel, B.; Parry, R.W. Hydrazine-mono- and -bisborane. *Inorg. Synth.* **1967**, *9*, 13–16. [CrossRef]
69. Pylypko, S.; Petit, E.; Yot, P.G.; Salles, F.; Cretin, M.; Miele, P.; Demirci, U.B. Key study on the potential of hydrazine bisborane for solid- and liquid-state chemical hydrogen storage. *Inorg. Chem.* **2015**, *54*, 4574–4583. [CrossRef] [PubMed]
70. Sun, W.; Gu, Q.; Guo, Y.; Guo, Z.; Liu, H.; Yu, X. Hydrazine bisborane as a promising material for chemical hydrogen storage. *Int. J. Hydrogen Energy* **2011**, *36*, 13640–13644. [CrossRef]
71. Harris, P.M.; Meibohm, E.P. The crystal structure of lithium borohydride $LiBH_4$. *J. Am. Chem. Soc.* **1947**, *69*, 1231–1232. [CrossRef]

72. El Kharbachi, A.; Pinatel, E.; Nuta, I.; Baricco, M. A thermodynamic assessment of $LiBH_4$. *Calphad Comput. Coupling Phase Diagrams Thermochem.* **2012**, *39*, 80–90. [CrossRef]
73. Züttel, A.; Rentsch, S.; Fischer, P.; Wenger, P.; Sudan, P.; Mauron, P.; Emmenegger, C. Hydrogen storage properties of $LiBH_4$. *J. Alloys Compd.* **2003**, *356–357*, 515–520. [CrossRef]
74. Pitt, M.P.; Paskevicius, M.; Brown, D.H.; Sheppard, D.A.; Buckley, C.E. Thermal stability of $Li_2B_{12}H_{12}$ and its role in the decomposition of $LiBH_4$. *J. Am. Chem. Soc.* **2013**, *135*, 6930–6941. [CrossRef]
75. Friedrichs, O.; Remhof, A.; Hwang, S.J.; Züttel, A. Role of $Li_2B_{12}H_{12}$ for the formation and decomposition of $LiBH_4$. *Chem. Mater.* **2010**, *22*, 3265–3268. [CrossRef]
76. Tu, G.; Xiao, X.; Qin, T.; Jiang, Y.; Li, S.; Ge, H.; Chen, L. Significantly improved de/rehydrogenation properties of lithium borohydride modified with hexagonal boron nitride. *RSC Adv.* **2015**, *5*, 51110–51115. [CrossRef]
77. Zhu, J.; Wang, H.; Cai, W.; Liu, J.; Ouyang, L.; Zhu, M. The milled $LiBH_4$/h-BN composites exhibiting unexpected hydrogen storage kinetics and reversibility. *Int. J. Hydrogen Energy* **2017**, *42*, 15790–15798. [CrossRef]
78. Cai, W.; Hou, J.; Tao, P.; Yang, Y. An insight into the dehydrogenation behaviour of $LiBH_4$ exhibiting remarkable kinetics enhanced by nanostructured h-BN. *J. Alloys Compd.* **2018**, *750*, 443–450. [CrossRef]
79. Zhu, J.; Wang, H.; Liu, J.; Ouyang, L.; Zhu, M. Achieving high dehydrogenation kinetics and reversibility of $LiBH_4$ by adding nanoporous h-BN to destabilize LiH. *J. Phys. Chem. C* **2018**, *122*, 23336–23344. [CrossRef]
80. Muthu, R.N.; Rajashabala, S.; Kannan, R. Hydrogen storage performance of lithium borohydride decorated activated hexagonal boron nitride nanocomposite for fuel cell applications. *Int. J. Hydrogen Energy* **2017**, *42*, 15586–15596. [CrossRef]
81. Tu, G.; Xiao, X.; Jiang, Y.; Qin, T.; Li, S.; Ge, H.; Wang, Q.; Chen, L. Composite cooperative enhancement on the hydrogen desorption kinetics of $LiBH_4$ by co-doping with $NbCl_5$ and hexagonal BN. *Int. J. Hydrogen Energy* **2015**, *40*, 10527–10535. [CrossRef]
82. Ma, Y.; Li, Y.; Liu, T.; Zhao, X.; Zhang, L.; Han, S.; Wang, Y. Enhanced hydrogen storage properties of $LiBH_4$ generated using a porous $Li_3BO_3$ catalyst. *J. Alloys Compd.* **2016**, *689*, 187–191. [CrossRef]
83. Li, Z.; Gao, M.; Gu, J.; Xian, K.; Yao, Z.; Shang, C.; Liu, Y.; Guo, Z.; Pan, H. In situ introduction of $Li_3BO_3$ and NbH leads to superior cyclic stability and kinetics of a $LiBH_4$-based hydrogen storage system. *ACS Appl. Mater. Interfaces* **2020**, *12*, 893–903. [CrossRef] [PubMed]
84. Wu, Y.; Jiang, X.; Chen, J.; Qi, Y.; Zhang, Y.; Fu, H.; Zheng, J.; Li, X. Boric acid destabilized lithium borohydride with a 5.6 wt% dehydrogenation capacity at moderate temperatures. *Dalt. Trans.* **2017**, *46*, 4499–4503. [CrossRef] [PubMed]
85. Roedern, E.; Hansen, B.R.S.; Ley, M.B.; Jensen, T.R. Effect of eutectic melting, reactive hydride composites, and nanoconfinement on decomposition and reversibility of $LiBH_4$-$KBH_4$. *J. Phys. Chem. C* **2015**, *119*, 25818–25825. [CrossRef]
86. Frommen, C.; Heere, M.; Riktor, M.D.; Sørby, M.H.; Hauback, B.C. Hydrogen storage properties of rare earth (RE) borohydrides (RE = La, Er) in composite mixtures with $LiBH_4$ and LiH. *J. Alloys Compd.* **2015**, *645*, S155–S159. [CrossRef]
87. Liu, Y.; Reed, D.; Paterakis, C.; Contreras Vasquez, L.; Baricco, M.; Book, D. Study of the decomposition of a $0.62LiBH_4$–$0.38NaBH_4$ mixture. *Int. J. Hydrogen Energy* **2017**, *42*, 22480–22488. [CrossRef]
88. Wang, L.; Rawal, A.; Quadir, M.Z.; Aguey-Zinsou, K.F. Nanoconfined lithium aluminium hydride ($LiAlH_4$) and hydrogen reversibility. *Int. J. Hydrogen Energy* **2017**, *42*, 14144–14153. [CrossRef]
89. He, Q.; Zhu, D.; Wu, X.; Dong, D.; Xu, M.; Tong, Z. Hydrogen desorption properties of $LiBH_4$/x$LiAlH_4$ (x = 0.5, 1, 2) composites. *Molecules* **2019**, *24*, 1861. [CrossRef]
90. Gu, R.; Wang, C.Y.; Liu, D.M.; Gao, C.; Li, Y.T.; Si, T.Z. De-/rehydrogenation properties and reaction mechanisms of $4LiBH_4$-$LiAlH_4$-$MgF_2$ system. *Int. J. Hydrogen Energy* **2015**, *40*, 10536–10541. [CrossRef]
91. Thaweelap, N.; Utke, R. Dehydrogenation kinetics and reversibility of $LiAlH_4$–$LiBH_4$ doped with Ti-based additives and MWCNT. *J. Phys. Chem. Solids* **2016**, *98*, 149–155. [CrossRef]
92. Li, Z.; Wang, H.; Ouyang, L.; Liu, J.; Zhu, M. Enhanced dehydrogenation of $LiBH_4{\cdot}NH_3$–$LiAlH_4$ composites. *Int. J. Hydrogen Energy* **2017**, *42*, 22406–22410. [CrossRef]
93. Halim Yap, F.A.; Ali, N.A.; Idris, N.H.; Ismail, M. Catalytic effect of $MgFe_2O_4$ on the hydrogen storage properties of $Na_3AlH_6$–$LiBH_4$ composite system. *Int. J. Hydrogen Energy* **2018**, *43*, 20882–20891. [CrossRef]
94. Liu, H.; Wang, X.; Zhou, H.; Gao, S.; Ge, H.; Li, S.; Yan, M. Improved hydrogen desorption properties of $LiBH_4$ by $AlH_3$ addition. *Int. J. Hydrogen Energy* **2016**, *41*, 22118–22127. [CrossRef]
95. Zhu, J.; Mao, Y.; Wang, H.; Liu, J.; Ouyang, L.; Zhu, M. Reaction route optimized $LiBH_4$ for high reversible capacity hydrogen storage by tunable surface-modified AlN. *ACS Appl. Energy Mater.* **2020**, *3*, 11964–11973. [CrossRef]
96. Meggouh, M.; Grant, D.M.; Deavin, O.; Brunelli, M.; Hansen, T.C.; Walker, G.S. Investigation of the dehydrogenation behavior of the $2LiBH_4$:$CaNi_5$ multicomponent hydride system. *Int. J. Hydrogen Energy* **2015**, *40*, 2989–2996. [CrossRef]
97. Liu, D.M.; Tan, Q.J.; Gao, C.; Sun, T.; Li, Y.T. Reversible hydrogen storage properties of $LiBH_4$ combined with hydrogenated $Mg_{11}CeNi$ alloy. *Int. J. Hydrogen Energy* **2015**, *40*, 6600–6605. [CrossRef]
98. Yang, L.; Zhao, S.; Liu, D.; Li, Y.; Si, T. Hydrogen storage properties and reactive mechanism of $LiBH_4$/$Mg_{10}$YNi-H composite. *Mater. Res.* **2019**, *22*, 1–6. [CrossRef]
99. Zhang, X.; Zhang, L.; Zhang, W.; Ren, Z.; Huang, Z.; Hu, J.; Gao, M.; Pan, H.; Liu, Y. Nano-synergy enables highly reversible storage of 9.2 wt% hydrogen at mild conditions with lithium borohydride. *Nano Energy* **2021**, *83*, 105839. [CrossRef]
100. Xu, J.; Li, Y.; Cao, J.; Meng, R.; Wang, W.; Chen, Z. Preparation of graphene-supported highly dispersed nickel nanoparticles for the improved generation of hydrogen from ball-milled $LiBH_4$. *Catal. Sci. Technol.* **2015**, *5*, 1821–1828. [CrossRef]

101. Xu, G.; Zhang, W.; Zhang, Y.; Zhao, X.; Wen, P.; Ma, D. $Fe_3O_4$ nanoclusters highly dispersed on a porous graphene support as an additive for improving the hydrogen storage properties of $LiBH_4$. *RSC Adv.* **2018**, *8*, 19353–19361. [CrossRef]
102. Zhang, L.; Zheng, J.; Xiao, X.; Wang, X.; Huang, X.; Liu, M.; Wang, Q.; Chen, L. A new strategy to remarkably improve the low-temperature reversible hydrogen desorption performances of $LiBH_4$ by compositing with fluorographene. *Int. J. Hydrogen Energy* **2017**, *42*, 20046–20055. [CrossRef]
103. Zhang, W.; Xu, G.; Chen, L.; Pan, S.; Jing, X.; Wang, J.; Han, S. Enhanced hydrogen storage performances of $LiBH_4$ modified with three-dimensional porous fluorinated graphene. *Int. J. Hydrogen Energy* **2017**, *42*, 15262–15270. [CrossRef]
104. Wang, K.; Kang, X.; Ren, J.; Wang, P. Nanostructured graphite-induced destabilization of $LiBH_4$ for reversible hydrogen storage. *J. Alloys Compd.* **2016**, *685*, 242–247. [CrossRef]
105. Lai, Q.; Quadir, M.Z.; Aguey-Zinsou, K.F. $LiBH_4$ electronic destabilization with nickel(II) phthalocyanine—Leading to a reversible hydrogen storage system. *ACS Appl. Energy Mater.* **2018**, *1*, 6824–6832. [CrossRef]
106. Zhou, H.; Wang, X.H.; Liu, H.Z.; Gao, S.C.; Yan, M. Improved hydrogen storage properties of $LiBH_4$ confined with activated charcoal by ball milling. *Rare Met.* **2019**, *38*, 321–326. [CrossRef]
107. Cai, R.; Sun, L.X.; Xu, F.; Zou, Y.J.; Chu, H.L. $LiBH_4$ confined in nitrogen-doped ordered mesoporous carbons for hydrogen storage. *Mater. Sci. Forum* **2016**, *852*, 858–863. [CrossRef]
108. Meng, X.H.; Wan, C.B.; Wang, Y.T.; Ju, X. Porous Ni@C derived from bimetallic Metal–Organic Frameworks and its application for improving $LiBH_4$ dehydrogenation. *J. Alloys Compd.* **2018**, *735*, 1637–1647. [CrossRef]
109. Vellingiri, L.; Annamalai, K.; Kandasamy, R.; Kombiah, I. Single-walled carbon nanotubes/lithium borohydride composites for hydrogen storage: Role of: In situ formed $LiB(OH)_4$, $Li_2CO_3$ and $LiBO_2$ by oxidation and nitrogen annealing. *RSC Adv.* **2019**, *9*, 31483–31496. [CrossRef]
110. Bao, Q.W.; Pan, W.Y.; Liu, H.; Liu, B.H.; Li, Z.P. Reversible hydrogen release and uptake for composites of $LiBH_4$ with the conjugated polymer poly(p-phenylene). *Int. J. Hydrogen Energy* **2016**, *41*, 1027–1034. [CrossRef]
111. Ding, Z.; Ma, Y.; Peng, D.; Zhang, L.; Zhao, Y.; Li, Y.; Han, S. Effects of the hierarchical pyrolysis polyaniline on reversible hydrogen storage of $LiBH_4$. *Prog. Nat. Sci. Mater. Int.* **2018**, *28*, 529–533. [CrossRef]
112. Zhao, Y.; Liu, Y.; Liu, H.; Kang, H.; Cao, K.; Wang, Q.; Zhang, C.; Wang, Y.; Yuan, H.; Jiao, L. Improved dehydrogenation performance of $LiBH_4$ by 3D hierarchical flower-like $MoS_2$ spheres additives. *J. Power Sources* **2015**, *300*, 358–364. [CrossRef]
113. Wang, J.; Wang, Z.; Li, Y.; Ke, D.; Lin, X.; Han, S.; Ma, M. Effect of nano-sized $Ce_2S_3$ on reversible hydrogen storage properties of $LiBH_4$. *Int. J. Hydrogen Energy* **2016**, *41*, 13156–13162. [CrossRef]
114. Dolotko, O.; Gupta, S.; Kobayashi, T.; McDonald, E.; Hlova, I.; Majzoub, E.; Balema, V.P.; Pruski, M.; Pecharsky, V.K. Mechanochemical reactions and hydrogen storage capacities in $MBH_4$–$SiS_2$ systems (M[dbnd]Li or Na). *Int. J. Hydrogen Energy* **2019**, *44*, 7381–7391. [CrossRef]
115. Bidabadi, A.S.; Varin, R.A.; Polanski, M.; Stobinski, L. Mechano-chemical activation of the ($3LiBH_4$ + $TiF_3$) system, its dehydrogenation behavior and the effects of ultrafine filamentary Ni and graphene additives. *RSC Adv.* **2016**, *6*, 93245–93258. [CrossRef]
116. Lai, Q.; Milanese, C.; Aguey-Zinsou, K.F. Stabilization of nanosized borohydrides for hydrogen storage: Suppressing the melting with $TiCl_3$ doping. *ACS Appl. Energy Mater.* **2018**, *1*, 421–430. [CrossRef]
117. Fan, Y.; Chen, D.; Liu, X.; Fan, G.; Liu, B. Improving the hydrogen storage performance of lithium borohydride by $Ti_3C_2$ MXene. *Int. J. Hydrogen Energy* **2019**, *44*, 29297–29303. [CrossRef]
118. Bösenberg, U.; Doppiu, S.; Mosegaard, L.; Barkhordarian, G.; Eigen, N.; Borgschulte, A.; Jensen, T.R.; Cerenius, Y.; Gutfleisch, O.; Klassen, T.; et al. Hydrogen sorption properties of $MgH_2$-$LiBH_4$ composites. *Acta Mater.* **2007**, *55*, 3951–3958. [CrossRef]
119. Ding, Z.; Lu, Y.; Li, L.; Shaw, L. High reversible capacity hydrogen storage through nano-$LiBH_4$ + nano-$MgH_2$ system. *Energy Storage Mater.* **2019**, *20*, 24–35. [CrossRef]
120. Ding, Z.; Shaw, L. Enhancement of hydrogen desorption from nanocomposite prepared by ball milling $MgH_2$ with in situ aerosol spraying $LiBH_4$. *ACS Sustain. Chem. Eng.* **2019**, *7*, 15064–15072. [CrossRef]
121. Ding, Z.; Zhao, X.; Shaw, L.L. Reaction between $LiBH_4$ and $MgH_2$ induced by high-energy ball milling. *J. Power Sources* **2015**, *293*, 236–245. [CrossRef]
122. Thiangviriya, S.; Utke, R. Improvement of dehydrogenation kinetics of $2LiBH_4$-$MgH_2$ composite by doping with activated carbon nanofibers. *Int. J. Hydrogen Energy* **2016**, *41*, 2797–2806. [CrossRef]
123. Plerdsranoy, P.; Chanthee, S.; Utke, R. Compaction of $LiBH_4$-$MgH_2$ doped with MWCNTs-$TiO_2$ for reversible hydrogen storage. *Int. J. Hydrogen Energy* **2017**, *42*, 978–986. [CrossRef]
124. Peng, D.; Li, Y.; Liu, Y.; Zhang, L.; Zhang, H.; Ding, Z.; Han, S. Effect of $LiBH_4$ on hydrogen storage properties of magnesium hydride-carbon composite. *J. Alloys Compd.* **2017**, *711*, 104–110. [CrossRef]
125. Thaweelap, N.; Thongtan, P.; Sitthiwet, C.; Thiangviriya, S.; Eiamlamai, P.; Utke, R. Hydrogen sorption, kinetics, reversibility, and reaction mechanisms of $MgH_2$-x$LiBH_4$ doped with activated carbon nanofibers for reversible hydrogen storage based laboratory powder and tank scales. *Int. J. Hydrogen Energy* **2017**, *42*, 24915–24926. [CrossRef]
126. Zhou, H.; Liu, H.Z.; Xu, L.; Gao, S.C.; Wang, X.H.; Yan, M. Hydrogen storage properties of Nb-compounds-catalyzed $LiBH_4$–$MgH_2$. *Rare Met.* **2017**, *36*, 723–728. [CrossRef]
127. Cheng, C.; Chen, M.; Xiao, X.; Huang, X.; Zheng, J.; Chen, L. Superior reversible hydrogen storage properties and mechanism of $LiBH_4$-$MgH_2$-Al doped with $NbF_5$ additive. *J. Phys. Chem. C* **2018**, *122*, 7613–7620. [CrossRef]

128. Puszkiel, J.A.; Gennari, F.C.; Larochette, P.A.; Ramallo-López, J.M.; Vainio, U.; Karimi, F.; Pranzas, P.K.; Troiani, H.; Pistidda, C.; Jepsen, J.; et al. Effect of Fe additive on the hydrogenation-dehydrogenation properties of 2LiH + $MgB_2$/2$LiBH_4$ + $MgH_2$ system. *J. Power Sources* **2015**, *284*, 606–616. [CrossRef]
129. Zhang, J.; Li, P.; Wan, Q.; Zhai, F.; Volinsky, A.A.; Qu, X. Superior destabilization effects of $LiBH_4$ with the addition of nano-sized nickel ferrite $NiFe_2O_4$. *RSC Adv.* **2015**, *5*, 81212–81219. [CrossRef]
130. Zhao, S.X.; Wang, C.Y.; Liu, D.M.; Tan, Q.J.; Li, Y.T.; Si, T.Z. Destabilization of $LiBH_4$ by $SrF_2$ for reversible hydrogen storage. *Int. J. Hydrogen Energy* **2018**, *43*, 5098–5103. [CrossRef]
131. Kumari, P.; Sharma, K.; Agarwal, S.; Awasthi, K.; Ichikawa, T.; Kumar, M.; Jain, A. The destabilization of $LiBH_4$ through the addition of $Bi_2Se_3$ nanosheets. *Int. J. Hydrogen Energy* **2020**, *45*, 23947–23953. [CrossRef]
132. Wang, H.; Cao, H.; Wu, G.; He, T.; Chen, P. The improved hydrogen storage performances of the multi-component composite: 2$Mg(NH_2)_2$-3LiH-$LiBH_4$. *Energies* **2015**, *8*, 6898–6909. [CrossRef]
133. Liu, L.; Wu, G.; Chen, W.; Xiong, Z.; He, T.; Chen, P. Synthesis and hydrogen storage properties of lithium borohydride urea complex. *Int. J. Hydrogen Energy* **2015**, *40*, 429–434. [CrossRef]
134. Wu, R.; Ren, Z.; Zhang, X.; Lu, Y.; Li, H.; Gao, M.; Pan, H.; Liu, Y. Nanosheet-like lithium borohydride hydrate with 10 wt % hydrogen release at 70°C as a chemical hydrogen storage candidate. *J. Phys. Chem. Lett.* **2019**, *10*, 1872–1877. [CrossRef] [PubMed]
135. Richter, B.; Ravnsbæk, D.B.; Sharma, M.; Spyratou, A.; Hagemann, H.; Jensen, T.R. Fluoride substitution in $LiBH_4$; Destabilization and decomposition. *Phys. Chem. Chem. Phys.* **2017**, *19*, 30157–30165. [CrossRef] [PubMed]
136. Lai, Q.; Yang, Y.; Aguey-Zinsou, K.F. Nanoconfinement of borohydrides in hollow carbon spheres: Melt infiltration versus solvent impregnation for enhanced hydrogen storage. *Int. J. Hydrogen Energy* **2019**, *44*, 23225–23238. [CrossRef]
137. Suwarno Ngene,, P.; Nale, A.; Eggenhuisen, T.M.; Oschatz, M.; Embs, J.P.; Remhof, A.; De Jongh, P.E. Confinement effects for lithium borohydride: Comparing silica and carbon scaffolds. *J. Phys. Chem. C* **2017**, *121*, 4197–4205. [CrossRef] [PubMed]
138. Wu, R.; Zhang, X.; Liu, Y.; Zhang, L.; Hu, J.; Gao, M.; Pan, H. A unique double-layered carbon nanobowl-confined lithium borohydride for highly reversible hydrogen storage. *Small* **2020**, *16*, 1–9. [CrossRef] [PubMed]
139. Wang, S.; Gao, M.; Xian, K.; Li, Z.; Shen, Y.; Yao, Z.; Liu, Y.; Pan, H. $LiBH_4$ nanoconfined in porous hollow carbon nanospheres with high loading, low dehydrogenation temperature, superior kinetics, and favorable reversibility. *ACS Appl. Energy Mater.* **2020**, *3*, 3928–3938. [CrossRef]
140. Shao, J.; Xiao, X.; Fan, X.; Huang, X.; Zhai, B.; Li, S.; Ge, H.; Wang, Q.; Chen, L. Enhanced hydrogen storage capacity and reversibility of $LiBH_4$ nanoconfined in the densified zeolite-templated carbon with high mechanical stability. *Nano Energy* **2015**, *15*, 244–255. [CrossRef]
141. Guo, L.; Li, Y.; Ma, Y.; Liu, Y.; Peng, D.; Zhang, L.; Han, S. Enhanced hydrogen storage capacity and reversibility of $LiBH_4$ encapsulated in carbon nanocages. *Int. J. Hydrogen Energy* **2017**, *42*, 2215–2222. [CrossRef]
142. Xian, K.; Nie, B.; Li, Z.; Gao, M.; Li, Z.; Shang, C.; Liu, Y.; Guo, Z.; Pan, H. $TiO_2$ decorated porous carbonaceous network structures offer confinement, catalysis and thermal conductivity for effective hydrogen storage of $LiBH_4$. *Chem. Eng. J.* **2021**, *407*, 127156. [CrossRef]
143. Gasnier, A.; Gennari, F.C. Graphene entanglement in a mesoporous resorcinol-formaldehyde matrix applied to the nanoconfinement of $LiBH_4$ for hydrogen storage. *RSC Adv.* **2017**, *7*, 27905–27912. [CrossRef]
144. Gasnier, A.; Luguet, M.; Pereira, A.G.; Troiani, H.; Zampieri, G.; Gennari, F.C. Entanglement of N-doped graphene in resorcinol-formaldehyde: Effect over nanoconfined $LiBH_4$ for hydrogen storage. *Carbon N. Y.* **2019**, *147*, 284–294. [CrossRef]
145. Gasnier, A.; Amica, G.; Juan, J.; Troiani, H.; Gennari, F.C. N-Doped graphene-rich aerogels decorated with nickel and cobalt nanoparticles: Effect on hydrogen storage properties of nanoconfined $LiBH_4$. *J. Phys. Chem. C* **2019**, *124*, 115–125. [CrossRef]
146. Thiangviriya, S.; Utke, R. $LiBH_4$ nanoconfined in activated carbon nanofiber for reversible hydrogen storage. *Int. J. Hydrogen Energy* **2015**, *40*, 4167–4174. [CrossRef]
147. Plerdsranoy, P.; Kaewsuwan, D.; Chanlek, N.; Utke, R. Effects of specific surface area and pore volume of activated carbon nanofibers on nanoconfinement and dehydrogenation of $LiBH_4$. *Int. J. Hydrogen Energy* **2017**, *42*, 6189–6201. [CrossRef]
148. Surrey, A.; Bonatto Minella, C.; Fechler, N.; Antonietti, M.; Grafe, H.J.; Schultz, L.; Rellinghaus, B. Improved hydrogen storage properties of $LiBH_4$ via nanoconfinement in micro- and mesoporous aerogel-like carbon. *Int. J. Hydrogen Energy* **2016**, *41*, 5540–5548. [CrossRef]
149. Sitthiwet, C.; Thiangviriya, S.; Thaweelap, N.; Meethom, S.; Kaewsuwan, D.; Chanlek, N.; Utke, R. Hydrogen sorption and permeability of compacted $LiBH_4$ nanoconfined into activated carbon nanofibers impregnated with $TiO_2$. *J. Phys. Chem. Solids* **2017**, *110*, 344–353. [CrossRef]
150. Zhou, H.; Zhang, L.; Gao, S.; Liu, H.; Xu, L.; Wang, X.; Yan, M. Hydrogen storage properties of activated carbon confined $LiBH_4$ doped with $CeF_3$ as catalyst. *Int. J. Hydrogen Energy* **2017**, *42*, 23010–23017. [CrossRef]
151. Sofianos, M.V.; Sheppard, D.A.; Silvester, D.S.; Lee, J.; Paskevicius, M.; Humphries, T.D.; Buckley, C.E. Electrochemical synthesis of highly ordered porous Al scaffolds melt-infiltrated with $LiBH_4$ for hydrogen storage. *J. Electrochem. Soc.* **2018**, *165*, D37–D42. [CrossRef]
152. Sofianos, M.V.; Sheppard, D.A.; Ianni, E.; Humphries, T.D.; Rowles, M.R.; Liu, S.; Buckley, C.E. Novel synthesis of porous aluminium and its application in hydrogen storage. *J. Alloys Compd.* **2017**, *702*, 309–317. [CrossRef]
153. Huang, J.; Yan, Y.; Ouyang, L.; Wang, H.; Zhu, M. Dehydrogenation mechanism of $LiBH_4$ by Poly(methyl methacrylate). *J. Alloys Compd.* **2015**, *645*, S100–S102. [CrossRef]

154. Plerdsranoy, P.; Wiset, N.; Milanese, C.; Laipple, D.; Marini, A.; Klassen, T.; Dornheim, M.; Gosalawit-Utke, R. Improvement of thermal stability and reduction of $LiBH_4$/polymer host interaction of nanoconfined $LiBH_4$ for reversible hydrogen storage. *Int. J. Hydrogen Energy* **2015**, *40*, 392–402. [CrossRef]
155. Fan, Y.; Chen, D.; Yuan, Z.; Chen, Q.; Fan, G.; Zhao, D.; Liu, B. Flexible, water-resistant and air-stable $LiBH_4$ nanoparticles loaded melamine foam with improved dehydrogenation. *Front. Chem.* **2020**, *8*, 1–9. [CrossRef]
156. Xu, X.; Zang, L.; Zhao, Y.; Liu, Y.; Wang, Y.; Jiao, L. Enhanced dehydrogenation performance of $LiBH_4$ by confinement in porous $NiMnO_3$ microspheres. *Int. J. Hydrogen Energy* **2017**, *42*, 25824–25830. [CrossRef]
157. Xu, X.; Zang, L.; Zhao, Y.; Zhao, Y.; Wang, Y.; Jiao, L. Hydrogen storage behavior of $LiBH_4$ improved by the confinement of hierarchical porous $ZnO/ZnCo_2O_4$ nanoparticles. *J. Power Sources* **2017**, *359*, 134–141. [CrossRef]
158. Zang, L.; Sun, W.; Liu, S.; Huang, Y.; Yuan, H.; Tao, Z.; Wang, Y. Enhanced hydrogen storage properties and reversibility of $LiBH_4$ confined in two-dimensional $Ti_3C_2$. *ACS Appl. Mater. Interfaces* **2018**, *10*, 19598–19604. [CrossRef]
159. Chen, X.; Li, Z.; Zhang, Y.; Liu, D.; Wang, C.; Li, Y.; Si, T.; Zhang, Q. Enhanced low-temperature hydrogen storage in nanoporous Ni-based alloy supported $LiBH_4$. *Front. Chem.* **2020**, *8*, 1–8. [CrossRef] [PubMed]
160. Kim, S.; Song, H.; Kim, C. Nanoconfinement effects of MCM-41 on the thermal decomposition of metal borohydrides. *Anal. Sci. Technol.* **2018**, *31*, 1–6. [CrossRef]
161. Wang, T.; Aguey-Zinsou, K.F. Controlling the growth of $LiBH_4$ nanoparticles for hydrogen storage. *Energy Technol.* **2019**, *7*, 1–9. [CrossRef]
162. Yao, Q.; Lu, Z.-H.; Zhang, R.; Zhang, S.; Chen, X.; Jiang, H.-L. A noble-metal-free nanocatalyst for highly efficient and complete hydrogen evolution from $N_2H_4BH_3$. *J. Mater. Chem. A* **2018**, *6*, 4386–4393. [CrossRef]
163. Lai, Q.; Wang, T.; Sun, Y.; Aguey-Zinsou, K. Rational design of nanosized light elements for hydrogen storage: Classes, synthesis, characterization, and properties. *Adv. Mater. Technol.* **2018**, *3*, 1700298. [CrossRef]
164. Mao, J.; Gregory, D.H. Recent advances in the use of sodium borohydride as a solid state hydrogen store. *Energies* **2015**, *8*, 430–453. [CrossRef]
165. Urgnani, J.; Torres, F.J.; Palumbo, M.; Baricco, M. Hydrogen release from solid state $NaBH_4$. *Int. J. Hydrogen Energy* **2008**, *33*, 3111–3115. [CrossRef]
166. Frankcombe, T.J. Proposed mechanisms for the catalytic activity of Ti in $NaAlH_4$. *Chem. Rev.* **2012**, *112*, 2164–2178. [CrossRef] [PubMed]
167. de Jongh, P.E.; Adelhelm, P. Nanosizing and nanoconfinement: New strategies towards meeting hydrogen storage goals. *ChemSusChem* **2010**, *3*, 1332–1348. [CrossRef] [PubMed]
168. Vajo, J.J.; Salguero, T.T.; Gross, A.F.; Skeith, S.L.; Olson, G.L. Thermodynamic destabilization and reaction kinetics in light metal hydride systems. *J. Alloys Compd.* **2007**, *446–447*, 409–414. [CrossRef]
169. Llamas-Jansa, I.; Aliouane, N.; Deledda, S.; Fonneløp, J.E.; Frommen, C.; Humphries, T.; Lieutenant, K.; Sartori, S.; Sørby, M.H.; Hauback, B.C. Chloride substitution induced by mechano-chemical reactions between $NaBH_4$ and transition metal chlorides. *J. Alloys Compd.* **2012**, *530*, 186–192. [CrossRef]
170. Kalantzopoulos, G.N.; Guzik, M.N.; Deledda, S.; Heyn, R.H.; Muller, J.; Hauback, B.C. Destabilization effect of transition metal fluorides on sodium borohydride. *Phys. Chem. Chem. Phys.* **2014**, *16*, 20483–20491. [CrossRef] [PubMed]
171. Llamas Jansa, I.; Kalantzopoulos, G.N.; Nordholm, K.; Hauback, B.C. Destabilization of $NaBH_4$ by transition metal fluorides. *Molecules* **2020**, *25*, 780. [CrossRef] [PubMed]
172. Zhao, N.; Zou, J.; Zeng, X.; Ding, W. Mechanisms of partial hydrogen sorption reversibility in a $3NaBH_4/ScF_3$ composite. *RSC Adv.* **2018**, *8*, 9211–9217. [CrossRef]
173. Huang, T.; Zou, J.; Zhao, N.; Zeng, X.; Ding, W. Reversible hydrogen storage system of $3NaBH_4$-$0.5ScF_3$-$0.5YF_3$: The synergistic effect of $ScF_3$ and $YF_3$. *J. Alloys Compd.* **2019**, *791*, 1270–1276. [CrossRef]
174. Kumar, S.; Singh, A.; Nakajima, K.; Jain, A.; Miyaoka, H.; Ichikawa, T.; Dey, G.K.; Kojima, Y. Improved hydrogen release from magnesium borohydride by $ZrCl_4$ additive. *Int. J. Hydrogen Energy* **2017**, *42*, 22342–22347. [CrossRef]
175. Mao, J.; Gu, Q.; Guo, Z.; Liu, H.K. Sodium borohydride hydrazinates: Synthesis, crystal structures, and thermal decomposition behavior. *J. Mater. Chem. A* **2015**, *3*, 11269–11276. [CrossRef]
176. Johnson, S.R.; David, W.I.F.; Royse, D.M.; Sommariva, M.; Tang, C.Y.; Fabbiani, F.P.A.; Jones, M.O.; Edwards, P.P. The monoammoniate of lithium borohydride, $Li(NH_3)BH_4$: An effective ammonia storage compound. *Chem. Asian J.* **2009**, *4*, 849–854. [CrossRef] [PubMed]
177. Soloveichik, G.; Her, J.-H.; Stephens, P.W.; Gao, Y.; Rijssenbeek, J.; Andrus, M.; Zhao, J.-C. Ammine magnesium borohydride complex as a new material for hydrogen storage: Structure and properties of $Mg(BH_4)_2 \cdot 2NH_3$. *Inorg. Chem.* **2008**, *47*, 4290–4298. [CrossRef] [PubMed]
178. Chu, H.; Wu, G.; Xiong, Z.; Guo, J.; He, T.; Chen, P. Structure and hydrogen storage properties of calcium borohydride diammoniate. *Chem. Mater.* **2010**, *22*, 6021–6028. [CrossRef]
179. Gu, Q.; Gao, L.; Guo, Y.; Tan, Y.; Tang, Z.; Wallwork, K.S.; Zhang, F.; Yu, X. Structure and decomposition of zinc borohydride ammonia adduct: Towards a pure hydrogen release. *Energy Environ. Sci.* **2012**, *5*, 7590. [CrossRef]
180. He, T.; Wu, H.; Wu, G.; Wang, J.; Zhou, W.; Xiong, Z.; Chen, J.; Zhang, T.; Chen, P. Borohydride hydrazinates: High hydrogen content materials for hydrogen storage. *Energy Environ. Sci.* **2012**, *5*, 5686–5689. [CrossRef]

181. He, T.; Wu, H.; Chen, J.; Zhou, W.; Wu, G.; Xiong, Z.; Zhang, T.; Chen, P. Alkali and alkaline-earth metal borohydride hydrazinates: Synthesis, structures and dehydrogenation. *Phys. Chem. Chem. Phys.* **2013**, *15*, 10487. [CrossRef]
182. Roedern, E.; Jensen, T.R. Synthesis, structures and dehydrogenation properties of zinc borohydride ethylenediamine complexes. *ChemistrySelect* **2016**, *1*, 752–755. [CrossRef]
183. Wang, M.; Ouyang, L.; Peng, C.; Zhu, X.; Zhu, W.; Shao, H.; Zhu, M. Synthesis and hydrolysis of $NaZn(BH_4)_3$ and its ammoniates. *J. Mater. Chem. A* **2017**, *5*, 17012–17020. [CrossRef]
184. Payandeh GharibDoust, S.; Heere, M.; Sørby, M.H.; Ley, M.B.; Ravnsbæk, D.B.; Hauback, B.C.; Černý, R.; Jensen, T.R. Synthesis, structure and properties of new bimetallic sodium and potassium lanthanum borohydrides. *Dalt. Trans.* **2016**, *45*, 19002–19011. [CrossRef] [PubMed]
185. Payandeh GharibDoust, S.; Ravnsbæk, D.B.; Černý, R.; Jensen, T.R. Synthesis, structure and properties of bimetallic sodium rare-earth (RE) borohydrides, $NaRE(BH_4)_4$, RE = Ce, Pr, Er or Gd. *Dalt. Trans.* **2017**, *46*, 13421–13431. [CrossRef] [PubMed]
186. Roedern, E.; Lee, Y.-S.; Ley, M.B.; Park, K.; Cho, Y.W.; Skibsted, J.; Jensen, T.R. Solid state synthesis, structural characterization and ionic conductivity of bimetallic alkali-metal yttrium borohydrides $MY(BH_4)_4$ (M = Li and Na). *J. Mater. Chem. A* **2016**, *4*, 8793–8802. [CrossRef]
187. Wu, Y.; Qi, Y.; Zheng, J.; Li, X. Synthesis and dehydrogenation properties of $NaZn(BH_4)_3$·en and $NaZn(BH_4)_3$·2en (en = ethylene diamine). *J. Energy Chem.* **2020**, *42*, 233–236. [CrossRef]
188. Christian, M.L.; Aguey-Zinsou, K.-F. Core–shell strategy leading to high reversible hydrogen storage capacity for $NaBH_4$. *ACS Nano* **2012**, *6*, 7739–7751. [CrossRef]
189. Wang, T.; Aguey-Zinsou, K.-F. Controlling the growth of $NaBH_4$ nanoparticles for hydrogen storage. *Int. J. Hydrogen Energy* **2020**, *45*, 2054–2067. [CrossRef]
190. Wang, T.; Aguey-Zinsou, K.-F. "Surfactant-free" sodium borohydride nanoparticles with enhanced hydrogen desorption properties. *ACS Appl. Energy Mater.* **2020**, *3*, 9940–9949. [CrossRef]
191. Salman, M.S.; Rawal, A.; Aguey-Zinsou, K.-F. Tunable $NaBH_4$ nanostructures revealing structure-dependent hydrogen release. *Adv. Energy Sustain. Res.* **2021**, *2*, 2100063. [CrossRef]
192. Wang, T.; Aguey-Zinsou, K.-F. Direct synthesis of $NaBH_4$ nanoparticles from $NaOCH_3$ for hydrogen storage. *Energies* **2019**, *12*, 4428. [CrossRef]
193. Nakamori, Y.; Li, H.W.; Kikuchi, K.; Aoki, M.; Miwa, K.; Towata, S.; Orimo, S. Thermodynamical stabilities of metal-borohydrides. *J. Alloys Compd.* **2007**, *446–447*, 296–300. [CrossRef]
194. Zavorotynska, O.; El-Kharbachi, A.; Deledda, S.; Hauback, B.C. Recent progress in magnesium borohydride $Mg(BH_4)_2$: Fundamentals and applications for energy storage. *Int. J. Hydrogen Energy* **2016**, *41*, 14387–14403. [CrossRef]
195. De Jongh, P.E.; Allendorf, M.; Vajo, J.J.; Zlotea, C. Nanoconfined light metal hydrides for reversible hydrogen storage. *MRS Bull.* **2013**, *38*, 488–494. [CrossRef]
196. Jain, A.; Agarwal, S.; Ichikawa, T. Catalytic tuning of sorption kinetics of lightweight hydrides: A review of the materials and mechanism. *Catalysts* **2018**, *8*, 651. [CrossRef]
197. Juahir, N.; Mustafa, N.S.; Halim Yap, F.A.; Ismail, M. Study on the hydrogen storage properties and reaction mechanism of $NaAlH_4$–$Mg(BH_4)_2$ (2:1) with and without $TiF_3$ additive. *Int. J. Hydrogen Energy* **2015**, *40*, 7628–7635. [CrossRef]
198. Bai, Y.; Pei, Z.; Wu, F.; Wu, C. Role of metal electronegativity in the dehydrogenation thermodynamics and kinetics of composite metal borohydride–$LiNH_2$ hydrogen storage materials. *ACS Appl. Mater. Interfaces* **2018**, *10*, 9514–9521. [CrossRef]
199. Morelle, F.; Jepsen, L.H.; Jensen, T.R.; Sharma, M.; Hagemann, H.; Filinchuk, Y. Reaction Pathways in $Ca(BH_4)_2$–$NaNH_2$ and $Mg(BH_4)_2$–$NaNH_2$ hydrogen-rich systems. *J. Phys. Chem. C* **2016**, *120*, 8428–8435. [CrossRef]
200. Zheng, J.; Xiao, X.; Zhang, L.; He, Y.; Li, S.; Ge, H.; Chen, L. Study on the dehydrogenation properties and reversibility of $Mg(BH_4)_2AlH_3$ composite under moderate conditions. *Int. J. Hydrogen Energy* **2017**, *42*, 8050–8056. [CrossRef]
201. Zheng, J.; Xiao, X.; Zhang, L.; Li, S.; Ge, H.; Chen, L. Facile synthesis of bowl-like 3D $Mg(BH_4)_2$–$NaBH_4$–fluorographene composite with unexpected superior dehydrogenation performances. *J. Mater. Chem. A* **2017**, *5*, 9723–9732. [CrossRef]
202. Zheng, J.; Xiao, X.; He, Y.; Chen, M.; Liu, M.; Li, S.; Chen, L. Enhanced reversible hydrogen desorption properties and mechanism of $Mg(BH_4)_2$-$AlH_3$-LiH composite. *J. Alloys Compd.* **2018**, *762*, 548–554. [CrossRef]
203. Gigante, A.; Leick, N.; Lipton, A.S.; Tran, B.; Strange, N.A.; Bowden, M.; Martinez, M.B.; Moury, R.; Gennett, T.; Hagemann, H.; et al. Thermal conversion of unsolvated $Mg(B_3H_8)_2$ to $BH_4^-$ in the presence of $MgH_2$. *ACS Appl. Energy Mater.* **2021**, *4*, 3737–3747. [CrossRef]
204. Moury, R.; Gigante, A.; Remhof, A.; Roedern, E.; Hagemann, H. Experimental investigation of $Mg(B_3H_8)_2$ dimensionality, materials for energy storage applications. *Dalt. Trans.* **2020**, *49*, 12168–12173. [CrossRef] [PubMed]
205. Han, M.; Zhao, Q.; Zhu, Z.; Hu, Y.; Tao, Z.; Chen, J. The enhanced hydrogen storage of micro-nanostructured hybrids of $Mg(BH_4)_2$–carbon nanotubes. *Nanoscale* **2015**, *7*, 18305–18311. [CrossRef] [PubMed]
206. Jiang, Z.; Yuan, J.; Han, H.; Wu, Y. Effect of carbon nanotubes on the microstructural evolution and hydrogen storage properties of $Mg(BH_4)_2$. *J. Alloys Compd.* **2018**, *743*, 11–16. [CrossRef]
207. Wahab, M.A.; Jia, Y.; Yang, D.; Zhao, H.; Yao, X. Enhanced hydrogen desorption from $Mg(BH_4)_2$ by combining nanoconfinement and a Ni catalyst. *J. Mater. Chem. A* **2013**, *1*, 3471–3478. [CrossRef]
208. Nale, A.; Pendolino, F.; Maddalena, A.; Colombo, P. Enhanced hydrogen release of metal borohydrides $M(BH_4)_n$ (M = Li, Na, Mg, Ca) mixed with reduced graphene oxide. *Int. J. Hydrogen Energy* **2016**, *41*, 11225–11231. [CrossRef]

209. Yuan, J.; Huang, H.; Jiang, Z.; Lv, Y.; Liu, B.; Zhang, B.; Yan, Y.; Wu, Y. Ni-doped carbon nanotube-$Mg(BH_4)_2$ composites for hydrogen storage. *ACS Appl. Nano Mater.* **2021**, *4*, 1604–1612. [CrossRef]
210. Saldan, I.; Frommen, C.; Llamas-Jansa, I.; Kalantzopoulos, G.N.; Hino, S.; Arstad, B.; Heyn, R.H.; Zavorotynska, O.; Deledda, S.; Sørby, M.H.; et al. Hydrogen storage properties of γ–$Mg(BH_4)_2$ modified by $MoO_3$ and $TiO_2$. *Int. J. Hydrogen Energy* **2015**, *40*, 12286–12293. [CrossRef]
211. Zavorotynska, O.; Saldan, I.; Hino, S.; Humphries, T.D.; Deledda, S.; Hauback, B.C. Hydrogen cycling in γ-$Mg(BH_4)_2$ with cobalt-based additives. *J. Mater. Chem. A* **2015**, *3*, 6592–6602. [CrossRef]
212. Zavorotynska, O.; Deledda, S.; Vitillo, J.G.; Saldan, I.; Guzik, M.N.; Baricco, M.; Walmsley, J.C.; Muller, J.; Hauback, B.C. Combined X-ray and raman studies on the effect of cobalt additives on the decomposition of magnesium borohydride. *Energies* **2015**, *8*, 9173–9190. [CrossRef]
213. Heere, M.; Zavorotynska, O.; Deledda, S.; Sørby, M.H.; Book, D.; Steriotis, T.; Hauback, B.C. Effect of additives, ball milling and isotopic exchange in porous magnesium borohydride. *RSC Adv.* **2018**, *8*, 27645–27653. [CrossRef]
214. Wang, X.; Xiao, X.; Zheng, J.; Hang, Z.; Lin, W.; Yao, Z.; Zhang, M.; Chen, L. The dehydrogenation kinetics and reversibility improvements of $Mg(BH_4)_2$ doped with Ti nano-particles under mild conditions. *Int. J. Hydrogen Energy* **2021**, *46*, 23737–23747. [CrossRef]
215. Zheng, J.; Wang, X.; Xiao, X.; Cheng, H.; Zhang, L.; Chen, L. Improved reversible dehydrogenation properties of $Mg(BH_4)_2$ catalyzed by dual-cation transition metal fluorides $K_2TiF_6$ and $K_2NbF_7$. *Chem. Eng. J.* **2021**, *412*, 128738. [CrossRef]
216. Li, Y.; Liu, Y.; Zhang, X.; Yang, Y.; Gao, M.; Pan, H. Hydrogen storage properties and mechanisms of a $Mg(BH_4)_2{\cdot}2NH_3$-$NaAlH_4$ combination system. *Int. J. Hydrogen Energy* **2016**, *41*, 2788–2796. [CrossRef]
217. Leng, H.; Xu, J.; Jiang, J.; Xiao, H.; Li, Q.; Chou, K.C. Improved dehydrogenation properties of $Mg(BH_4)_2{\cdot}2NH_3$ combined with $LiAlH_4$. *Int. J. Hydrogen Energy* **2015**, *40*, 8362–8367. [CrossRef]
218. Li, Y.; Liu, Y.; Zhang, X.; Zhou, D.; Lu, Y.; Gao, M.; Pan, H. An ultrasound-assisted wet-chemistry approach towards uniform $Mg(BH_4)_2{\cdot}6NH_3$ nanoparticles with improved dehydrogenation properties. *J. Mater. Chem. A* **2016**, *4*, 8366–8373. [CrossRef]
219. Yang, Y.; Liu, Y.; Li, Y.; Zhang, X.; Gao, M.; Pan, H. Towards the endothermic dehydrogenation of nanoconfined magnesium borohydride ammoniate. *J. Mater. Chem. A* **2015**, *3*, 11057–11065. [CrossRef]
220. Yang, Y.; Liu, Y.; Li, Y.; Gao, M.; Pan, H. Fluorine-substituted $Mg(BH_4)_2{\cdot}2NH_3$ with improved dehydrogenation properties for hydrogen storage. *J. Mater. Chem. A* **2015**, *3*, 570–578. [CrossRef]
221. Hansen, B.R.S.; Paskevicius, M.; Li, H.-W.; Akiba, E.; Jensen, T.R. Metal boranes: Progress and applications. *Coord. Chem. Rev.* **2016**, *323*, 60–70. [CrossRef]
222. Chu, H.; Qiu, S.; Zou, Y.; Xiang, C.; Zhang, H.; Xu, F.; Sun, L.; Zhou, H. Improvement on hydrogen desorption performance of calcium borohydride diammoniate doped with transition metal chlorides. *J. Phys. Chem. C* **2014**, *119*, 913–918. [CrossRef]
223. Chen, J.; Chua, Y.S.; Wu, H.; Xiong, Z.; He, T.; Zhou, W.; Ju, X.; Yang, M.; Wu, G.; Chen, P. Synthesis, structures and dehydrogenation of magnesium borohydride–ethylenediamine composites. *Int. J. Hydrogen Energy* **2015**, *40*, 412–419. [CrossRef]
224. Li, Z.; He, T.; Wu, G.; Ju, X.; Chen, P. The synthesis, structure and dehydrogenation of calcium borohydride hydrazinates. *Int. J. Hydrogen Energy* **2015**, *40*, 5333–5339. [CrossRef]
225. Wu, H.; Zhou, X.; Rodriguez, E.E.; Zhou, W.; Udovic, T.J.; Yildirim, T.; Rush, J.J. A new family of metal borohydride guanidinate complexes: Synthesis, structures and hydrogen-storage properties. *J. Solid State Chem.* **2016**, *242*, 186–192. [CrossRef]
226. Chong, M.; Autrey, T.; Jensen, C.M. Lewis base complexes of magnesium borohydride: Enhanced kinetics and product selectivity upon hydrogen release. *Inorganics* **2017**, *5*, 89. [CrossRef]
227. Lai, Q.; Aguey-Zinsou, K.F. Destabilisation of $Ca(BH_4)_2$ and $Mg(BH_4)_2$: Via confinement in nanoporous $Cu_2S$ hollow spheres. *Sustain. Energy Fuels* **2017**, *1*, 1308–1319. [CrossRef]
228. Lai, Q.; Pratthana, C.; Yang, Y.; Rawal, A.; Aguey-Zinsou, K.-F. Nanoconfinement of complex borohydrides for hydrogen storage. *ACS Appl. Nano Mater.* **2021**, *4*, 973–978. [CrossRef]
229. Schneemann, A.; Wan, L.F.; Lipton, A.S.; Liu, Y.-S.; Snider, J.L.; Baker, A.A.; Sugar, J.D.; Spataru, C.D.; Guo, J.; Autrey, T.S.; et al. Nanoconfinement of molecular magnesium borohydride captured in a bipyridine-functionalized Metal–Organic Framework. *ACS Nano* **2020**, *14*, 10294–10304. [CrossRef] [PubMed]
230. Wang, X.; Xiao, X.; Zheng, J.; Huang, X.; Chen, M.; Chen, L. In-situ synthesis of amorphous $Mg(BH_4)_2$ and chloride composite modified by $NbF_5$ for superior reversible hydrogen storage properties. *Int. J. Hydrogen Energy* **2020**, *45*, 2044–2053. [CrossRef]
231. Sulaiman, N.N.; Ismail, M.; Timmiati, S.N.; Lim, K.L. Improved hydrogen storage performances of $LiAlH_4$ + $Mg(BH_4)_2$ composite with $TiF_3$ addition. *Int. J. Energy Res.* **2021**, *45*, 2882–2898. [CrossRef]
232. Yuan, J.; Chen, J.; Huang, H.; Lv, Y.; Liu, B.; Li, Z.; Zhang, B.; Lv, W.; Wu, Y. Enhanced hydrogen storage properties of $NaBH_4$–$Mg(BH_4)_2$ composites by $NdF_3$ addition. *Prog. Nat. Sci. Mater. Int.* **2021**. [CrossRef]
233. Wahab, M.A.; Young, D.J.; Karim, A.; Fawzia, S.; Beltramini, J.N. Low-temperature hydrogen desorption from $Mg(BH_4)_2$ catalysed by ultrafine Ni nanoparticles in a mesoporous carbon matrix. *Int. J. Hydrogen Energy* **2016**, *41*, 20573–20582. [CrossRef]
234. Clémençon, D.; Davoisne, C.; Chotard, J.N.; Janot, R. Enhancement of the hydrogen release of $Mg(BH_4)_2$ by concomitant effects of nano-confinement and catalysis. *Int. J. Hydrogen Energy* **2019**, *44*, 4253–4262. [CrossRef]
235. Leick, N.; Strange, N.A.; Schneemann, A.; Stavila, V.; Gross, K.; Washton, N.; Settle, A.; Martinez, M.B.; Gennett, T.; Christensen, S.T. $Al_2O_3$ atomic layer deposition on nanostructured γ-$Mg(BH_4)_2$ for $H_2$ storage. *ACS Appl. Energy Mater.* **2021**, *4*, 1150–1162. [CrossRef]

236. Zheng, J.; Yao, Z.; Xiao, X.; Wang, X.; He, J.; Chen, M.; Cheng, H.; Zhang, L.; Chen, L. Enhanced hydrogen storage properties of high-loading nanoconfined $LiBH_4$–$Mg(BH_4)_2$ composites with porous hollow carbon nanospheres. *Int. J. Hydrogen Energy* **2021**, *46*, 852–864. [CrossRef]
237. Javadian, P.; Sheppard, D.A.; Buckley, C.E.; Jensen, T.R. Hydrogen storage properties of nanoconfined $LiBH_4$-$Ca(BH_4)_2$. *Nano Energy* **2015**, *11*, 96–103. [CrossRef]
238. Zheng, J.; Cheng, H.; Wang, X.; Chen, M.; Xiao, X.; Chen, L. $LiAlH_4$ as a "Microlighter" on the fluorographite surface triggering the dehydrogenation of $Mg(BH_4)_2$: Toward more than 7 wt % hydrogen release below 70 °C. *ACS Appl. Energy Mater.* **2020**, *3*, 3033–3041. [CrossRef]
239. Petit, J.F.; Miele, P.; Demirci, U.B. Ammonia borane $H_3N$-$BH_3$ for solid-state chemical hydrogen storage: Different samples with different thermal behaviors. *Int. J. Hydrogen Energy* **2016**, *41*, 15462–15470. [CrossRef]
240. Nakagawa, Y.; Zhang, T.; Kitamura, M.; Isobe, S.; Hino, S.; Hashimoto, N.; Ohnuki, S. A systematic study of the effects of metal chloride additives on $H_2$ desorption properties of ammonia borane. *J. Chem. Eng. Data* **2016**, *61*, 1924–1929. [CrossRef]
241. Simagina, V.I.; Vernikovskaya, N.V.; Komova, O.V.; Kayl, N.L.; Netskina, O.V.; Odegova, G.V. Experimental and modeling study of ammonia borane-based hydrogen storage systems. *Chem. Eng. J.* **2017**, *329*, 156–164. [CrossRef]
242. Shin, S.; Jin, J.H.; Jung, J. Thermolytic dehydrogenation of cotton-structured $SiO_2$-Ammonia borane nanocomposite. *J. Ind. Eng. Chem.* **2020**, *88*, 278–284. [CrossRef]
243. Ergüven, H.; Kantürk Figen, A.; Pişkin, S. Ammonia borane–boron composites for hydrogen release: Thermolysis kinetics. *Energy Sources Part A Recover Util. Environ. Eff.* **2017**, *39*, 613–617. [CrossRef]
244. Gangal, A.; Edla, R.; Manna, J.; Sharma, P. Effect of misch metal nanoparticles on thermal decomposition of ammonia borane. *J. Res. Nanotechnol.* **2015**, *2015*, 1–8. [CrossRef]
245. Biliškov, N.; Vojta, D.; Kótai, L.; Szilágyi, I.M.; Hunyadi, D.; Pasinszki, T.; Flinčec Grgac, S.; Borgschulte, A.; Züttel, A. High influence of potassium bromide on thermal decomposition of ammonia borane. *J. Phys. Chem. C* **2016**, *120*, 25276–25288. [CrossRef]
246. Huang, J.; Tan, Y.; Gu, Q.; Ouyang, L.; Yu, X.; Zhu, M. Ammonia borane modified zirconium borohydride octaammoniate with enhanced dehydrogenation properties. *J. Mater. Chem. A* **2015**, *3*, 5299–5304. [CrossRef]
247. Kim, G.J.; Boone, A.M.; Chesnut, M.; Shin, J.H.; Jung, J.; Hwang, H.T. Enhanced thermal dehydrogenation of ammonia borane by d-mannitol. *Ind. Eng. Chem. Res.* **2020**, *59*, 620–626. [CrossRef]
248. Kim, G.J.; Hunt, S.G.; Hwang, H.T. Effect of maleic acid on onset temperature and $H_2$ release kinetics for thermal dehydrogenation of ammonia borane. *Int. J. Hydrogen Energy* **2020**, *45*, 33751–33758. [CrossRef]
249. Shin, S.; Jin, J.H.; Jung, J. Sugar acid–assisted thermolysis of all-solid-state ammonia borane hydrogen fuel. *Energy Technol.* **2020**, *8*, 1–7. [CrossRef]
250. Roy, B.; Manna, J.; Sharma, P. Effect of Ni-alloys on thermal decomposition of ammonia borane. *J. Alloys Compd.* **2015**, *645*, S234–S238. [CrossRef]
251. Luo, J.; Wang, J.; Feng, X.; Cai, J.; Yao, W.; Song, J.; Chen, C.; Luo, D. Mechanistic insight into the promoting effect of magnesium nickel hydride on the dehydrogenation of ammonia borane. *Int. J. Hydrogen Energy* **2018**, *43*, 1681–1690. [CrossRef]
252. Wan, L.; Chen, J.; Tan, Y.; Gu, Q.; Yu, X. Ammonia borane destabilized by aluminium hydride: A mutual enhancement for hydrogen release. *Int. J. Hydrogen Energy* **2015**, *40*, 1047–1053. [CrossRef]
253. Dovgaliuk, I.; Le Duff, C.S.; Robeyns, K.; Devillers, M.; Filinchuk, Y. Mild dehydrogenation of ammonia borane complexed with aluminum borohydride. *Chem. Mater.* **2015**, *27*, 768–777. [CrossRef]
254. Huang, H.; Wang, C.; Li, Q.; Wang, R.; Yang, Y.; Muhetaer, A.; Huang, F.; Han, B.; Xu, D. Efficient and full-spectrum photothermal dehydrogenation of ammonia borane for low-temperature release of hydrogen. *Adv. Funct. Mater.* **2021**, *31*, 1–9. [CrossRef]
255. Castilla-Martinez, C.A.; Moury, R.; Demirci, U.B. Amidoboranes and hydrazinidoboranes: State of the art, potential for hydrogen storage, and other prospects. *Int. J. Hydrogen Energy* **2020**, *45*, 30731–30755. [CrossRef]
256. Milanović, I.; Biliškov, N. Mechanochemical pretreatment of ammonia borane: A new procedure for sodium amidoborane synthesis. *Int. J. Hydrogen Energy* **2020**, *45*, 7938–7946. [CrossRef]
257. Lee, C.H.; Nakagawa, Y.; Isobe, S.; Hashimoto, N.; Sugino, S.; Miyaoka, H.; Ichikawa, T. Synthesis of sodium-magnesium amidoborane by sodium amide: An investigation of functional properties for hydrogen/ammonia storage. *J. Alloys Compd.* **2019**, *801*, 645–650. [CrossRef]
258. Wu, C.; Wu, G.; Xiong, Z.; David, W.I.F.; Ryan, K.R.; Jones, M.O.; Edwards, P.P.; Chu, H.; Chen, P. Stepwise phase transition in the formation of lithium amidoborane. *Inorg. Chem.* **2010**, *49*, 4319–4323. [CrossRef] [PubMed]
259. Liu, X.; Wang, S.; Wu, Y.; Li, Z.; Jiang, L.; Guo, X.; Ye, J. Dehydrogenation properties of two phases of $LiNH_2BH_3$. *Int. J. Hydrogen Energy* **2019**, *5*, 1–8. [CrossRef]
260. Ghaani, M.R.; Catti, M. Dehydrogenation properties of the $LiNH_2BH_3/MgH_2$ and $LiNH_2BH_3/LiBH_4$ bi-component hydride systems for hydrogen storage applications. *Mater. Renew. Sustain. Energy* **2018**, *7*, 1–6. [CrossRef]
261. Owarzany, R.; Jaroń, T.; Leszczyński, P.J.; Fijalkowski, K.J.; Grochala, W. Amidoboranes of rubidium and caesium: The last missing members of the alkali metal amidoborane family. *Dalt. Trans.* **2017**, *46*, 16315–16320. [CrossRef]
262. Kazakov, I.V.; Butlak, A.V.; Shelyganov, P.A.; Suslonov, V.V.; Timoshkin, A.Y. Reversible structural transformations of rubidium and cesium amidoboranes. *Polyhedron* **2017**, *127*, 186–190. [CrossRef]
263. Davydova, E.I.; Lisovenko, A.S.; Timoshkin, A.Y. Complex beryllium amidoboranes: Structures, stability, and evaluation of their potential as hydrogen storage materials. *J. Comput. Chem.* **2017**, *38*, 401–405. [CrossRef] [PubMed]

264. Shcherbina, N.A.; Kazakov, I.V.; Timoshkin, A.Y. Synthesis and characterization of barium amidoborane. *Russ. J. Gen. Chem.* **2017**, *87*, 2875–2877. [CrossRef]
265. Dovgaliuk, I.; Jepsen, L.H.; Safin, D.A.; Łodziana, Z.; Dyadkin, V.; Jensen, T.R.; Devillers, M.; Filinchuk, Y. A composite of complex and chemical hydrides yields the first Al-based amidoborane with improved hydrogen storage properties. *Chem. Eur. J.* **2015**, *21*, 14562–14570. [CrossRef] [PubMed]
266. Nakagawa, Y.; Shinzato, K.; Nakagawa, T.; Nakajima, K.; Isobe, S.; Goshome, K.; Miyaoka, H.; Ichikawa, T. Synthesis, structural characterization, and hydrogen desorption properties of $Na[Al(NH_2BH_3)_4]$. *Int. J. Hydrogen Energy* **2017**, *42*, 6173–6180. [CrossRef]
267. Milanović, I.; Biliškov, N.; Užarević, K.; Lukin, S.; Etter, M.; Halasz, I. Mechanochemical synthesis and thermal dehydrogenation of novel calcium-containing bimetallic amidoboranes. *ACS Sustain. Chem. Eng.* **2021**, *9*, 2089–2099. [CrossRef]
268. Chernysheva, A.M.; Shelyganov, P.A.; Kazakov, I.V.; Timoshkin, A.Y. Complex amidoboranes $M^2[M^1(NH_2BH_3)_4]$ ($M^1$ = Al, Ga; $M^2$ = Li, Na, K, Rb, Cs). *Russ. J. Gen. Chem.* **2017**, *87*, 665–669. [CrossRef]
269. Yang, J.; Beaumont, P.R.; Humphries, T.D.; Jensen, C.M.; Li, X. Efficient synthesis of an aluminum amidoborane ammoniate. *Energies* **2015**, *8*, 9107–9116. [CrossRef]
270. He, T.; Wu, H.; Wu, G.; Li, Z.; Zhou, W.; Ju, X.; Xie, D.; Chen, P. Lithium amidoborane hydrazinates: Synthesis, structure and hydrogen storage properties. *J. Mater. Chem. A* **2015**, *3*, 10100–10106. [CrossRef]
271. Li, Z.; He, T.; Wu, G.; Chen, W.; Chua, Y.S.; Guo, J.; Xie, D.; Ju, X.; Chen, P. Synthesis, structure and the dehydrogenation mechanism of calcium amidoborane hydrazinates. *Phys. Chem. Chem. Phys.* **2016**, *18*, 244–251. [CrossRef]
272. Jørgensen, M.; Lee, Y.-S.; Bjerring, M.; Jepsen, L.H.; Akbey, Ü.; Cho, Y.W.; Jensen, T.R. Disorder induced polymorphic transitions in the high hydrogen density compound $Sr(BH_4)_2(NH_3BH_3)_2$. *Dalt. Trans.* **2018**, *47*, 16737–16746. [CrossRef]
273. Valero-Pedraza, M.J.; Gascón, V.; Carreón, M.A.; Leardini, F.; Ares, J.R.; Martín, Á.; Sánchez-Sánchez, M.; Banãres, M.A. Operando Raman-mass spectrometry investigation of hydrogen release by thermolysis of ammonia borane confined in mesoporous materials. *Microporous Mesoporous Mater.* **2016**, *226*, 454–465. [CrossRef]
274. Sullivan, J.A.; Herron, R.; Phillips, A.D. Towards an understanding of the beneficial effect of mesoporous materials on the dehydrogenation characteristics of $NH_3BH_3$. *Appl. Catal. B Environ.* **2017**, *201*, 182–188. [CrossRef]
275. Rueda, M.; Sanz-Moral, L.M.; Segovia, J.J.; Martín, Á. Improvement of the kinetics of hydrogen release from ammonia borane confined in silica aerogel. *Microporous Mesoporous Mater.* **2017**, *237*, 189–200. [CrossRef]
276. Roy, B.; Manna, J.; Pal, U.; Hajari, A.; Bishnoi, A.; Sharma, P. An: In situ study on the solid state decomposition of ammonia borane: Unmitigated by-product suppression by a naturally abundant layered clay mineral. *Inorg. Chem. Front.* **2018**, *5*, 301–309. [CrossRef]
277. Feng, Y.; Zhou, X.; Yang, J.; Gao, X.; Yin, L.; Zhao, Y.; Zhang, B. Encapsulation of ammonia borane in Pd/Halloysite nanotubes for efficient thermal dehydrogenation. *ACS Sustain. Chem. Eng.* **2020**, *8*, 2122–2129. [CrossRef]
278. So, S.H.; Jang, J.H.; Sung, S.J.; Yang, S.J.; Nam, K.T.; Park, C.R. Demonstration of the nanosize effect of carbon nanomaterials on the dehydrogenation temperature of ammonia borane. *Nanoscale Adv.* **2019**, *1*, 4697–4703. [CrossRef]
279. Yang, Z.; Zhou, D.; Chen, B.; Liu, Z.; Xia, Q.; Zhu, Y.; Xia, Y. Improved hydrogen release from ammonia borane confined in microporous carbon with narrow pore size distribution. *J. Mater. Chem. A* **2017**, *5*, 15395–15400. [CrossRef]
280. Bravo Diaz, L.; Hanlon, J.M.; Bielewski, M.; Milewska, A.; Gregory, D.H. Ammonia borane based nanocomposites as solid-state hydrogen stores for portable power applications. *Energy Technol.* **2018**, *6*, 583–594. [CrossRef]
281. Cao, Z.; Ouyang, L.; Felderhoff, M.; Zhu, M. Low temperature dehydrogenation properties of ammonia borane within carbon nanotube arrays: A synergistic effect of nanoconfinement and alane. *RSC Adv.* **2020**, *10*, 19027–19033. [CrossRef]
282. Li, Z.; Liu, W.; Yang, H.; Sun, T.; Liu, K.; Wang, Z.; Niu, C. Improved thermal dehydrogenation of ammonia borane by MOF-5. *RSC Adv.* **2015**, *5*, 10746–10750. [CrossRef]
283. Kong, S.; Dai, R.; Li, H.; Sun, W.; Wang, Y. Microwave hydrothermal synthesis of Ni-based Metal-Organic Frameworks and their derived yolk-shell NiO for Li-ion storage and supported ammonia borane for hydrogen desorption. *ACS Sustain. Chem. Eng.* **2015**, *3*, 1830–1838. [CrossRef]
284. Yang, H.; Li, Z.; Liu, K.; Meng, F.; Niu, C. Clean hydrogen release from ammonia borane in a metal-organic framework with unsaturated coordinated $Tm^{3+}$. *J. Phys. Chem. C* **2015**, *119*, 2260–2265. [CrossRef]
285. Wang, X.; Xie, L.; Huang, K.W.; Lai, Z. A rationally designed amino-borane complex in a metal organic framework: A novel reusable hydrogen storage and size-selective reduction material. *Chem. Commun.* **2015**, *51*, 7610–7613. [CrossRef] [PubMed]
286. Liao, C.W.; Tseng, P.S.; Chang, B.K.; Wang, C.Y. Facilitated hydrogen release kinetics from amine borane functionalization on gate-opening metal-organic framework. *Surf. Coatings Technol.* **2018**, *350*, 12–19. [CrossRef]
287. Chung, J.Y.; Liao, C.W.; Chang, Y.W.; Chang, B.K.; Wang, H.; Li, J.; Wang, C.Y. Influence of Metal-Organic Framework porosity on hydrogen generation from nanoconfined ammonia borane. *J. Phys. Chem. C* **2017**, *121*, 27369–27378. [CrossRef]
288. Wu, Y.J.; Wang, C.Y. Insight into the catalytic effects of open metal sites in Metal-Organic Frameworks on hydride dehydrogenation via nanoconfinement. *ACS Sustain. Chem. Eng.* **2019**, *7*, 16013–16025. [CrossRef]
289. Zhang, L.; Xia, G.; Ge, Y.; Wang, C.; Guo, Z.; Li, X.; Yu, X. Ammonia borane confined by nitrogen-containing carbon nanotubes: Enhanced dehydrogenation properties originating from synergetic catalysis and nanoconfinement. *J. Mater. Chem. A* **2015**, *3*, 20494–20499. [CrossRef]
290. Yang, Z.; Sun, H.; Li, H.; Li, F.; Qijing, H.; Zhang, Y. Enhancing the thermal dehydrogenation properties of ammonia borane (AB) by using monodisperse $MnO_2$ hollow spheres (MHS). *J. Alloys Compd.* **2019**, *781*, 111–117. [CrossRef]

291. Salameh, C.; Moussa, G.; Bruma, A.; Fantozzi, G.; Malo, S.; Miele, P.; Demirci, U.B.; Bernard, S. Robust 3D boron nitride nanoscaffolds for remarkable hydrogen storage capacity from ammonia borane. *Energy Technol.* **2018**, *6*, 570–577. [CrossRef]
292. Richard, J.; Cid, S.L.; Rouquette, J.; Van Der Lee, A.; Bernard, S.; Haines, J. Pressure-induced insertion of ammonia borane in the siliceous zeolite, silicalite-1F. *J. Phys. Chem. C* **2016**, *120*, 9334–9340. [CrossRef]
293. Sun, W.; Li, H.; Wang, Y. Graphene-supported nickel chloride and cobalt chloride nanoparticles as highly efficient catalysts for dehydrogenation of ammonia borane. *Int. J. Hydrogen Energy* **2015**, *40*, 15389–15397. [CrossRef]
294. Champet, S.; Van Den Berg, J.; Szczesny, R.; Godula-Jopek, A.; Gregory, D.H. Nano-inclusion in one step: Spontaneous ice-templating of porous hierarchical nanocomposites for selective hydrogen release. *Sustain. Energy Fuels* **2019**, *3*, 396–400. [CrossRef]
295. Peil, S.; Wisser, D.; Stähle, M.; Roßmann, P.K.; Avadhut, Y.S.; Hartmann, M. Hydrogen release from ammonia borane nanoconfined in Metal-Organic Frameworks with MIL-53 topology. *J. Phys. Chem. C* **2021**, *125*, 9990–10000. [CrossRef]
296. Nathanson, A.S.; Ploszajski, A.R.; Billing, M.; Cook, J.P.; Jenkins, D.W.K.; Headen, T.F.; Kurban, Z.; Lovell, A.; Bennington, S.M. Ammonia borane-polyethylene oxide composite materials for solid hydrogen storage. *J. Mater. Chem. A* **2015**, *3*, 3683–3691. [CrossRef]
297. Ploszajski, A.R.; Billing, M.; Cockcroft, J.K.; Skipper, N.T. Crystalline structure of an ammonia borane-polyethylene oxide cocrystal: A material investigated for its hydrogen storage potential. *CrystEngComm* **2018**, *20*, 4436–4440. [CrossRef]
298. Ploszajski, A.R.; Billing, M.; Nathanson, A.S.; Vickers, M.; Bennington, S.M. Freeze-dried ammonia borane-polyethylene oxide composites: Phase behaviour and hydrogen release. *Int. J. Hydrogen Energy* **2018**, *43*, 5645–5656. [CrossRef]
299. Seemaladinne, R.; Pati, S.; Kharel, K.; Bafana, A.; al-Wahish, A.; Wujcik, E.K.; Günaydın-Şen, Ö. Ammonia borane with polyvinylpyrrolidone as a hydrogen storage material: Comparison of different molecular weights. *J. Phys. Chem. Solids* **2017**, *110*, 394–400. [CrossRef]
300. Alipour, J.; Shoushtari, A.M.; Kaflou, A. Ammonia borane confined by poly(methyl methacrylate)/multiwall carbon nanotube nanofiber composite, as a polymeric hydrogen storage material. *J. Mater. Sci.* **2015**, *50*, 3110–3117. [CrossRef]
301. Roy, B.; Hajari, A.; Manna, J.; Sharma, P. Supported ammonia borane decomposition through enhanced homopolar B-B coupling. *Dalt. Trans.* **2018**, *47*, 6570–6579. [CrossRef]
302. Demirci, U.B. Mechanistic insights into the thermal decomposition of ammonia borane, a material studied for chemical hydrogen storage. *Inorg. Chem. Front.* **2021**, *8*, 1900–1930. [CrossRef]
303. Petit, J.F.; Demirci, U.B. Mechanistic insights into dehydrogenation of partially deuterated ammonia borane $NH_3BD_3$ being heating to 200°C. *Inorg. Chem.* **2019**, *58*, 489–494. [CrossRef]
304. Song, Y.; Ma, N.; Ma, X.; Fang, F.; Chen, X.; Guo, Y. Synthesis of ammonia borane nanoparticles and the diammoniate of diborane by direct combination of diborane and ammonia. *Chem. Eur. J.* **2016**, *22*, 6228–6233. [CrossRef]
305. Lai, Q.; Rawal, A.; Quadir, M.Z.; Cazorla, C.; Demirci, U.B.; Aguey-Zinsou, K.F. Nanosizing ammonia borane with nickel: A path toward the direct hydrogen release and uptake of B–N–H systems. *Adv. Sustain. Syst.* **2018**, *2*, 1–14. [CrossRef]
306. Valero-Pedraza, M.J.; Cot, D.; Petit, E.; Aguey-Zinsou, K.F.; Alauzun, J.G.; Demirci, U.B. Ammonia borane nanospheres for hydrogen storage. *ACS Appl. Nano Mater.* **2019**, *2*, 1129–1138. [CrossRef]
307. Pylypko, S.; Petit, J.F.; Ould-Amara, S.; Hdhili, N.; Taihei, A.; Chiriac, R.; Ichikawa, T.; Cretin, M.; Miele, P.; Demirci, U.B. Metal hydride-hydrazine borane: Towards hydrazinidoboranes or composites as hydrogen carriers. *Int. J. Hydrogen Energy* **2015**, *40*, 14875–14884. [CrossRef]
308. Moury, R.; Demirci, U.B.; Ban, V.; Filinchuk, Y.; Ichikawa, T.; Zeng, L.; Goshome, K.; Miele, P. Lithium hydrazinidoborane: A polymorphic material with potential for chemical hydrogen storage. *Chem. Mater.* **2014**, *26*, 3249–3255. [CrossRef]
309. Moury, R.; Demirci, U.B.; Ichikawa, T.; Filinchuk, Y.; Chiriac, R.; Van Der Lee, A.; Miele, P. Sodium hydrazinidoborane: A chemical hydrogen-storage material. *ChemSusChem* **2013**, *6*, 667–673. [CrossRef] [PubMed]
310. Chua, Y.S.; Pei, Q.; Ju, X.; Zhou, W.; Udovic, T.J.; Wu, G.; Xiong, Z.; Chen, P.; Wu, H. Alkali metal hydride modification on hydrazine borane for improved dehydrogenation. *J. Phys. Chem. C* **2014**, *118*, 11244–11251. [CrossRef]
311. Wu, H.; Zhou, W.; Pinkerton, F.E.; Udovic, T.J.; Yildirim, T.; Rush, J.J. Metal hydrazinoborane $LiN_2H_3BH_3$ and $LiN_2H_3BH_3{\cdot}2N_2H_4BH_3$: Crystal structures and high-extent dehydrogenation. *Energy Environ. Sci.* **2012**, *5*, 7531. [CrossRef]
312. Castilla-Martinez, C.A.; Granier, D.; Charmette, C.; Maurin, G.; Yot, P.G.; Demirci, U.B. Rubidium hydrazinidoborane: Synthesis, characterization and hydrogen release properties. *Int. J. Hydrogen Energy* **2019**, *44*, 28252–28261. [CrossRef]
313. Castilla-Martinez, C.A.; Granier, D.; Charmette, C.; Cartier, J.; Yot, P.G.; Demirci, U.B. Cesium hydrazinidoborane, the last of the alkali hydrazinidoboranes, studied as potential hydrogen storage material. *Int. J. Hydrogen Energy* **2020**, *45*, 16634–16643. [CrossRef]
314. Moury, R.; Petit, J.F.; Demirci, U.B.; Ichikawa, T.; Miele, P. Pure hydrogen-generating "doped" sodium hydrazinidoborane. *Int. J. Hydrogen Energy* **2015**, *40*, 7475–7482. [CrossRef]
315. Ould-Amara, S.; Granier, D.; Chiriac, R.; Toche, F.; Yot, P.G.; Demirci, U.B. Lithium hydrazinidoborane ammoniate $LiN_2H_3BH_3{\cdot}0.25NH_3$, a derivative of hydrazine borane. *Materials* **2017**, *10*, 750. [CrossRef]
316. Ould-Amara, S.; Yadav, V.; Petit, E.; Maurin, G.; Yot, P.G.; Demirci, U.B. Calcium hydrazinidoborane: Synthesis, characterization, and promises for hydrogen storage. *Int. J. Hydrogen Energy* **2019**, *45*, 2022–2033. [CrossRef]
317. Castilla-Martinez, C.A.; Roussignol, L.; Demirci, U.B. Magnesium hydrazinidoborane: Synthesis, characterization and features for solid-state hydrogen storage. *Int. J. Hydrogen Energy* **2021**, *46*, 33164–33175. [CrossRef]
318. Fu, H.; Yang, J.; Wang, X.; Xin, G.; Zheng, J.; Li, X. Preparation and dehydrogenation properties of lithium hydrazidobis(borane) ($LiNH(BH_3)NH_2BH_3$). *Inorg. Chem.* **2014**, *53*, 7334–7339. [CrossRef]

319. Hajari, A.; Roy, B.; Sharma, P. Metal-free rapid dehydrogenation kinetics and better regeneration yield of ammonia borane. *Int. J. Hydrogen Energy* **2021**, *46*, 24214–24224. [CrossRef]
320. Tan, Y.; Zhang, L.; Chen, X.; Yu, X. Reductive dechlorination of $BCl_3$ for efficient ammonia borane regeneration. *Dalt. Trans.* **2015**, *44*, 753–757. [CrossRef] [PubMed]
321. Nakagawa, T.; Uesato, H.; Burrell, A.K.; Ichikawa, T.; Miyaoka, H.; Davis, B.L.; Kojima, Y. Surface-controlled conversion of ammonia borane from boron nitride. *Energies* **2020**, *13*, 5569. [CrossRef]